Ph.D. Dissertation

International Doctoral School in Information

and Communication Technology

DISI - University of Trento

Innovative Wireless Localization Techniques and Applications

Alessandro Polo

Advisor:
Prof. Giacomo Oliveri
University of Trento

February 2018

To my family, to Georgia and to all friends, for having trust and understanding until now and hopefully for years to come.

A special thanks to all friends and colleagues of the ELEDIA Research Center.

Abstract

Innovative methodologies for the wireless localization of users and related applications are addressed in this thesis.

In last years, the widespread diffusion of pervasive wireless communication (e.g., Wi-Fi) and global localization services (e.g., *GPS*) has boosted the interest and the research on location information and services. Location-aware applications are becoming fundamental to a growing number of consumers (e.g., navigation, advertising, seamless user interaction with smart places), private and public institutions in the fields of energy efficiency, security, safety, fleet management, emergency response. In this context, the position of the user - *where* is often more valuable for deploying services of interest than the identity of the user itself - *who*.

In detail, opportunistic approaches based on the analysis of electromagnetic field indicators (i.e., received signal strength and channel state information) for the presence detection, the localization, the tracking and the posture recognition of cooperative and non-cooperative (device-free) users in indoor environments are proposed and validated in real world test sites. The methodologies are designed to exploit existing wireless infrastructures and commodity devices without any hardware modification.

In outdoor environments, global positioning technologies are already available in commodity devices and vehicles, the research and knowledge transfer activities are actually focused on the design and validation of algorithms and systems devoted to support decision makers and operators for increasing efficiency, operations security, and management of large fleets as well as localized sensed information in order to gain situation awareness. In this field, a decision support system for emergency response and Civil Defense assets management (i.e., personnel and vehicles equipped with *TETRA* mobile radio) is described in terms of architecture and results of two-years of experimental validation.

This thesis is in partial fulfillment for the degree of Doctor of Philosophy at the Department of Information Engineering and Computer Science of the University of Trento, Italy. The work, carried out between 2012 and 2017 at the ELEDIA Research Center, has been published in peer-reviewed journals and conferences.

Keywords
Wireless positioning, device-free localization, target users detection, electromagnetic modeling, received signal strength, channel state information, location-aware decision support systems, multi-objective evolutionary optimization, fleet management, emergency-response, terrestrial trunked radio (TETRA).

Published Journal Papers

[R01] F. Viani, F. Robol, A. Polo, P. Rocca, G. Oliveri, and A. Massa, "Wireless architectures for heterogeneous sensing in smart home applications - Concepts and real implementations," *Proceedings of the IEEE* - Special Issue on 'The Smart Home,' Invited Paper, vol. 101, no. 11, pp. 2381-2396, November 2013.

[R02] F. Viani, A. Polo, M. Donelli, and E. Giarola, "A relocable and resilient distributed measurement system for electromagnetic exposure assessment," *IEEE Sensors Journal*, vol. 16, no. 11, pp. 4595-4604, June 2016.

[R03] H. Ahmadi, A. Polo, T. Moriyama, M. Salucci, and F. Viani, "Semantic wireless localization of Wi-Fi terminals in smart buildings," *Radio Science - Special Issue on 'Innovative Microwave Devices, Methods and Applications,' Invited Paper*, vol. 51, no. 6, pp. 876-892, June 2016.

[R04] F. Viani, M. Bertolli, and A. Polo, "Low-cost wireless system for agrochemical dosage reduction in precision farming," *IEEE Sensors Journal*, vol. 17, no. 1, pp. 5-6, January 2017.

[R05] F. Viani, A. Polo, P. Garofalo, N. Anselmi, M. Salucci, and E. Giarola, "Evolutionary optimization applied to wireless smart lighting in energy-efficient museums," *IEEE Sensors Journal*, vol. 17, no. 5, pp. 1213-1214, March 2017.

[R06] H. Ahmadi, F. Viani, A. Polo, and R. Bouallegue, "Learning ensemble strategy for static and dynamic localization in wireless sensor networks," *International Journal of Network Management*, vol. 27, no. 4, pp. 1-10, July 2017.

[R07] F. Viani, M. Bertolli, M. Salucci, and A. Polo, "Low-cost wireless monitoring and decision support for water saving in agriculture," *IEEE Sensors Journal*, vol. 17, no. 13, pp. 4299-4309, July 2017.

[R08] F. Viani and A. Polo, "A forecasting strategy based on wireless sensing for thermal comfort optimization in smart buildings," *Microwave and Optical Technology Letters*, vol. 59, no.11, pp. 2913-2917, November 2017.

[R09] G. Oliveri, G. Gottardi, F. Robol, A. Polo, L. Poli, M. Salucci, M. Chuan, C. Massagrande, P. Vinetti, M. Mattivi, R. Lombardi, and A. Massa, "Co-design of unconventional array architectures and antenna elements for 5G base stations," *IEEE Transactions on Antennas and Propagation* - Special Issue on 'Antennas and Propagation Aspects of 5G Communications,' vol. 65, no. 12, pp. 6752-6767, Dec. 2017.

[R10] F. Viani, M. D. Migliore, A. Polo, M. Salucci, and A. Massa, "An iterative classification strategy for multi-resolution wireless sensing of passive targets," *Electronics Letters*, vol. 54, no. 2, pp.101-103, Jan, 2018.

Published International Conference Papers

[C01] G. Menduni, F. Viani, F. Robol, E. Giarola, A. Polo, G. Oliveri, P. Rocca, and A. Massa, "A WSN-based architecture for the E-Museum - The experience at 'Sala dei 500' in Palazzo Vecchio (Florence)," *Proc. 2013 IEEE AP-S International Symposium*, Lake Buena Vista, Florida, USA, pp. 1114-1115, July 7-12, 2013.

[C02] F. Viani, F. Robol, A. Polo, E. Giarola, and A. Massa, "Localization strategies in WSNs as applied to landslide monitoring," *2013 American Geophysical Union Fall Meeting*, San Francisco, USA, p. A5, December 9-13, 2013 (Invited paper; Session title: 'New technologies in landslide monitoring and risk management' - A. Pasuto and L. Schenato).

[C03] A. Polo, F. Viani, E. Giarola, G. Oliveri, P. Rocca, and A. Massa, "Semantic wireless localization enabling advanced services in museums," *8th European Conference on Antennas and Propagation* (EUCAP 2014), The Hague, The Netherlands, pp. 443-446, April 6-11, 2014.

[C04] A. Polo, F. Robol, C. Nardin, S. Marchesi, A. Zorer, L. Zappini, F. Viani, and A. Massa, "Decision support system for fleet management based on TETRA terminals geolocation," *8th European Conference on Antennas and Propagation* (EUCAP 2014), The Hague, The Netherlands, pp. 1195-1198, April 6-11, 2014

[C05] F. Viani, A. Polo, F. Robol, G. Oliveri, P. Rocca, and A. Massa, "Crowd detection and occupancy estimation through indirect environmental measurements," *8th European Conference on Antennas and Propagation* (EUCAP 2014), The Hague, The Netherlands, pp. 2127-2130, April 6-11, 2014.

[C06] F. Viani, E. Giarola, A. Polo, G. Vannuccini, L. Longo, and A. Massa, "Decision support system for museum management through distributed wireless sensing," *Museums and the Web* (MWF 2014), Florence, Italy, February 19-21, 2014.

[C07] F. Viani, A. Polo, E. Giarola, F. Robol, P. Rocca, P. Garofalo, S. De Vigili, G. Benedetti, L. Zappini, A. Zorer, S. Marchesi, and A. Massa, "Semantic wireless localization for innovative indoor/outdoor services," *Proc. 2014 IEEE AP-S International Symposium and USNC-URSI Radio Science Meeting*, Memphis, Tennessee, USA, pp. 402-403, July 6-12, 2014.

[C08] F. Viani, E. Giarola, F. Robol, A. Polo, A. Lazzareschi, T. Moriyama, and A. Massa, "Passive wireless localization strategies for security in large indoor areas," *Proc. 2014 IEEE Antenna Conference on Antenna Measurements and Applications* (IEEE CAMA 2014), Antibes Juan-les-Pins, France, pp. 1-3, November 16-19, 2014.

[C09] A. Polo, F. Viani, L. Zappini, S. Marchesi, A. Zorer, and A. Massa, "Advances in decision-making support tools for fleet management in emergency and security applications," *Proc. 2014 IEEE Antenna Conference on Antenna Measurements and Applications* (IEEE CAMA 2014), Antibes Juan-les-Pins, France, pp. 1-3, November 16-19, 2014.

[C10] F. Viani, F. Robol, E. Giarola, A. Polo, A. Toscano, and A. Massa, "Wireless monitoring of heterogeneous parameters in complex museum scenario," *Proc. 2014 IEEE Antenna Conference on Antenna Measurements and Applications* (IEEE CAMA 2014), Antibes Juan-les-Pins, France, pp. 1-3, November 16-19, 2014.

[C11] F. Robol, F. Viani, A. Polo, E. Giarola, P. Garofalo, C. Zambiasi, and A. Massa, "Opportunistic crowd sensing in Wi-Fi-enabled indoor areas," *Proc. 2015 IEEE AP-S International Symposium and USNC-URSI Radio Science Meeting*, Vancouver, BC, Canada, pp. 274-275, July 19-25, 2015.

[C12] T. Moriyama, A. Polo, F. Viani, and A. Massa, "Improved wireless localization of mobile devices in smart indoor scenarios," *Proc. 2015 IEEE Mediterranean Microwave Symposium* (MMS 2015), Lecce, Italy, November 30 - December 2, 2015.

[C13] L. Paucar, A. Diaz, F. Viani, F. Robol, A. Polo, and A. Massa, "Decision support for smart irrigation by means of wireless distributed sensors," *Proc. 2015 IEEE Mediterranean Microwave Symposium* (MMS 2015), Lecce, Italy, November 30 - December 2, 2015.

[C14] L. Zappini, S. Marchesi, A. Polo, F. Viani, and A. Massa, "Evolutionary optimization strategies applied to wireless fleet management in emergency scenarios," *Proc. 2015 IEEE Mediterranean Microwave Symposium* (MMS 2015), Lecce, Italy, November 30 - December 2, 2015.

[C15] L. Tenuti, G. Oliveri, F. Viani, A. Polo, M. Donelli, and A. Massa, "A frequency-hopping BCS strategy for imaging buried objects," *Proc. 2015 IEEE Mediterranean Microwave Symposium* (MMS 2015), Lecce, Italy, November 30 - December 2, 2015.

[C16] F. Viani, N. Anselmi, M. Donelli, P. Garofalo, G. Gottardi, G. Oliveri, L. Poli, A. Polo, P. Rocca, M. Salucci, L. Tenuti, and A. Massa, "On the role of information in inversion and synthesis â challenges, tools, and trends," *Proc. 2015 IEEE Mediterranean Microwave Symposium* (MMS 2015), Lecce, Italy, November 30 - December 2, 2015.

[C17] F. Viani, A. Polo, and E. Giarola, "Exploiting EM simulation modelling for wireless indoor localization," *10th European Conference on Antennas and Propagation* (EUCAP 2016), Davos, Switzerland, April 10-15, 2016.

[C18] F. Viani, F. Robol, A. Polo, and E. Giarola, "Wildlife road-crossing monitoring system: Advances and test site validation," *10th European Conference on Antennas and Propagation* (EUCAP 2016), Davos, Switzerland, April 10-15, 2016.

[C19] F. Viani, F. Robol, M. Bertolli, A. Polo, H. Ahmadi, R. Bouallegue, and A. Massa, "A wireless monitoring system for phytosanitary treatment in smart farming applications," *Proc. 2016 IEEE AP-S International Symposium and USNC-URSI Radio Science Meeting*, Fajardo, Puerto Rico, pp. 2001-2002, June 26 - July 1, 2016.

[C20] H. Ahmadi, F. Viani, A. Polo, and R. Bouallegue, "An improved anchor selection strategy for wireless localization of WSN nodes," *2016 IEEE Symposium on Computers and Communication* (ISCC), Messina, Italy, June 27-30, 2016.

[C21] F. Viani, A. Polo, F. Robol, A. Ferro, and E. Giarola, "Experimental validation of a wireless distributed system for smart public lighting management," *2016 IEEE International Smart Cities Conference*,

Trento, Italy, pp. 1-6, September 12-15, 2016 (Special Session title: 'Decision Support Strategies based on Wireless Sensing and Monitoring for Smart Cities Management' - F. Viani and A. Polo).

[C22] F. Viani, A. Polo, E. Giarola, G. Benedetti, S. Zanetti, and F. Robol, "Performance assessment of a smart road management system for the wireless detection of wildlife road-crossing," *2016 IEEE International Smart Cities Conference*, Trento, Italy, pp. 1-6, September 12-15, 2016 (Special Session title: 'Decision Support Strategies based on Wireless Sensing and Monitoring for Smart Cities Management' - F. Viani and A. Polo).

[C23] P. Chakravorty, D. Mandal, A. Polo, and F. Viani, "Antenna system strategies for wireless sensor networks in resource hungry smart cities," *2016 IEEE International Smart Cities Conferenc*e, Trento, Italy, pp. 1-4, September 12-15, 2016 (Special Session title: 'Decision Support Strategies based on Wireless Sensing and Monitoring for Smart Cities Managemen' - F. Viani and A. Polo).

[C24] A. Polo, F. Viani, F. Robol, S. Marchesi, L. Zappini, and A. Massa, "Optimization strategies for fleet management based on wireless terminals localization in smart cities scenarios," *2016 IEEE International Smart Cities Conference*, Trento, Italy, pp. 1-4, September 12-15, 2016 (Special Session title: 'Decision Support Strategies based on Wireless Sensing and Monitoring for Smart Cities Management' - F. Viani and A. Polo).

[C25] H. Ahmadi, F. Viani, A. Polo, and R. Bouallegue, "An accurate ensemble-based wireless localization strategy for wireless sensor networks," *24th International Conference on Software*, Telecommunications, and Computer Networks (SoftCOM 2016), Split, Croatia, pp. 1-5, September 22-24, 2016.

[C26] H. Ahmadi, F. Viani, A. Polo, and R. Bouallegue, "Improved target tracking using regression tree in wireless sensor networks," *2016 IEEE/ACS International Conference of Computer Systems and Applications* (AICCSA), Agadir, Morocco, pp. 1-6, November 29 - December 2, 2016.

[C27] G. Oliveri, F. Robol, A. Polo, R. Lombardi, M. Chuan, M. Mattivi, C. Massagrande, P. Vinetti, C. Mazzucco, and A. Massa, "Design of compact printed antennas for 5G base stations," *11th European Conference on Antennas and Propagation* (EUCAP 2017), Paris, France, pp. 3090-3093, March 19-24, 2017.

[C28] F. Viani, A. Polo, E. Giarola, M. Salucci, and A. Massa, "Principal component analysis of CSI for the robust wireless detection of passive targets," *2017 International Applied Computational Electromagnetics Society Symposium* (ACES 2017), Firenze, Italy, pp. 1-2, March 26-30, 2017 (Invited paper; Special Session title: 'Electromagnetic Techniques for the Internet of Things' - A. Costanzo and P. Nepa).

[C29] F. Viani, A. Polo, and M. D. Migliore, "Device-free human monitoring using channel state information," *6th Asia-Pacific Conference on Antennas and Propagation* (APCAP 2017), Xiâan, China, October 16-19, 2017 (Invited paper; Session title: 'Current Trends and Advances in Computational Inverse Scattering: Theory, Techniques, and Application' - A. Massa, M. Li, and M. Salucci).

Published National Conference Papers

[N01] E. Giarola, S. Marchesi, A. Polo, F. Robol, F. Viani, L. Zappini, A. Zorer, and A. Massa, "Innovative wireless solutions for smart cities," Atti XX Riunione Nazionale di Elettromagnetismo (XX RiNEm), Padova, pp. 385-388, 15-18 Settembre 2014.

[N02] A. Polo, "Exploiting Frequency Diversity in Propagation-based Wireless Localization of Mobile Devices," Atti XXI Riunione Nazionale di Elettromagnetismo (XXI RiNEm), Parma, 12-14 Settembre 2016.

[N03] H. Ahmadi, M. S. Dao, E. Giarola, A. Polo, F. Robol, F. Viani, and A. Massa, "Distributed wireless sensing, monitoring, and decision support: current activities @ ELEDIA Research Center," Atti XXI Riunione Nazionale di Elettromagnetismo (XXI RiNEm), Parma, pp. 156-159, 12-14 Settembre 2016.

[N04] A. Polo and A. Massa, "Wireless-based decision support systems and fleet management @ ELEDIA Research Center," Atti XXI Riunione Nazionale di Elettromagnetismo (XXI RiNEm), Parma, pp. 160-163, 12-14 Settembre 2016.

Awards

[AW1] Winner Project Idea Proposal: "DOMiNO - a decision support system for critical missions and fleet management in civil and TETRA scenario," *InSIEm - Giovani verso l'Impresa*, Padova, XX Riunione Nazionale di Elettromagnetismo (XX RiNEm), Padova, 16 Settembre 2014.

[AW2] Yarman-Carlin Student Award. Third Prize for the paper "Improved wireless localization of mobile devices in smart indoor scenarios," *2015 IEEE 15th Mediterranean Microwave Symposium* (MMS 2015) pp.212-215, Lecce, Italy, 2015.

Thesis Outline

The thesis is organized as follows. Firstly, Chapter 1 introduces the motivations, the application scenarios and the architectures of wireless technologies for the presence detection, the localization and the human monitoring of both cooperative and non-cooperative (device-free) target users.

In Chapter 2, an innovative and opportunistic methodology for the accurate positioning of wireless devices in indoor scenarios is addressed. The proposed approach is based on training-less self-calibrating numerical electromagnetic propagation modeling of the wireless communications. It relies on existing commodity wireless infrastructures and it exploits the minimal information about the environment required by the algorithm (i.e., location of Wi-Fi Access Points and blueprint of the building) for improving the accuracy accordingly to probabilistic and semantic considerations.

In Chapter 3, non-cooperative target users are considered. Unlike many device-free localization techniques, the proposed methodologies do not require any kind of hardware customization. Indeed, the wireless monitoring of a standard communication link established between two commercial wireless devices (e.g., a Wi-FI Access Point and a client) is opportunistically exploited for human presence detection, localization and posture recognition.

In Chapter 4, the focus is on the application of location-based technologies and services in outdoor environments (e.g., *GPS*, *TETRA*) for supporting decision makers and operators within the field of distributed wireless monitoring and fleet management for institutional and emergency-response agencies. A full-scale prototype software tool experimentally validated by hundreds of professionals of the civil defense of the Trentino region is illustrated.

Contents

List of Tables

List of Figures

Chapter 1

Introduction

The problem of guaranteeing a reliable, accurate, and robust localization information (especially in indoor scenarios) is a fundamental challenge at the intersection of many information engineering disciplines because of its importance and impact from the scientific and industrial viewpoint.

While *ICT* services were initially focused on transmitting identity, request and response for accomplishing explicit user needs, recently with the widespread diffusion of pervasive wireless communication networking such as indoor Wi-Fi technologies and with the advent of (*GPS*-enabled) smart-phones, the paradigm has evolved in order to provide services able to understand, assist and forecast user activities without standard command-and-control interactions. This new approach moves the focus from *who are you* to *where are you* information as user habits and location are exploited for characterizing user profile and consequently his real-time needs. Nowadays both the industry and the consumers have realized the benefits that location-based services bring, applications like search, maps and navigation are becoming fundamental to a growing number of consumers, and they are still gaining more and more interest as they provide new opportunities in the mobile value chain. Indeed, the range of applications requiring an accurate localization of people, goods, or devices is vast, also governments and authorities are interested in services dedicated to emergency-call positioning, emergency-response and fleet management, road-traffic optimization, tracking vulnerable and elderly people, and so on. While location-based services enable a dynamic user experience and interactivity, offering a new level of convenience that was not possible before and that changes the way businesses and institutions interact with customers and other enterprises, they also raise many concerns about user privacy. These concerns are particularly relevant for non-cooperative localization and human monitoring, in this scenario device-free solutions that also preserve the user identification and privacy such as the wireless electromagnetic-based localization techniques presented in this work constitute of a valid alternative to the computer-vision approaches often adopted within security and surveillance applications.

1.1 Scenarios and Motivations

1.1.1 Smart Home and Internet of Things

The home technology is moving rapidly from the programmable thermostat to an era where all home systems are integrated into a centralized control one accessible from multiple entry points like touch pads, computer screens, telephones, and other wireless mobile devices, such as smart-phones and tablets. The result is a highly personalized environment, a house that reacts to individual needs and wants, and even anticipates changes. This perspective is a clear consequence of the dramatic impact that pervasive technologies have had on society.
In such a framework, a widely diffused viewpoint on the smart home and its implementation, more specifically the home automation, is related to the idea of comfort that can be explained as follows: "*Morning brings a graduated alarm that plays some of your favorite music. The volume builds slowly and the bedroom curtains gently part until you react and tell the alarm. Meanwhile, the bathroom floors are already warming in anticipation of your arrival, and the coffee-maker starts brewing up* [1]." The problem complexity, the competition between vendors, the multiple incompatible standards, and the high expenses, have limited the diffusion of smart home technologies in the real scenario. Only a niche of users is disposed nowadays to (or can) spend money for those expensive and luxury facilities. Other needs are considered more essential with respect to the strictly comfort-based functionalities. As a consequence, much of the potential that would technically be available are still confined to research projects, test beds, or industrial experiments, as clearly shown by the rich state of the art produced in the last years [2][3][4][5][6]. Consequently, the researchers are now focusing on testing and deploying technologies in real environments and for long-term periods by reducing the system complexity and implementing solutions providing more evident and tangible advantages to the everyday life of the end users. Among smart home functionalities, the following ones are here considered as most interesting applications and case studies of wireless localization system because of their direct impact on environmental efficiency (i.e., energy and money saving), safety and security for both private users and public services:

- *Smart power management for energy cost reduction.* With the growth of the smart grid research area, concerned with the intelligent control of electricity usage, the smart home plays a key role in the interaction between the grid and the consumers [3]. Power management systems are undergoing an increasing deployment in private homes all over the world because of the government decisions for fulfilling the optimization of resources and from the end-users perspective of reducing the costs of in-home power consumptions. Many solutions have been proposed for integrating smart meter devices capable of simultaneously communicating with both the energy distributors and the household [7][8]. Toward this end, two main guidelines

have been established. The one is to collect energy information through the standard utility meter that gives aggregate information about the consumption of the home [9]. The other direction is that of monitoring individual appliances of interest by means of in-home distributed smart meters and communicate the recorded data to a central data processing unit [10]. This latter solution has been sometimes considered costly and complex to implement because of the need of infrastructure [8]. However, many drawbacks related to wiring, costs, and complexity are going to be overcome thanks to the diffusion of wireless architectures [6, 11, 12, 13, 14, 15, 16, 17, 18].

- *Assistive services for elderly people monitoring and security.* Health-care systems have attracted enormous attention worldwide [19][20] and many national associations have reported the urgent need for in-home assistance due to the high cost of institutional living [21]. In this framework, the social security and health-care systems are taking advantage of the out coming assistive technologies [4] that can be integrated in smart home scenarios. Several projects have been developed [22, 23, 24, 25, 26, 27] giving emphasis and priority to the functionalities provided to the end users. Smart homes have been equipped with various sensors to improve the detection of anomalies or behavioral changes [28, 29, 30, 31]. Starting from the sensors acquisitions, data fusion techniques are mandatory to extract useful evolutions inside the large set of information. Despite all these efforts, some drawbacks like privacy and reliability are still limiting the wide diffusion and commercialization of such systems. A solution is that of focusing on the unobtrusiveness as a key issue to improve user satisfaction and acceptance. This mainstream has been pursued testing more and more pervasive, non-invasive, and low cost technologies [6][32] capable of inferring the user behavior, while avoiding the installation of cameras or microphones. Towards this end, wireless technologies are very promising tools enabling flexible adding/removing of components and facilitating the scalability and the integrability of small devices within other existing wireless backbones [33, 34, 35].

It is worth noticing that previous topics present common challenges from both a technological and methodological point of view. The actual state of the art presents many lessons learned from experiences in project activities and the difficulties that are limiting the proliferation of next-generation smart homes have been pointed out [36]. From the technological perspective, the main challenges are related to the non-scalable integration of heterogeneous technologies that often cannot communicate together, require hard wiring, are ad-hoc designed and cannot be evolved, updated, or easily replaced [4]. The lack of a common and flexible infrastructure hosting heterogeneous functionalities according to the user needs often comes out and it represents a key challenge to be considered in the development of smart home concepts. Because of these problems, taking

advantages of exploiting wireless networks as a means for sensing and actuation is considered to be inevitable.

Whether the initial objective of the home intelligence was to automatically control devices and systems according to specific rules previously implemented [37], nowadays, the purpose of the algorithms is to enable an interactive home environment capable of adapting its operations to accommodate the users. The main requirement to enable interactions is to gather information not only on the environment, but also related to the users presence and location-based activities. The methodologies for the activity recognition vary as greatly as the types of adopted technologies and corresponding sensed data [38]. Currently used methods are mostly based on machine-learning models such as Bayes classifiers [39, 40], Markov models [41, 42], artificial neural networks [43, 44], and support vector machines [45][46] thanks to their ability to create context models from measured data and to adapt them according to the changing behavior and needs, and their computational efficiency (i.e., real-time response) enabling integration in low power wireless devices with constrained resources. The obtained results demonstrate that such approaches are promising for behavior classification and prediction. However, once applied to real test-cases, single methods would not suffice to bring forward the best systemic solution, while the combination of different techniques could lead to more sophisticated hybrid intelligent systems [10]. It has also to be noticed that evolutionary optimization strategies [47] have been profitably exploited in many applicative fields thanks to their ability to solve complex problems with high number of unknowns. Such a feature has been exploited and integrated in hybrid algorithms for decision making to find optimal user preferences adapting to new knowledge without deleting the existing one [48, 49]. Each solution is effective for a limited set of conditions mainly due to the specific initialization given by the experts and to the kind of adopted sensors. Up to now, the decision making phase is still considered a support tool where the user has to interact to give additional information [50]. In these years, researchers began to recognize the importance of improving and applying methodologies for behavior monitoring and decision making also in the fields of assistance services [51][52] and power management [43]. In this regard, the implementation of distributed intelligence on top of wireless platforms like Wireless Sensor Networks (WSN) and Internet of Things (IoT) has emerged as a promising solution and is attracting more and more attention [53] as the increasing capabilities of very low-cost embedded wireless devices (e.g., System on Chip micro-boards such as *ESP8266*, which is sold at few euros) supporting easy re-programmability and offering to developers interesting features for localization (i.e., Wi-Fi connectivity) and monitoring (i.e, digital inputs for sensors and output for actuation). The work on active and passive localization presented in the thesis has been designed to exploit these kind of new opportunities and the new indoor networking paradigms in terms of communication standard (i.e., *IEEE 802.11g/n/ac/ax*) and availability of inter-connected devices. In fact, each

wireless device of the network, being cooperative or not, will provide some valuable information to a localization system based on the electromagnetic analysis of wireless links and channels.

1.1.2 Fleet and Emergency Management

In last decade, the spread of outdoor digital wireless communication systems and low-cost global positioning services that are embedded in commodity products such as smart-phones and vehicles, as well as professional networks such as the terrestrial trunked radio (*ETSI TETRA*) [54] and digital mobile radio (*ETSI DMR*) for civil defense and critical applications is offering more and more opportunities for the adoption in real-world scenario of location-based systems supporting the pervasive environmental monitoring, the goods tracking, the fleet and the emergency-response management (Fig. 1.1). In the outdoor scenario, different global navigation satellite systems (*GNSS*) have been established as de-facto standard for civilian and military positioning (i.e., with different level of restrictions and accuracy) at worldwide level:

- Global Positioning System (*GPS*) from United States of America;
- Global Navigation Satellite system (*GLONASS*) from Russia;
- BeiDou Navigation Satellite System (*BeiDou / BDS*) from China;
- and *GALILEO*, the newest solution from European Community, that is actually being finalized and activated.

Modern organizations such as goods transportation industry and crisis management agencies share the need of tracking, dispatching and coordinating many heterogeneous resources distributed on the field (e.g., trucks, ambulances, fire-engines, helicopters, drones) for the accomplishment of simple tasks as well as critical missions. In the last decades, more and more natural and man-made emergencies have occurred (e.g., urban accidents, forest fires, flooding, landslides, tsunamis, toxic chemical spills) with widespread consequences on the population and on the societal costs [55, 56]. Consequently, the interest in the improved crisis management has grown at worldwide level. As an example, one third of the budget is reserved for societal needs in the forthcoming *H2020* calls of the European Commission [57].

The fleet and emergency management scenario deals with a highly dynamic, uncertain, and dangerous environment where the exchange of information and the coordination between civil defense actors are essential for mission accomplishment. The situation room operators have to take quick and proper decisions according to their interpretation of the situational picture. This is possible only when professional managers and first responders have access to the required information, and when the assets are ready to intervene with very low latency

[58]. Location-based Decision Support Systems (*DSS*) are aimed at assisting decision makers, operators and control rooms for different tasks in which the position of assets and localized information themselves (such as weather and traffic conditions) play a crucial role in the evaluation of efficient solutions for mission management problems such as vehicle coordination, goods routing and mission planning. Modern *DSS* have benefit from the new communication, sensing, and positioning technologies in order to provide real-time awareness to the situation room and to support the decision making process in complex and dynamic emergency situations [59]. In Chapter 4, a prototype (*TRL-7*) that supports the environmental monitoring and the fleet management operations for civil defense situation rooms and operators is presented.

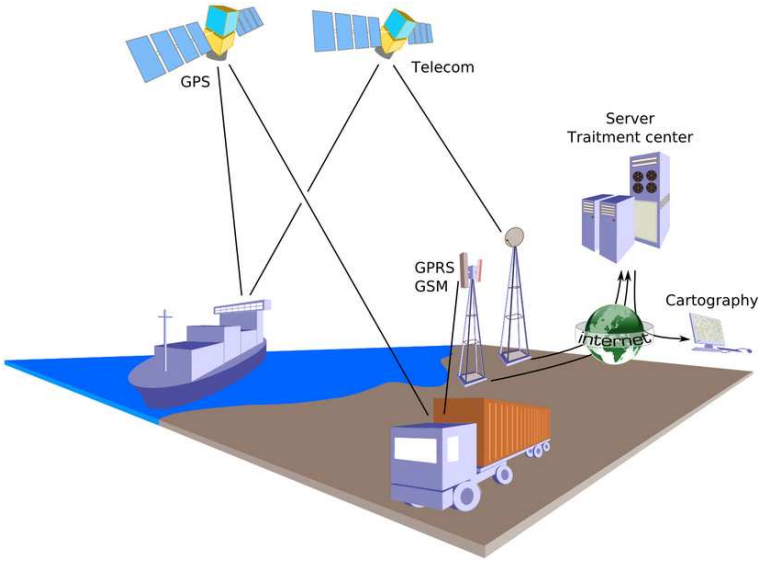

Figure 1.1: *Outdoor Localization Scenario.* Fleet assets are equipped with Global Positioning System (GPS) device that provides real-time location (e.g., latitude, longitude, direction, speed) to the central operation center. Bidirectional voice and data communication, including command and control channel, is provided by TETRA, 2G, 3G, 4G and soon 5G mobile communication technologies.

1.2 Wireless Approaches and Architectures

The electromagnetic (*EM*) field generated by a radio transceiver integrated in wireless devices, such as home router, smart TVs, personal computers, smartphones and tablets has its own sensing capabilities as any other dedicated sensor. The *EM* field that propagates throughout the environment "collects" information about physical and electrical characteristics of objects in the form of radio-frequency (*RF*) perturbations. Accordingly, the problem of human presence and movements estimation can be recast as the following inverse problem one

[47]: "*Starting from measurements of electromagnetic field, reconstructing the characteristics of the propagation scenario that fit the measured data*". Almost all wireless transceivers including low-cost and low-power devices provide a raw information on the *RF* signal quality, the Received Signal Strength (*RSS*) indicator. Modern communication standards, such as *IEEE 802.11n/ac* Wi-Fi, are designed to acquire, exploit and provide more detailed information as the Channel State Information (*CSI*) that describes the *EM* channel response in Single-Input Single-Output (*SISO*) and Multiple-Input Multiple-Output (*MIMO*) configuration. Such indicators measure the magnitude of the received *EM* field and it "contains" a valuable information for the estimation of the human behavior. As a matter of fact, human positions are inferred by measuring the absorption, the reflection, the scattering of the *EM* field caused by the human bodies. It has to be noticed that, unlike most of standard sensors, *EM* sensors permeate the home environment since the primary role of the *RF* signal is to provide wireless connectivity throughout the home (and often not limited to the perimeter of the house). It is worth noticing that people has already accepted the presence of home wireless network to enable Internet connectivity service, thus implicitly accepting the presence of *EM* sensing. Accordingly, the measurement of *RSS* and eventually *CSI* of any wireless network device turns out to be a transparent procedure that does not require dedicated sensors and gives a preliminary estimation of user activities.

This opportunistic way of exploiting *EM* signals is here adopted both for *passive* (i.e., the target does not need to carry any *RF* transceiver to be localized)[60, 61, 62, 63, 64, 65] and *active* (i.e., the target is an active *RF* node of the wireless network) [66] localization and tracking of targets moving throughout areas monitored with wireless technologies. Consequently, the following classification arises from the role of the user:

- *Cooperative user*. The end user actively interacts with the components of the system. The personal wireless devices such as smart-phones, *IoT* sensor or actuator, or other dedicated wearable sensors are used by the cooperative user for a direct communication with the smart home infrastructure. In such a configuration, the user is a mobile node of the network and it is recognized by the system through the identification of the associated devices. The localization and the behavior interpretation is based on the processing of data actively exchanged with the wireless network devices. Cooperative users refer to an active localization strategy;

- *Non-cooperative user*. Unlike cooperative users, no wearable devices are present and no direct communication with the system is established by the user. The user is part of the environment instead of being part of the wireless network infrastructure. Therefore, the behavior monitoring depends on the ability of the system to sense the environmental changes and, in particular, the perturbation caused by the user presence and movements. Passive

localization strategies have to be adopted in order to acquire representative parameters influenced by the human body presence.

The integration of our active and passive approaches in the same wireless hardware backbone enables the behavior estimation of both cooperative and non-cooperative users, thus enhancing the system performance in several domestic situations. The reference scenario of a smart home where our heterogeneous wireless devices coexist to cooperatively extract information on cooperative and non-cooperative users is shown in Fig. 1.2. As it can be seen, the non-cooperative target can be monitored by passive strategy while cooperative target may be localized also by active architecture (yellow links with the Wi-Fi access points in the map). Both active and passive localization systems are present, but users should not be aware of their existence. The non-invasiveness of our smart home system is guaranteed since inhabitants are not compelled to follow procedures or activate devices. As a consequence, the best way to make our system transparent is to integrate the functionalities in existing devices that user is already used to interact with. Let us consider that almost everyone has a cellphone nowadays and smart-phones with integrated Wi-Fi connectivity are becoming popular. Moreover, the number of houses without at least a personal computer and an Internet connection is rapidly reducing. Under these assumptions, our proposed active strategies can leverage the presence of a minimal wireless infrastructure for the localization of devices like smart-phones and tablets.

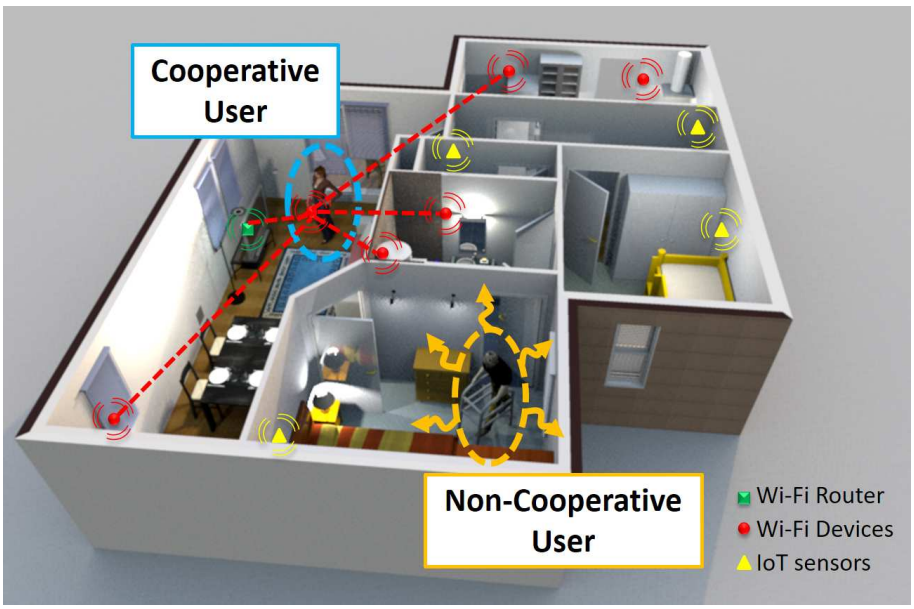

Figure 1.2: *Indoor Localization Scenario.* Cooperative and non-cooperative users localized through active and passive localization strategies.

1.3 State of the Art

In this Section, a short survey of the State of the Art in the field of wireless active and passive localization is reported.

1.3.1 Active Localization

The widespread diffusion of wireless technologies and systems in both public and private environment has stimulated the exploitation of electromagnetic (EM) waves to enable location-based services for cooperative users. In particular, one of the most applications of interest is the positioning and the tracking of mobile terminals such as users' smart-phone and tablet. the Different theoretical principles of the EM propagation have been introduced in the formulation of the localization methods, providing different performance according to the application requirements and objectives. The angle of arrival (AOA) [67], the time difference of arrival ($TDOA$) [68, 69], the ultra-wideband (UWB) frequency spectrum [70, 71], the backscattering of radio frequency identification ($RFID$) [72, 73] are examples of EM propagation features enabling the wireless localization. However, the approaches based on such principles often require expensive and complex hardware, which is not readily available in most of the application scenarios. On the contrary, the well-known received signal strength (RSS) indicator can be easily measured by commercial wireless devices without any modification. Nevertheless the relationship between RSS and distance between antennas is trivial only in the theoretical free-space propagation model. In real indoor environments, the EM propagation exhibits scattering, diffraction and reflection phenomena which are not considered by the free-space model [74, 75]. The presence of static and dynamic obstacles strongly interferes with RSS behavior in terms of expected value and high space-time fluctuations. The complexity of the wireless propagation and the instability of RSS data has been addressed in the state of the art by fingerprinting strategies, which collect a large number of RSS measurements in known positions to create a kind of look-up table between the RSS signatures and the target positions [76]. The methods based on the fingerprinting are accurate but they require extensive and expensive data collection campaigns for system training as well as frequent recalibration when small environment changes occur [77]. RSS can be also exploited by the propagation-based approach, these methods numerically compute the attenuation of the transmitted signal due to the wireless propagation in complex media using analytical models. In particular, starting from the signal attenuation, the transmitter-receiver distance is estimated according to the defined propagation rules. The position of the target is then estimated respect to the (a-priori known) positions of fixed anchors (e.g., the Wi-Fi access points). This kind of propagation-based approaches do not require time-consuming trainings nor frequent calibrations, but the localization accuracy is strongly related to the precision of the propagation model.

1.3.2 Passive Localization

In the last years, the passive wireless localization, also called device-free localization (*DFL*), has revealed strong interest in many applications related to building management, security, surveillance, healthcare monitoring, and many other fields where location-based services need the detection and localization of non-cooperative people in indoor scenarios [62][78]. The main advantage of the passive strategies is that the target needs neither to carry active devices, nor to cooperate to the localization procedure. Different technologies have been used to enable the presence and the motion detection of device-free targets, including ultrawideband (*UWB*) radar-based systems [79], computer vision [80], wireless local area network *(WLAN)*[81][82], wireless sensor networks [60][83], and cellular networks [84]. In particular, the increasing interest for contact-free and privacy-preserving target sensing has stimulated the research of methodologies for the presence detection [85], people counting [86], localization [87], motion tracking [78], behaviour monitoring [88], gesture recognition [89][90], vital signs monitoring [91][92], up to emotion detection [93] of humans in indoor spaces. However, the adopted wireless architectures have been often customized and deployed in a specific way in order to solve such complex and challenging problems, to the best of the authors' knowledge, target features like the presence, position, movement, posture have been studied individually with specific system requirements and theoretical assumptions. However, in real-world scenarios, these features are usually combined and mixed together generating the common daily-life human activities.

The basic principle of *DFL* based on electromagnetic (*EM*) propagation of radio-frequency (*RF*) wireless networks relies on the fact that the *RF* propagation is affected by the changes in the environment, including the time-varying presence and position of people acting as *EM* scatterers, especially if wireless systems operate at the microwave frequencies of the common wireless standards, such as the *IEEE802.11* (i.e., Wi-Fi) or the *IEEE802.15.4* (e.g., Bluetooth and Zigbee). Recently, another trend arised in the scientific community is focused on the opportunistic exploitation of existing wireless devices to enable the so-called ubiquitous sensing paradigm [94], with less and less impact and changes to be applied on the radio-frequency systems.

One of the main challenges related to the target detection problem is the capability to implement a low-cost, low-overhead, and robust system, which is able to estimate the information of interest without special hardware or additional sensors. In this regard, most of the aforementioned solutions provide reliable performance under relevant assumptions, which often limit the application and diffusion in real-world and large-scale scenarios. For example, sensor-based solutions are affected by environmental changes, they require frequent calibrations in time-varying conditions, and the installation procedures are expensive and time consuming. Even if the sensor-less solutions are more robust to calibration issues and sensors' faults, most of the state of the art techniques have been usu-

ally evaluated in controlled environments [95] or in small-scale test fields [96]. Concerning WSN-based systems, they often constrain the size of the detection area to guarantee a high density of wireless links and a full-coverage radio map [62].

Wi-Fi is one of the most diffused wireless technologies in both public and private areas, and its exploitation for wireless target sensing enables the disruptive proliferation of new location-based applications. The state of the art on device-free target sensing through Wi-Fi is rapidly growing and the current achievements point out the feasibility to extract the aforementioned target information from the properties of the wireless signals. Among the solutions available in the state of the art for passive wireless localization, [95] and [60] have modeled the localization problem as a machine learning problem for the real-time estimation of target positions in wireless environments, through the real-time processing of the received signal strength (RSS). More recently, [62] and [97] have formulated the target localization as a radio tomographic imaging (RTI) problem, solving the position estimation as an ill-posed inverse problem with a regularization method. Many other reference works have been proposed to solve the numerous challenges of RSS-based passive localization, introducing more and more complex algorithms for performance improvement and for multi-target localization [85][98][99], including compressive sensing [100][101], Bayesian grid [102], support vector machines (SVM) [61][103], Diffraction models [104], Kalman filters [105]. Most of such solutions present common requirements for the correct detection and localization of targets. The most relevant are (i) the high number of wireless links to collect enough information about the spatial distribution of the RSS perturbations, (ii) the need of target motion during the data acquisition to make the EM perturbation non-negligible (in particular for variance-based approaches [106]), (iii) the acquisition of large training data set with targets in known and predefined positions, and often (iv) the customization of the wireless devices adopted for RSS measurement. Even if the available solutions provide outstanding performance, the aforementioned requirements make their diffusion and real-world exploitation not so straightforward.

Chapter 2

Semantic Wireless Localization of Cooperative Users

In this Chapter, an innovative and opportunistic methodology for the localization of cooperative wireless devices in indoor scenarios is addressed.

In particular, a training-less localization approach based on a numerical propagation model of wireless transmission calibrated online also with a semantic representation of the scenario is proposed. The objectives of the proposed solution are (*i*) to improve the localization accuracy exploiting additional environment information, (*ii*) to avoid the time-consuming survey of a specific indoor site as in the case of fingerprinting approaches, (*iii*) to prevent the need of updating or calibrating the localization system (as usually required by learning-by-example solutions), and (*iv*) to reduce the computational complexity of the localization procedure to guarantee real-time performance. The parameters of the propagation model are constantly optimized by means of an evolutionary optimization technique, the proposed cost function has been formulated to consider in the calibration both the spatio-temporal changes of the indoor *EM* propagation as well as the semantic representation of the environment, which has been recast as a two-dimensional probability map. Such a probability has been estimated exploiting the available blueprint of the considered indoor area including the geometry of the walls, rooms, corridors, obstacles, and restricted areas, which determine the subset of positions where the targets can be located.

2.1 *RSS*-based *EM* Propagation Approach

One of the main challenges for accurate *RSS*-based localization is related to the scalability of the methodology due to the complex *EM* propagation in indoor environments. In fact, solutions that work well in a given test scenario (e.g., a room or floor of a specific building) might suffer from different environmental and network infrastructure characteristic in other sites (e.g., moving furniture, changing location of access points). Indeed, the presence of obstacles with various shape, size, and material causes different and complex propagation phenomena like scattering, diffraction, reflection, and absorption of the transmitted wireless signals. Moreover, the presence of moving people makes the propagation even more complex, since the human bodies are also scatterers, which introduce unpredictable perturbations of the *RSS* indicator. While passive solutions exploit such perturbations for the localization of the targets [60, 107, 108], the active ones suffer the *RSS* instability. The *RSS* fingerprinting (*FP*) has been widely adopted [76, 109, 110, 111] by active methods as a practical solution to reduce the negative effects of the *RSS* instability. However, the collection of a large set of *RSS* fingerprints in multiple positions of the considered area is required. Such samples are used to build a fingerprint database, also called *radio-map*, in which the collected *RSS* values are related with the recorded target locations. Successively, the position estimation is performed looking at the best match between the new *RSS* acquisitions and the available samples in the fingerprint database. Although satisfactory localization accuracy is obtained by *FP* methods, the site survey is complex and time-consuming, especially in large domains like museums, airports, and shopping centers. Many *FP*-based approaches aimed at reducing the size of the database or the complexity of the *radio-map* generation have been investigated. In [101], the theory of compressive sensing has been adopted to significantly reduce the number of *RSS* measurements. An autonomous *FP* mechanism based on the inertial sensors of the mobile terminals for the self-localization of fingerprints has been proposed in [109]. [112] introduced a method for database construction during target walking, in order to reduce the site survey effort. Even if such methods simplify the training phase, the *FP* still presents weaknesses in the long-term operation due to the unavoidable changes in the conditions of the environment. Accordingly, the fingerprint database requires periodical and time consuming updates and calibrations [113]. Some solutions have been investigated to automatically update the *RSS* recordings through incremental learning approaches [114, 115] but they still need an accurate initialization of the training procedure.

An alternative approach to the *FP*-based methodologies is represented by the numerical characterization of the wireless propagation. Such training-less solutions do not require the acquisition of large databases because the position estimation is based on the online comparison of the *RSS* measurement with the output of numerical propagation models. The numerical formulation of the

underlying *EM* propagation is exploited to estimate the transmitter-receiver distance as a fundamental information to localize the target [116]. In [117], the common one-slope and two-slopes log-distance path-loss models have been used, while a more accurate third-order polynomial extension has been introduced in [118]. The ray-tracing modeling has been exploited in [119] in order to consider the effects of human bodies in the proximity of the transmitter. It has to be noticed that more accurate models provide a more feasible *RSS* estimation, but the higher accuracy often requires site-specific customization as well as complex calibrations when environmental changes occur. Accordingly, the proper trade-off between the prediction accuracy and the model simplicity has to be found. Different strategies have been studiled to improve the quality of the models without increasing the complexity. A deep statistical analysis of *RSS* has been performed in [120] in order to better characterize the *RSS* indoor distribution, and in [121] a machine learning strategy for the mitigation of the non-line-of-sight (*NLOS*) indoor propagation has been proposed. However, even if the learning strategy is not site-dependent, a time-consuming training phase is still required.

The constant growth of the state of the art on indoor positioning points out that the accurate and robust localization of moving devices using common wireless technologies is still an open issue. Many research efforts are recently focused on the exploitation and fusion of different sources of information. In this regard, the new paradigm of *semantic localization* has been recently proposed [122, 123, 124, 125]. The semantic localization is referred to the estimation of target position not only from a physical point of view, but also in relation to the properties of the environment and of the objects located in the proximity of the target. Such an approach requires the prior characterization of the domain, which can be inferred from a topological map of the environment.

2.2 Mathematical Formulation

Let us consider the two-dimensional (*2D*) office area organized in corridors and offices shown in Figure 2.1. The considered domain $D = \{0 \leq x \leq X_D;\, 0 \leq y \leq Y_D\}$ is inhomogeneous and constituted by a set of objects and obstacles (e.g., furniture and walls) of different shape and size, which determine the spatial sub-domain D_O. The area under test is infrastructured with a set of P wireless APs deployed in known and fixed spatial positions $\underline{r}_p$, $p = 1, ..., P$, where $\underline{r} = (x, y)$ is the position vector. The area is occupied by a target identified by its position $\underline{r}_T$ and equipped with a mobile wireless terminal. The available APs are detected by the mobile terminal using the standard Wi-Fi scanning procedure. Figure 2.2 schematically shows different solutions for the *RSS* data collection and processing, which can be performed by a remote processing unit [Fig. 2.2(a) and Fig. 2.2(b)], receiving the *RSS* data and providing the location estimation, or by the terminal itself [Fig. 2.2(c)].

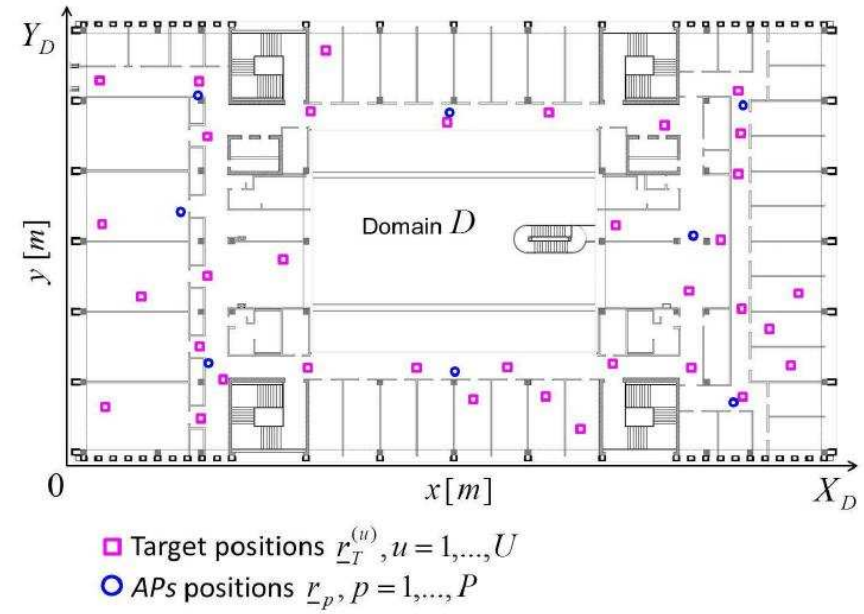

(*a*)

(*b*)

Figure 2.1: *Semantic Localization* - Indoor localization domain. Two-dimensional map of the considered indoor office area (*a*), and snapshot of the existing wireless infrastructure exploited for opportunistic localization (*b*).

Once the scan is completed, the target device in position $\underline{r}_T$ has collected the *RSS* values $\rho_i\,(\underline{r}_T, \underline{r}_i)$, $i = 1, ..., I$, $I \leq P$, where I is the subset of the transmitting *APs* located within the wireless coverage of the target. More in detail, the *remote* solution can be implemented with two different communication

modes. Since the scan procedure can be executed whether the device is connected or disconnected from the Wi-Fi network, the interconnection with the remote unit can be established through the Wi-Fi network [Fig. 2.2(a)] or exploiting other wireless architectures (e.g., *2G/3G/4G* networks) [Fig. 2.2(b)]. This last solution is particularly useful when the access to the local Wi-Fi is limited or prevented to the device at hand.

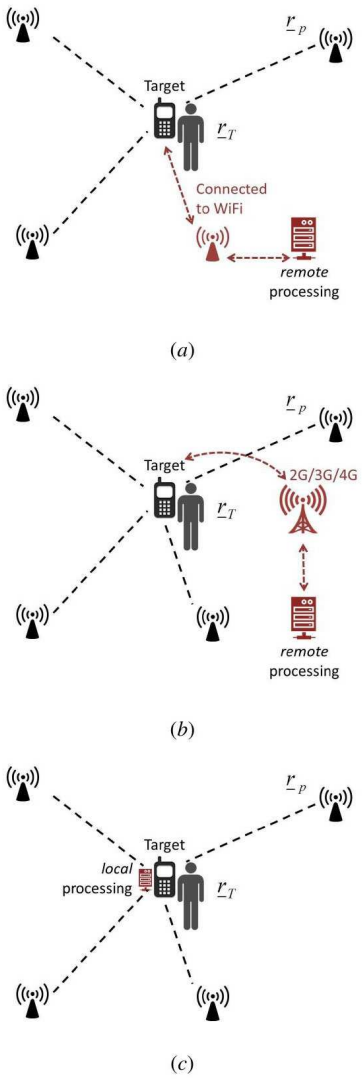

Figure 2.2: *Semantic Localization* - Wireless architectures for indoor localization. *Remote* solution with connected terminal (a), *Remote* with disconnected terminal (b), and *Local* solution with computation on the wireless terminal (c).

2.2.1 Semantic Description of the Target-Environment Interaction

Let us assume that the obstacles within D are solid and impenetrable and that the targets can move throughout the target domain $D_T = D - D_O$. In order to improve the quality of the target localization within D_T, the proposed strategy aims to extend the geometrical characteristics of D exploiting a semantic interpretation of the spatial relation between the environment and the target. Toward this end, let us partition the localization domain D into a two-dimensional lattice of $N = N_X \times N_Y$ cells, each one corresponding to a square area of sides ΔX and ΔY and centered in $\underline{r}_n$, $n = 1, ..., N$. The semantic status of each cell can be *accessible* $[g_n = g(\underline{r}_n) = 1, \underline{r}_n \in D_T]$ or *restricted* $[g_n = g(\underline{r}_n) = 0, \underline{r}_n \in D_O]$ according to the absence or presence of obstacles within the cell, respectively [Fig. 2.3(a)]. Besides the binary status, the state transition between an *accessible* and a *restricted* cell can be also considered to model how likely the target occupies the domain in proximity of obstacles. Starting from the a-priori assumption that the user behavior and movements are influenced by the presence of obstacles in the environment, a spatial probability model is defined to enrich the knowledge about the target surroundings from a context-aware perspective. Toward this end, the probability $\Gamma(\underline{r})$ that a target occupies a position within D can be fully described by means of the coefficients g_n, $n = 1, ..., N$, of the following expansion

$$\Gamma(\underline{r}) = \sum_{n=1}^{N} g_n \beta_n(\underline{r}) \tag{2.1}$$

where $\beta_n(\underline{r})$, $n = 1, ..., N$, are the basis functions chosen according to the desired probability pattern between an *accessible* and a *restricted* cell. Different transition patterns can be adopted to describe how the probability decreases when the target approaches an obstacle. As an example, to formulate a linear transition of such a probability, triangular basis functions $\beta_n(\underline{r}) = Tr_n(\underline{r}, \theta)$ centered in positions $\underline{r} = \underline{r}_n$, $n = 1, ..., N$, can be adopted, where θ is the interior angle at the base of the triangular function. Alternatively, in order to model a Gaussian probability transition, the basis function is formulated as follows

$$\beta_n(\underline{r}) = \omega_n\left(\underline{r}, \sigma_T^2\right) = \int_D \frac{1}{(2\pi\sigma_T^2)} e^{-\frac{1}{2\sigma_T^2}(\|\underline{r}-\underline{r}'\|)^2} d\underline{r}' \tag{2.2}$$

where σ_T^2 is the variance of the Gaussian distribution. Summarizing, besides the shape of the basis function, the probability function $\Gamma(\underline{r})$ is calculated in the whole domain D in order to obtain values $\Gamma(\underline{r}) = 1$ where the target is supposed to move ($\underline{r} \in D_T$), while $\Gamma(\underline{r}) = 0$ is forced in the sub-domain D_O where the target presence is unfeasible. A graphical representation of the function $\Gamma(\underline{r})$ evaluated with the two reference basis functions $\tau_n(\underline{r}, \theta)$ and $\omega_n(\underline{r}, \sigma_T^2)$ is pictorially shown in Fig. 2.3(b). Such a semantic interpretation of the solution space through the definition of the function $\Gamma(\underline{r})$ can be inferred from the

two-dimensional blueprint of the considered floor. Additional information about known obstacles introducing dedicated interactions of moving targets with their physical surroundings can be considered for the generation of a more detailed function $\Gamma(\underline{r})$.

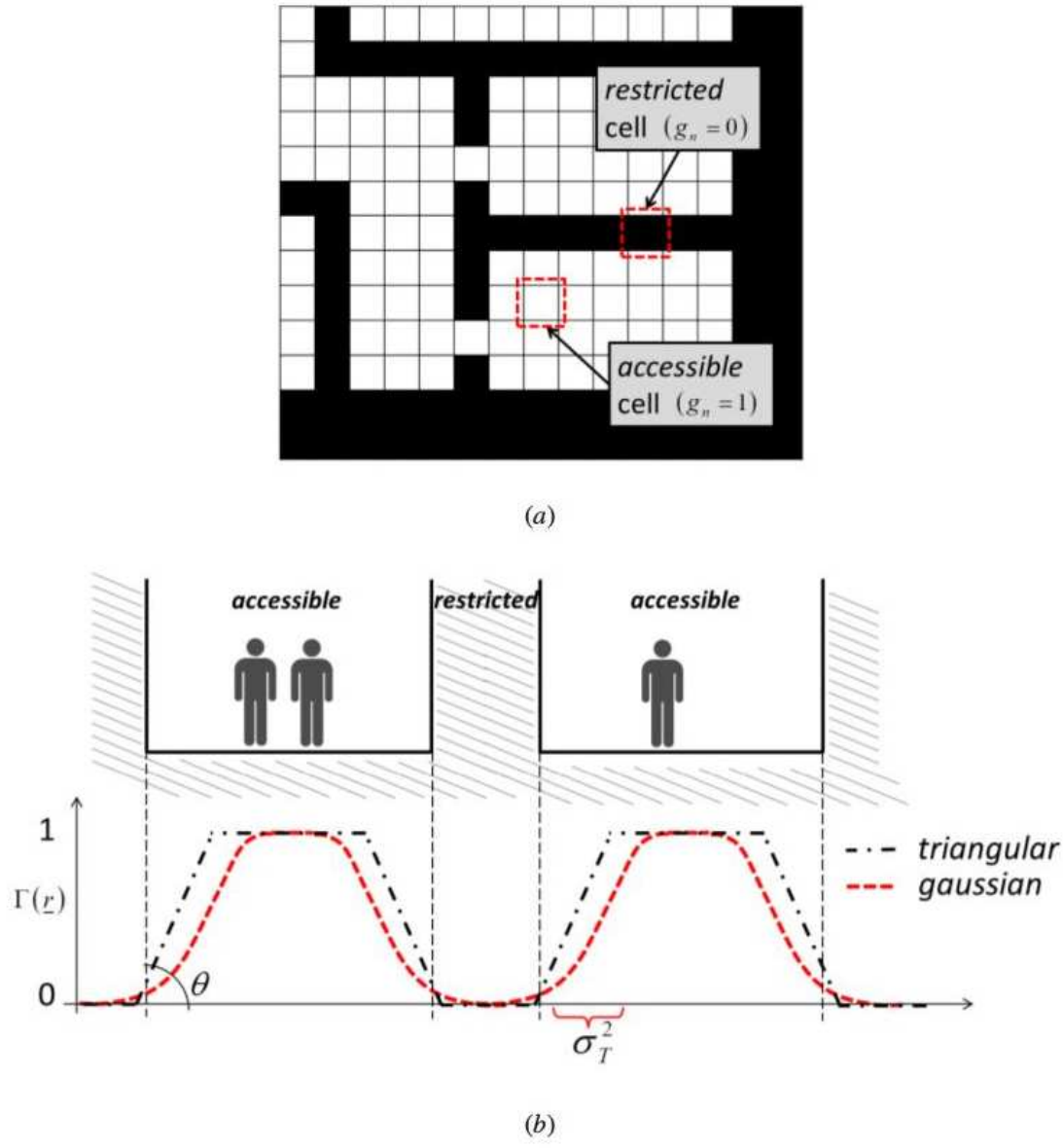

Figure 2.3: *Semantic Localization* - Example of a two dimensional lattice composed by *accessible* [$g_n = 1$, $r_n \in D_T$] and *restricted* [$g_n = 0$, $r_n \in D_O$] cells (a), and graphical representation of the probabilistic function Γ generated with triangular and Gaussian basis functions (b).

2.2.2 Real-time Wireless Localization Strategy

The acquired *RSS* data can be numerically estimated using the well-known path-loss model

$$\hat{\rho}_i\left(\underline{r}_T, \underline{r}_i\right) = \rho_i^0\left(d_0\right) - 10\alpha_i \log\left(\frac{\left\|\underline{r}_T - \underline{r}_i\right\|}{d_0}\right) - \varepsilon_{noise} \quad i = 1, ..., I \tag{2.3}$$

where $\rho_i^0\left(d_0\right)$ is the *RSS* measured at the reference distance d_0, α_i is the path-loss exponent, and ε_{noise} is the noise term modeled as a Gaussian distributed random variable with zero mean and variance σ_{noise}^2. Accordingly, the output of the propagation model can be controlled by the input parameters $\underline{\xi}_i = [\rho_i^0,\, \alpha_i,\, \underline{r}_T], i = 1, ..., I$. Taking into consideration the high spatial variability of the *EM* propagation in the indoor domain, each wireless link between the target and the set of $i = 1, ..., I$ scanned *APs* is affected by different propagation phenomena and a dedicated calibration of the corresponding numerical model is required in order to accurately predict the simulated values $\hat{\rho}_i\left(\underline{r}_T, \underline{r}_i\right)$, $i = 1, ..., I$, given a target position $\underline{r}_T$. The arising model calibration problem is recast as an optimization problem formulated as follows

$$\hat{\underline{\xi}}_{opt} = \min_{\underline{\xi}} \Phi\left\{\underline{\xi} \middle| \, \rho_i\left(\underline{r}_T, \underline{r}_i\right);\, i = 1, ..., I\right\} \tag{2.4}$$

where $\underline{\xi} = \left[\underline{\xi}_i;\, i = 1, ..., I\right]$ is the set of the input parameters describing the $i = 1, ..., I$ path-loss models, and $\hat{\underline{\xi}}_{opt} = [\hat{\rho}_i^0,\, \hat{\alpha}_i,\, \hat{\underline{r}}_T;\, i = 1, ..., I]$ is the estimated solution obtained through the minimization of the function

$$\Phi\left(\underline{\xi}\right) = \frac{1}{\Gamma\left(\underline{r}_T\right)} \times \frac{\sum_{i=1}^{I}\left[\rho_i^0\left(d_0\right) - 10\alpha_i \log\left(\frac{\left\|\underline{r}_T - \underline{r}_i\right\|}{d_0}\right) - \rho_i\left(\underline{r}_T, \underline{r}_i\right)\right]^2}{\sum_{i=1}^{I} \rho_i\left(\underline{r}_T, \underline{r}_i\right)^2}. \tag{2.5}$$

The minimization of (2.5) has been performed by means of a suitable *PSO* implementation [126] developed according to the guidelines in [127]. Starting from each of the trial parameter sets $\underline{\xi}^{(m,k)}$, ($m = 1, ..., M$, being the trial index, and $k = 1, ..., K$, the iteration index of the optimization process) defined by the *PSO*, the trial target positions $\hat{\underline{r}}_T^{(m,k)}$, $m = 1, ..., M$, $k = 1, ..., K$, represent the solutions computed during the optimization process. The iterative process continues until $k = K$ or $\Phi\left(\hat{\underline{\xi}}_{opt}\right) < \chi$, where χ is the predefined convergence threshold. Such termination criteria are fundamental when solving the localization problem directly on the wireless terminals because the maximum convergence time has to be controlled according to the application requirements. The maximum processing time can be formulated as $\tau = K\Delta\tau$, where $\Delta\tau$ is the duration of a single iteration of the *PSO*. In summary, the final solution $\hat{\underline{r}}_T^{opt}\big|_{\underline{\xi}=\hat{\underline{\xi}}_{opt}}$ belongs to the optimized parameter set that (i) minimizes the difference between the numerical and measured *RSS*, and (ii) maximizes the probability that the target is in a valid position from the semantic point of view and according to the probability function in (2.1).

2.3 Experimental Assessment

The effectiveness and the feasibility of the proposed approach have been assessed in a real test field (Fig. 2.1) through an extensive experimental validation. The size of the considered building floor, at the ELEDIA Research Center laboratories, are $X_D = 80$ $[m]$ and $Y_D = 46$ $[m]$. The *APs* of the existing Wi-Fi network are deployed in known positions $\underline{r}_p$, $p = 1, ..., P$, $P = 8$, graphically shown in Fig. 2.1(a). The existing wireless network is compliant to the standards *IEEE 802.11b/g/n* and the working frequency of the wireless links adopted for the localization purposes is $f = 2.4$ $[GHz]$. In order to guarantee the opportunistic exploitation of the available wireless infrastructures, any kind of customization has been applied to the configuration and the position of the involved hardware. Different commercial mobile devices (namely, a smartphone *Samsung Galaxy S4 mini*, hereinafter the *smartphone*, and a tablet *Sony Xperia Z*, the *tablet*) have been used by the moving target to collect the *RSS* data. A dedicated *Android*-based application has been developed to enable the acquisition, processing, transmission, and visualization of the data, as shown in Figure 2.4.

The available floor map of the domain D reported in Fig. 2.5(a) has been processed in order to compute the probability function $\Gamma(\underline{r})$. More in detail, the map has been discretized in the two-dimensional lattice of $N_X = 1435$ and $N_Y = 826$ cells of sides $\Delta X = \Delta Y = 0,56$ $[m]$, and the coefficients g_n, $n = 1, ..., N$, have been set to obtain the black-and-white representation shown in Fig. 2.5(b). The black regions ($g_n = 0$, $\underline{r}_n \in D_O$) represent the sub-domain D_O as a combination of *restricted* cells, and the white regions ($g_n = 1$, $\underline{r}_n \in D_T$) are composed by *accessible* cells. The *RSS* test set has been collected in a set of $\underline{r}_T^{(u)}$, $u = 1, ..., U$, $U = 35$ positions (Fig. 2.6) randomly chosen within the sub-domain D_T. In each position, $Z = 150$ acquisitions have been repeated to collect the *RSS* $\underline{\rho}^{(u)} = \left[\rho_i^{(z)}\left(\underline{r}_T^{(u)}, \underline{r}_i\right); i = 1, ..., I; z = 1, ..., Z\right]$ considering different target postures and orientations in order to reproduce the common variability of the target behavior in real conditions.

The localization performance has been assessed in terms of the localization error $\lambda = \left\|\underline{r}_T - \hat{\underline{r}}_T^{opt}\right\|$ computed as the Euclidean distance between the actual and the estimated target position. The first-order error statistics $\lambda_{min} = \min_u\left[\min_z\left(\lambda^{(z,u)}\right)\right]$, $\lambda_{max} = \max_u\left[\max_z\left(\lambda^{(z,u)}\right)\right]$, $\lambda = \frac{1}{U \times Z}\sum_{u=0}^{U}\sum_{z=0}^{Z}\lambda^{(z,u)}$ and the variance $var(\lambda) = \frac{1}{U \times Z}\sum_{u=1}^{U}\sum_{z=1}^{Z}\left(\lambda^{(z,u)} - \bar{\lambda}\right)^2$ have been also evaluated.

(a)

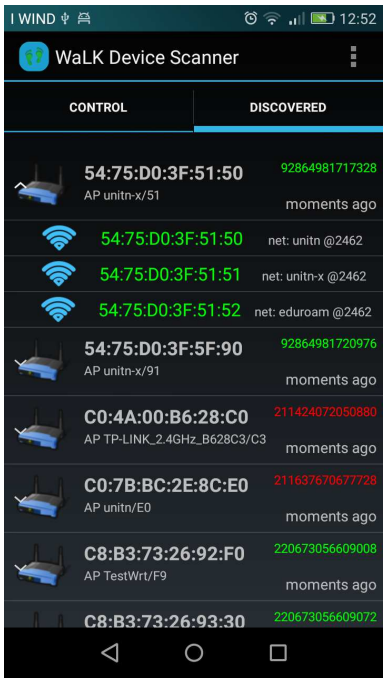

(b)

Figure 2.4: *Semantic Localization* - The software front-end of the central localization system *(a)* showing the real-time map and signal strength of wireless links measured on the connected device. *(b)* The App scanning for nearby wireless devices - links.

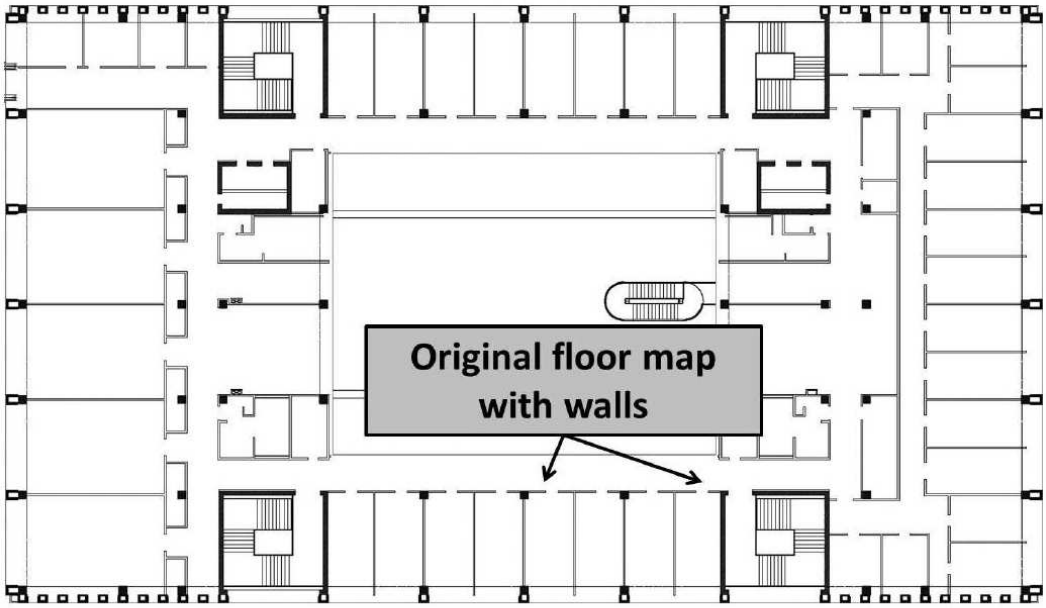

(*a*)

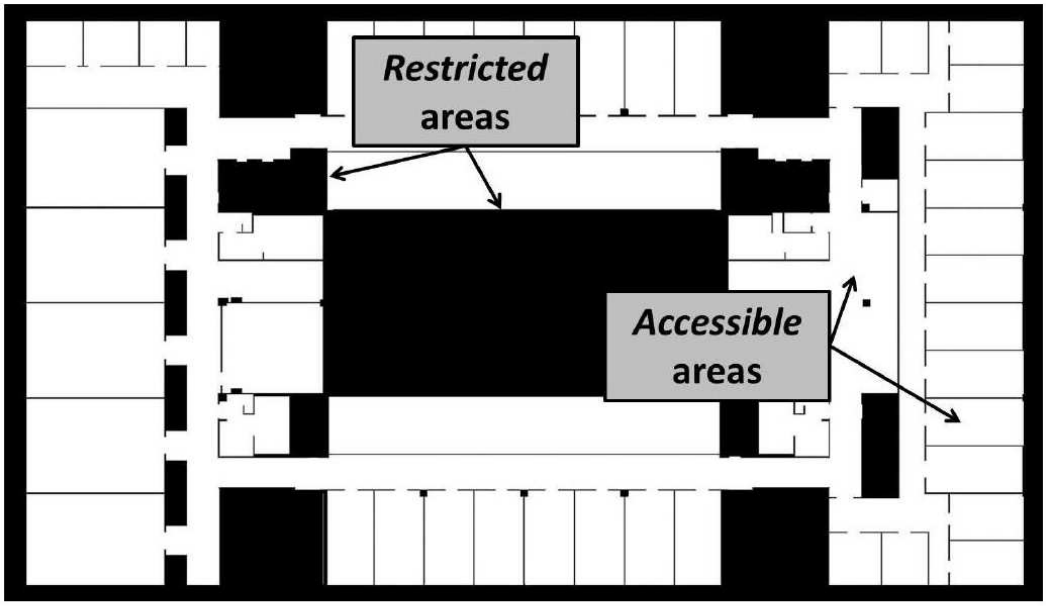

(*b*)

Figure 2.5: *Semantic Localization* - Floor map of the considered domain D (a) used for the generation of the binary representation of *accessible* (white regions) and *restricted* (black regions) areas (b).

2.3.1 Performance Analysis of the Proposed Semantic Approach

The first experiment aims at presenting the performance improvement caused by the introduction of the proposed semantic interpretation of the environment. Toward this end, the optimal configuration of the probability function $\Gamma(\underline{r})$ as well as the optimal *PSO* parameters have been adopted for the performance comparison with the standard *PSO*-based localization method (i.e., using a flat semantic function $\Gamma(\underline{r}) = 1, \forall \underline{r} \in D$). More in detail, the Gaussian basis function $\omega_n(\underline{r}, \sigma_T^2)$ has been selected, with the optimal variance $\sigma_T^2 = 0.5\ [m]$. The *PSO* adopted for this validation has been calibrated with a population formed by $M = 15$ trial solutions, and the termination criteria have been configured with threshold $\chi = 10^{-4}$ and a maximum number of iteration $K = 200$. The remaining *PSO* parameters have been set as in [126] and according to the reference literature [127]. The propagation model parameters have been optimized within the ranges $-48\ [dBm] < \rho_i^0 < -44\ [dBm]$ and $2.2 < \alpha_i < 4.8$.

The average localization error $\bar{\lambda}_u$, $u = 1, ..., U$, $U = 35$ has been evaluated in all the test positions (Fig. 2.6) applying the *standard* approach as well as the *semantic* one, results are shown in Figure 2.7. As it can be noticed, lower localization errors have been obtained introducing the semantic contribution in all the considered positions. The error statistics reported in Tab. I point out a reduction of the minimum $(1 - \left[100 \times \frac{\lambda_{min}^{(smt)}}{\lambda_{min}^{(std)}}\right] = 61.9\ [\%])$, maximum $(1 - \left[100 \times \frac{\lambda_{max}^{(smt)}}{\lambda_{max}^{(std)}}\right] = 35.1\ [\%])$, and average errors $(1 - \left[100 \times \frac{\overline{\lambda}^{(smt)}}{\overline{\lambda}^{(std)}}\right] = 20.6\ [\%])$ as well as a reduction of the error variance $(1 - \left[100 \times \frac{var(\lambda)^{(smt)}}{var(\lambda)^{(std)}}\right] = 54.7\ [\%])$, which is an important indicator of an improved stability of the localization process. The uncertainty of the estimations is strictly related to the variance of the localization error, and such an improvement given by the semantic contribution points out a higher reliability of the target localization with a mean error variance $var(\lambda)^{(smt)} = 7.94\ [m]$ (Tab. 2.1).

	Localization Error λ $[m]$			
	λ_{min} $[m]$	λ_{max} $[m]$	λ $[m]$	$var(\lambda)$ $[m]$
standard	0.21	33.82	7.84	17.56
semantic	0.08	21.95	6.22	7.94

Table 2.1: *Semantic Localization.* Error statistics of the *standard* and the *semantic* (Gaussian basis function, $\sigma_T^2 = 0.5\ [m]$) approaches.

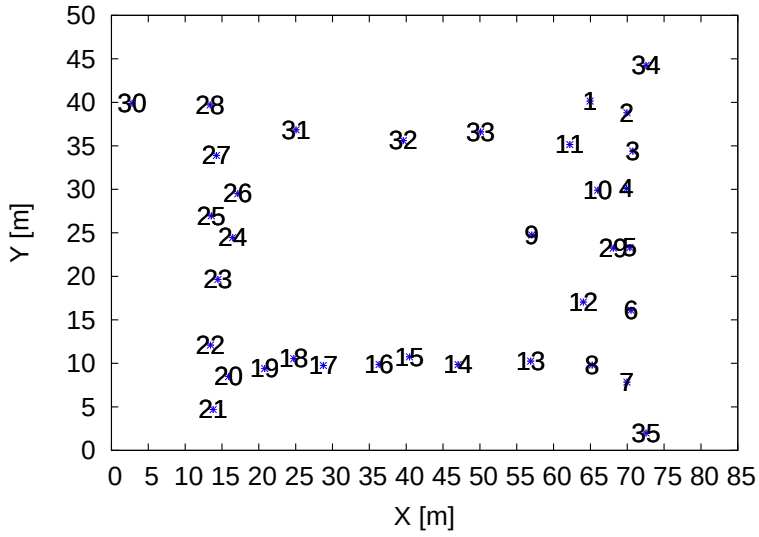

Figure 2.6: *Semantic Localization* - Floor map of the considered domain D indicating the coordinates of target tests $u = 1, ..., U$, $U = 35$.

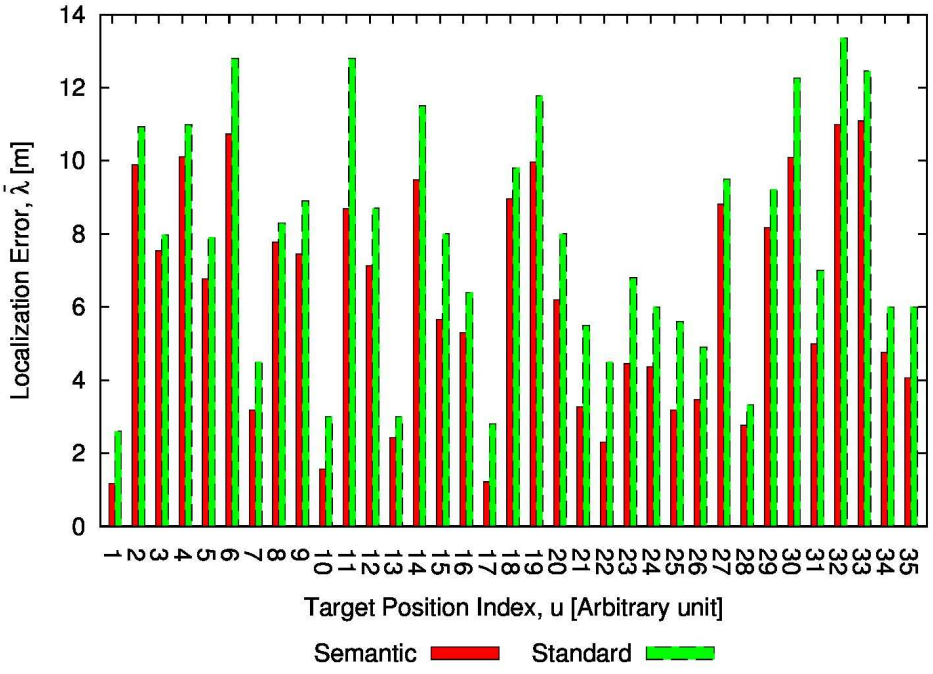

Figure 2.7: *Semantic Localization.* Average localization error $\bar{\lambda}_u$, $u = 1, ..., U$, $U = 35$, calculated with the *standard* and the *semantic* (Gaussian model, $\sigma_T^2 = 0.5$ $[m]$) approaches.

Besides the reduction of the localization error, the proposed approach improves the capability to correctly identify the room where the target is located. A common problem for location-based services in indoor sites, which are organized in multiple and adjacent corridors and rooms, is to assign the target to the proper sub-domain. As an example, two adjacent offices divided by a wall are geometrically very close but they can have very different features, such as the intended use. Figure 2.8 shows the estimated target positions of a target located in a corridor [Fig. 2.8(a)] and in an adjacent office [Fig. 2.8(b)] within the experimental test field. The results obtained with the *standard* and the *semantic* approaches are reported in order to compare the spatial distributions of the solutions. Such a comparison clearly shows the impact of the probability function introduced by the *semantic* approach. Besides the reduction of the average localization error, one of the main advantages of the semantic information is to bound the solutions in the feasible spatial sub-domains, also reducing the wrong interpretation of the target position respect to its surrounding.

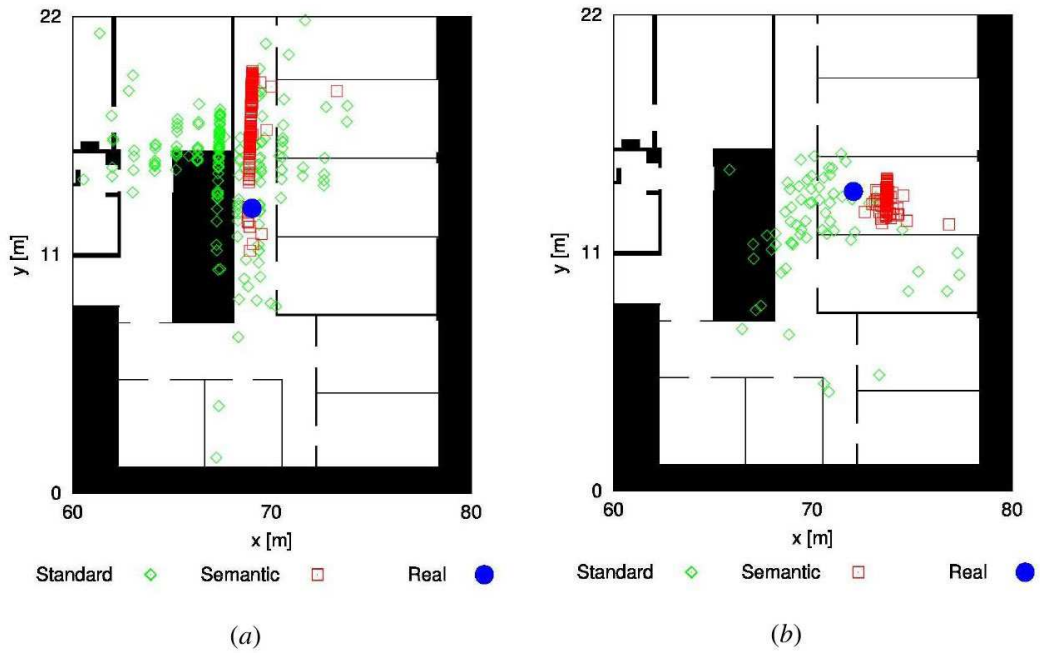

Figure 2.8: *Semantic Localization.* Target positions estimated with the *standard* and the *semantic* approaches with target in two adjacent but semantically different positions, namely on the corridor (a) and within an office (b).

2.3.2 Probabilistic Map and Optimization Parameters Calibration

In order to point out the robustness of the proposed solution using different parameters configurations, the second experiment deals with the calibration of the probabilistic function and of the input parameters of the *PSO* strategy. The impact of different semantic contributions on the localization performance has been analyzed using both the triangular and the Gaussian basis functions formulated in Sect. 2.2.1 for the generation of $\Gamma(\underline{r})$. The triangular basis function $Tr(\underline{r}, \theta)$ has been generated with different angles in the range $\theta \in [45° \div 90°]$, while the variance of the Gaussian function $\omega_n(\underline{r}, \sigma_T^2)$ has been changed in the range $\sigma_T^2 \in [0\ [m] \div 1.0\ [m]]$ in order to evaluate the effects of the different transition shapes between *accessible* and *restricted* cells. The arising localization error has been considered as the performance indicator. Figure 2.9 shows the average localization error $\overline{\lambda}$ calculated on the whole dataset of *RSS* acquisitions $Z_u = 150$, $u = 1, ..., U$, $U = 35$. As it can be observed, the error trends obtained with both the triangular [Fig. 2.9(a)] and the Gaussian [Fig. 2.9(b)] basis functions present a minimum. Although the two minimum values are quite close to each other ($\overline{\lambda}^{(tri)}\Big|_{\theta=63°} = 6.42\ [m]$ and $\overline{\lambda}^{(gau)}\Big|_{\sigma_T^2=0.5\,[m]} = 6.25\ [m]$), the Gaussian function outperforms the triangular one. Moreover, the error variability is also lower ($\Delta\overline{\lambda}^{(tri)} = 0.81\ [m]$ and $\Delta\overline{\lambda}^{(gau)} = 0.66\ [m]$, where $\Delta\overline{\lambda}^{(tri)} = \max_\theta\left(\overline{\lambda}^{(tri)} =\right) - \min_\theta\left(\overline{\lambda}^{(tri)}\right)$ and $\Delta\overline{\lambda}^{(gau)} = \max_{\sigma_T^2}\left(\overline{\lambda}^{(gau)}\right) - \min_{\sigma_T^2}\left(\overline{\lambda}^{(gau)}\right)$) pointing out a higher stability of the Gaussian profile. In order to get an insight into the effects of the considered basis functions on the optimization strategy, the minimization of the cost function in (2.5) has been analyzed. In Fig. 2.10, the evolution of the fitness function Φ_k, $k = 1, ..., K$, is reported to show the convergence of the *PSO* algorithm toward the optimal solution. To fairly compare the two configurations with the calibrated triangular ($\theta = 63°$) and the Gaussian ($\sigma_T^2 = 0.5\ [m]$) basis functions, the same representative test data set has been used. The termination criteria as well as the remaining *PSO* parameters have been set as described in Sect. 2.3.1). The Gaussian approach enables a faster ($\Phi_k^{(gau)}\Big|_{k=100} = 0.9 \times 10^{-5}$ and $\Phi_k^{(tri)}\Big|_{k=100} = 3.1 \times 10^{-3}$) and a higher ($\Phi_k^{(gau)}\Big|_{k=500} = 0.6 \times 10^{-5}$ and $\Phi_k^{(tri)}\Big|_{k=500} = 1.4 \times 10^{-3}$) convergence compared to the triangular one. The effects of the *PSO* population size on the localization error has been also verified (the Gaussian basis function has been selected for this experiment) in order to identify the minimum number of trial solutions which guarantees satisfactory performances. In fact, the reduction of the population size is fundamental in the framework of mobile applications from the computational point of view, as also

analyzed in Sect. 2.3.4. As it can be observed (Fig. 2.11), the localization error is higher for small populations, as expected, and is minimum with $M = 15$.

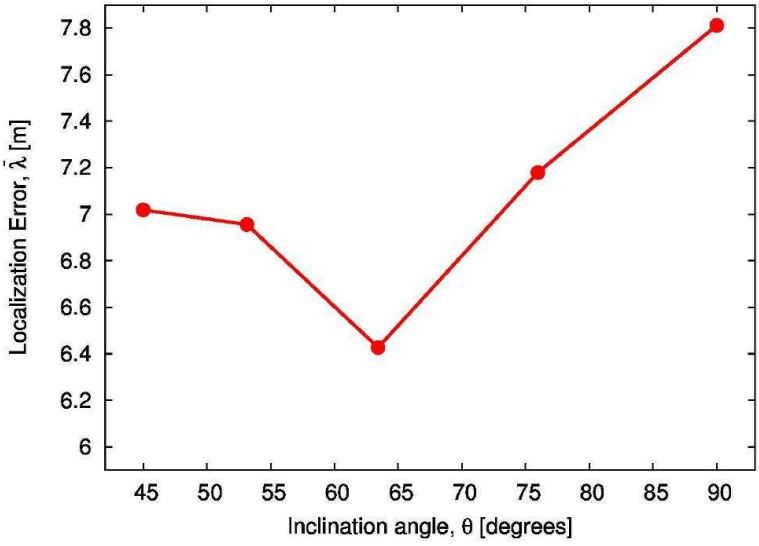

(*a*)

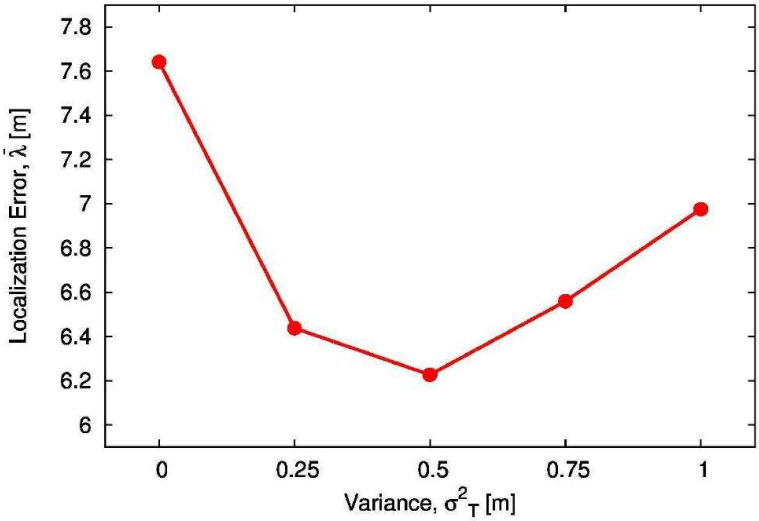

(*b*)

Figure 2.9: *Semantic Localization* - Calibration of the probabilistic function Γ. Localization error $\bar{\lambda}$ versus the angle θ of the triangular basis function (a), and versus the variance σ^2 of the Gaussian basis function (b).

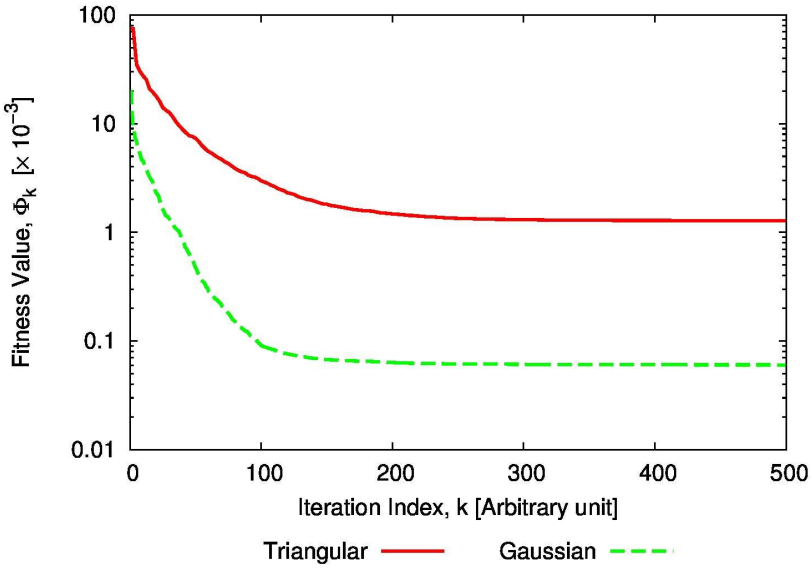

Figure 2.10: *Semantic Localization* - Fitness function. Convergence comparison using the *triangular* ($\theta = 63°$) and the *Gaussian* ($\sigma^2 = 0.5$ $[m]$) basis functions for the generation of Γ.

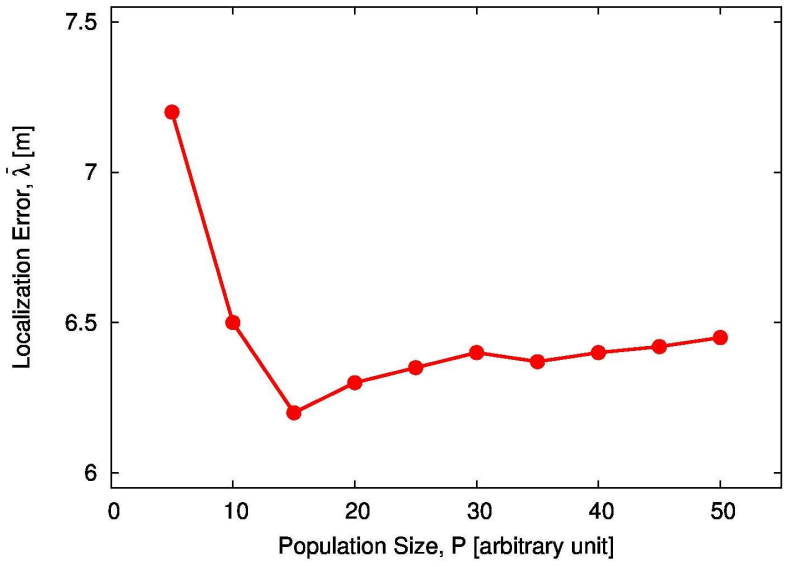

Figure 2.11: *Semantic Localization* - Localization error $\bar{\lambda}$ versus the *PSO* population size obtained with the semantic approach, *Gaussian* basis function ($\sigma_T^2 = 0.5$ $[m]$).

2.3.3 Comparison with a State of the Art Trilateration Technique

The third experiment is aimed at confirming the validity and the robustness of the proposed semantic approach over a standard localization method based on the principle of trilateration. The parameter configuration adopted in Sect. 2.3.1 and motivated in Sect. 2.3.2 has been used for this comparison. The trilateration techniques use distance measurements computed by fixed anchors to estimate the unknown spatial coordinates of the target. Such methods are usually based on linear or non-linear least square estimators. The state-of-the-art implementation here adopted is based on the Levenberg-Marquardt algorithm (*LMA*) [128] for the minimization of the quasi-likelihood function

$$\Theta\left(\underline{\hat{r}}_T\right) = \sum_{i=1}^{I}\left[\zeta_i - \widehat{\zeta}_i\right]^2 = \sum_{i=1}^{I}\left[\zeta_i - \|\underline{\hat{r}}_T - \underline{r}_i\|\right]^2 \tag{2.6}$$

where $\widehat{\zeta}_i$, $i = 1, ..., I$, are the anchors-target distances (assuming $\underline{r}_i$, $i = 1, ..., I$, the positions of the Wi-Fi *APs*, $I \geq 3$ being the number of the available fixed anchors) estimated by the trilateration approach, while $\zeta_i = \|\underline{r}_T - \underline{r}_i\|$, $i = 1, ..., I$, are the distances computed using the same path-loss propagation model formulated in (2.3). More in detail, starting from the measured *RSS*, the path-loss distance is computed as

$$\zeta_i = \frac{10^{\left[\rho_i^0(d_0) - \rho_i(\underline{r}_T, \underline{r}_i)\right]}}{10\alpha_i}, \quad i = 1, ..., I, \tag{2.7}$$

where the model parameters $\rho_i^0(d_0)$ and α_i, $i = 1, ..., I$, have been a-priori calibrated with the average values inferred from the results obtained during the experiments described in the previous Sections ($\rho_i^0(d_0) = \rho^0 = -45.4$ $[dBm]$ and $\alpha_i = \alpha = 2.4$). The localization error obtained with the trilateration method has been computed and compared with the results of the proposed semantic approach (Fig. 2.12). Such a comparison clearly shows the outperforming capabilities of the proposed optimization strategy ($1 - \left[100 \times \frac{\overline{\lambda}^{(smt)}}{\overline{\lambda}^{(lat)}}\right] = 56.8$ $[\%]$) and points out the strong limitations of range-based approaches, like the trilateration ($\overline{\lambda}^{(lat)} = 14.4$ $[m]$), in dealing with the high complexity of the indoor wireless propagation, which reflects in the high instability of the measured *RSS*.

In order to further highlight the advantages given by the adaptive calibration of the wireless propagation model minimizing the cost function in (2.5) over the predefined distance model in (2.7) used by the standard trilateration, Fig. 2.13 compares the relation between the received signal strength and the anchor-target distance. The measured *RSS* values are reported to show the actual behavior of the considered indoor wireless propagation. It has to be noticed that the proposed semantic approach adaptively calibrate the model parameters

at each data acquisition, while the trilateration approach exploits a predefined propagation models. As it can be noticed, the *RSS* trend estimated with the semantic approach is more accurate than the trilateration one, which is very sensitive to small changes of the predefined model parameters, as pointed out by the curves obtained with $\alpha = 2.0$ and $\alpha = 3.0$ (small variations of α cause high variations of the distance estimations).

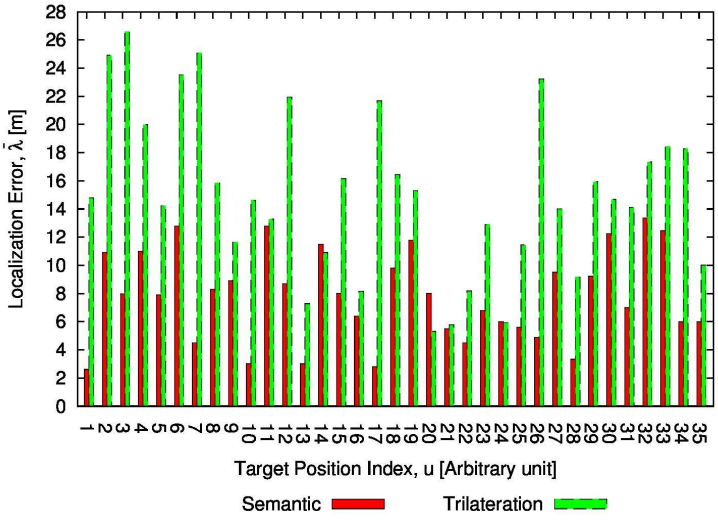

Figure 2.12: *Semantic Localization* - Comparison of the localization error $\bar{\lambda}$ between the semantic approach and a state-of-the-art trilateration method.

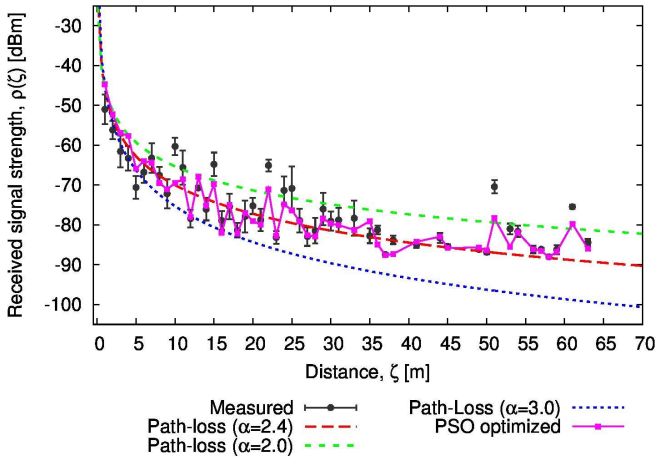

Figure 2.13: *Semantic Localization* - Path-loss models computed with the semantic approach and the trilateration method compared with the *RSS* measurements.

2.3.4 Computational Performance Analysis on Different Platforms

The last experiment is aimed to assess the computational performance of the proposed method tested with the *remote* and the *local* architectural solutions (Fig. 2.2). Toward this end, three different typologies of processing platforms have been compared, namely the *server* (a quad-core desktop PC with $8\,GB$ of RAM) adopted for the *remote* architecture, while the *smartphone* and the *tablet* for the *local* solution. As far as the localization accuracy is concerned, the target positions $\underline{r}_T^{(u)}$, $u = 1, ..., U$, $U = 35$, have been estimated using the three hardware platforms. The results of the comparison (Fig. 2.14) point out that the same localization error has been obtained, regardless the platform typology. Such results have been computed using the proposed PSO-based strategy initialized with the parameters $\chi = 10^{-4}$, $K = 500$, and $M = 15$. The computational time of the optimization procedure has been analyzed taking into consideration the computational resources of the *smartphone* and *tablet* terminals in order to evaluate the feasibility of the *local* architecture. Fig. 2.15 presents the computational time [Fig. 2.15(a)] and the localization error [Fig. 2.15(b)] versus the iteration number k. Such an analysis points out the relation between the computational time and the localization performance, enabling the identification of the best trade-off according to the application requirements.

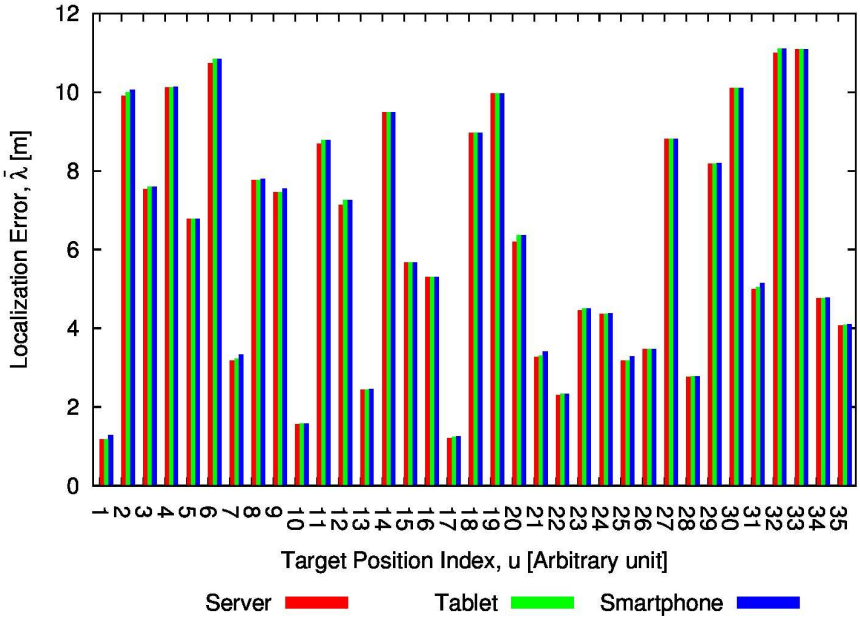

Figure 2.14: *Semantic Localization* - Average localization error $\bar{\lambda}$ obtained with the *server*, *smartphone*, and *tablet* platforms in the considered target position $u = 1, ..., U$, $U = 35$.

The obtained results suggest that the maximum number of iterations can be set to $K = 200$, as also confirmed by the analysis reported in Tab. 2.2 about the variations of the average localization error $\bar{\lambda}$ and the processing time τ versus the number of *PSO* iterations. With reference to the *smartphone* platform, the localization performance are stable when $K \geq 200$, corresponding to a processing time $\tau|_{K=200} = 2.02$ $[s]$.

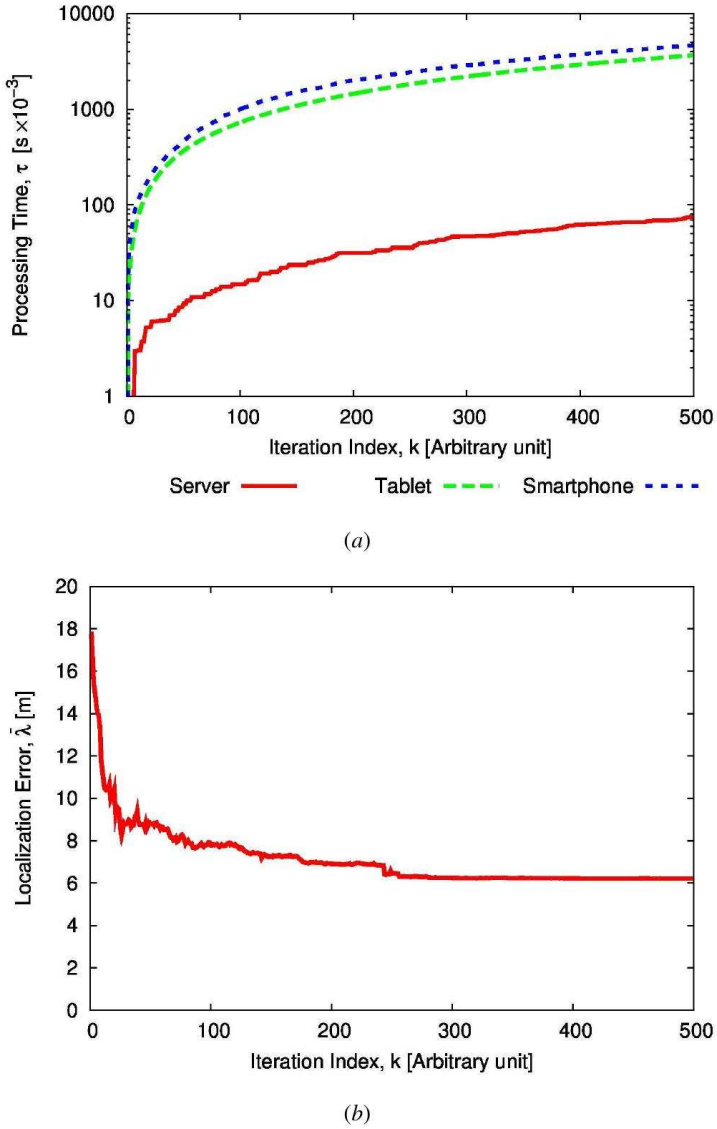

Figure 2.15: *Semantic Localization* - Computational performance analysis. Computational time τ (a) and localization error $\bar{\lambda}$ (b) versus the iteration number.

	$K = 100$	$K = 200$	$K = 300$	$K = 400$	$K = 500$
Average error λ $[m]$	7.92	6.81	6.32	6.19	6.02
Processing time τ $[s]$					
server	0.02	0.04	0.05	0.06	0.07
tablet	0.70	1.21	1.81	2.91	3.81
smartphone	1.01	2.02	2.80	3.55	4.75

Table 2.2: *Semantic Localization* - Processing time τ and average localization error $\bar{\lambda}$ versus the maximum iteration numbers K.

2.4 Conclusions

In this Chapter, an innovative semantic strategy for the indoor localization of wireless terminals has been proposed. The challenging indoor localization problem has been solved exploiting the available geometrical information about the considered scenario. The features of the objects like the walls and the fixed furniture (extracted from the topological map of the building floor) have been used to introduce a semantic interpretation of the target-environment relation. The probability that a target occupies a position has been modeled in a probabilistic map of the indoor domain. Such a semantic information together with the *RSS* data measured by the wireless device has been exploited to calibrate in real-time the parameters of a simple path-loss propagation model. Toward this end, a training-less optimization procedure has been formulated in order to avoid the complex and time-consuming site survey usually required by the widely adopted fingerprinting methods.

The effectiveness of the proposed approach has been assessed dealing with the localization of Wi-Fi-enabled smartphones and tablets in a real indoor scenario. The obtained experimental results have shown that:

- the proposed semantic interpretation of the environment improves the localization performance with a reduction of the localization error higher than 20 [%];
- the Gaussian profile with variance $\sigma_T^2 = 0.5$ $[m]$ is suitable to model the semantic spatial relation between the positions of the moving targets and the obstacles in the environment;
- the use of a training-less procedure allows the adaptive and real-time calibration of the indoor propagation model in order to take in consideration the time-varying propagation phenomena;
- the proposed localization approach outperforms the standard trilateration method with a percentage reduction of the average localization error higher than 58 [%];

- the proposed *PSO*-based optimization strategy is executed by the mobile platforms with a computational time compliant with the common requirements of the indoor location-based applications ($\tau \simeq 2$ $[s]$);
- the localization performance are stable regardless the considered hardware platforms (i.e., *server*, *smartphone*, and *tablet*) where the proposed method is executed.

Chapter 3

Opportunistic Localization of Device-free Passive Targets

In this Chapter, innovative methodologies for the opportunistic monitoring of transceiver-free targets by using existing wireless infrastructures is addressed.

The main goal of the proposed works is to opportunistically exploit wireless link established between two commercial wireless devices (e.g., an access point and a client) for the real-time monitoring of humans in the considered domain. As opposed to many device-free localization techniques, the adopted configuration is designed to minimize the system complexity and to avoid any kind of hardware customization as required in most of real-world applications. In particular, Received Signal Strength (*RSS*) indicator and Channel State Information (*CSI*) of commodity Wi-Fi devices are exploited for *(i)* human presence detection, *(ii)* localization and *(iii)* posture recognition. A selected set of experiments carried out in a real indoor test site are presented in order to assess the current advantages and limitations of the proposed methodologies.

3.1 *RSS*-based Presence Detection

This Section addresses the challenge of detecting non-cooperative device-free targets through the opportunistic exploitation of the simplest wireless architecture that can be installed in whichever indoor wireless scenario. Commodity Wi-Fi access points have been used in [81][86][95] as an existing hardware backbone, which can be opportunistically used as target detector to enable a set of applications, such as intrusion detection, border protection, surveillance, and healthcare services. Good detection capabilities have been obtained, but it has to be noticed that the considered experiments always consider multiple wireless links. The common assumption is that the environment is noisy and that many false detections can be generated if the systems are based on a single link. As an example, in [81] a refinement module generates a global anomaly score by summing the individual anomalies computed for each stream. In [86], the system *Nuzzer* has been tested in large-scale typical environments, without special hardware and using six raw data streams. *Nuzzer* aims to track multiple entities and applies fingerprinting in order to reach satisfactory performance. The authors declare that the main limitation of *Nuzzer* is the substantial calibration effort related to the construction of the passive radio map, however this is necessary when fingerprinting strategies are adopted. The proposed work aims at improving the robustness of the detection methodology in order to further reduce the number of the required wireless links without affecting the detection performance and avoiding time-consuming fingerprinting. The main goal is to enable a reliable target detection even using a single wireless link, which is the simplest building-block of any wireless architecture and can be easily replicated propagating the detection performance regardless of the number of wireless devices and links.

Toward this end, let us suppose to exploit the *RSS* of a single wireless link between a transmitter and a receiver. Representative and real-world examples are the home wireless networks typically composed by a single access point (AP) with a wireless device (e.g., a desktop computer) connected, or a wireless bridge for internet connectivity between two areas located in different positions of a historical building. In such daily-life scenarios the deployment of dense wireless networks composed by many *APs* is unfeasible, but different location-based services may be of interest for the end-users. In this conditions, the main assumption is that any kind of modification can be applied to the existing devices and the available *RSS* readings have to be exploited in a transparent and simple way. The proposed method is aimed at maximizing the reliability of the passive target detection applying a customized algorithm based on the analysis of the *RSS* time series in the frequency domain. More in detail, in order to enhance the effects of the target presence on the *RSS* data stream, an empirical mode decomposition (EMD) has been applied for the denoising of the raw input series. Successively, the denoised sequences have been transformed in the frequency domain by means of a discrete Fourier transform (DFT) for the extraction and

filtering of the *DFT* coefficients. Finally, the small set of denoised and filtered coefficients have been used as features for the training of a learning by examples (*LBE*) method based on a *SVM* binary classifier. The output of the *SVM*-based detector is the probability that a target occupies the area in proximity of the wireless link. The proposed method has been experimentally validated in a real indoor test site using a single *IEEE802.11* wireless link operating at the 2.4 [GHz] Industrial-Scientific-Medical (*ISM*) frequency band. A selected set of experiments have been reported and discussed in order to point out the performance in terms of failure rate and to estimate the spatial coverage of the indoor detection respect to the length of the wireless link.

3.1.1 Rationale of the Detection Procedure

The building blocks of the proposed detection methodology are schematically represented in Fig. 3.1 and summarized in the following:

- ***RSS denoising***. The first step is aimed at removing from the *RSS* time series the noise components due to the environment and to the hardware non-idealities using the *EMD* technique. Since any kind of customization has been applied to the involved hardware, a dedicated denoising strategy is required for the robust analysis of the noisy information acquired by commercial platforms. The *EMD* is a non-parametric data-driven analysis tool proposed by N. E. Huang [129] for the time-domain decomposition of non-linear and non-stationary signals. As opposed to other well-known decomposition methods (e.g., wavelet), *EMD* does not require a set of basis functions to analyze the input signal, reducing the overall complexity of the algorithm. *EMD* has been widely used for the suppression of acoustic distortions in noisy speech signals, where different indices of non-stationarity exist due to the high variability of the environmental noise [130]. Such properties are here exploited for the enhancement of the target signature in the *RSS* data. The details of the denoising procedure are given in Sect. 3.1.2.1.

- ***Feature extraction and selection***. Analyzing the spectral characteristics of the signal provides a different representation of the *RSS* non-stationarity. Most of the literature processes the *RSS* data in the time domain [107]-[132], and less attention has been given to the analysis of the target effects on the *RSS* in the frequency domain. The goal of such an approach is to identify the frequency contributions of interest in terms of Fourier coefficients. Toward this end, the frequency domain representation of the denoised data is obtained by applying the *DFT*. The distance between two transformed *RSS* sequences, one in absence and one in presence of targets, is computed and the most relevant differential *DFT* coefficients

are selected to further isolate the signal components related to the target absence/presence. The feature extraction procedure and the successive selection through the coefficients band-pass filtering are detailed in Sect. 3.1.2.2.

- ***Training phase***. The automatic learning of the unknown relation between the filtered *DFT* coefficients and the target absence/presence is addressed offline by means of a customized *SVM*-based classifier. A set of *RSS* data streams are acquired in known conditions, both in absence and in presence of humans inside the monitored domain. The distance between the two *RSS* streams transformed in the frequency domain and the statistics (i.e., the mean and the variance) of the *DFT* coefficients are the features of the *SVM* training set. The definition of the training procedure and the generation of the decision function are described in Sect. 3.1.2.3.

- ***Target detection phase***. Once the learning process is completed, the online detection is performed on unforeseen *RSS* data streams. The *SVM*-based detector classifies in real-time the test data with labels "target absence" or "target presence" and estimates the class probability, as well. The *SVM* test phase and the formulation of the detection probability are presented in Sect. 3.1.2.3.

3.1.2 Mathematical Formulation

Let us consider a single wireless link in the domain Ω between the transmitter and the receiver located in the known positions $\underline{r}_{TX}$ and $\underline{r}_{RX}$, respectively, $\underline{r} = (x_\Omega, y_\Omega, z_\Omega)$ being the position vector. Heterogeneous obstacles like furniture and walls occupy the domain, as well as a variable number of $p = 1, ..., P$ human targets. Let $\mathbf{S}(t) = \{s(t - k\Delta t)\,;\, k = 0, ..., K-1\}$ denote the *RSS* vector available at the receiver at the time instant t and composed of K readings stored with a constant sampling rate Δt. The *RSS* time series is analyzed by applying a sliding time window $\underline{\omega}(t) = [s(t - U\Delta t + u\Delta t)\,;\, u = 0, ..., U-1]$ of length $U \leq K$ and ending at the time instant t.

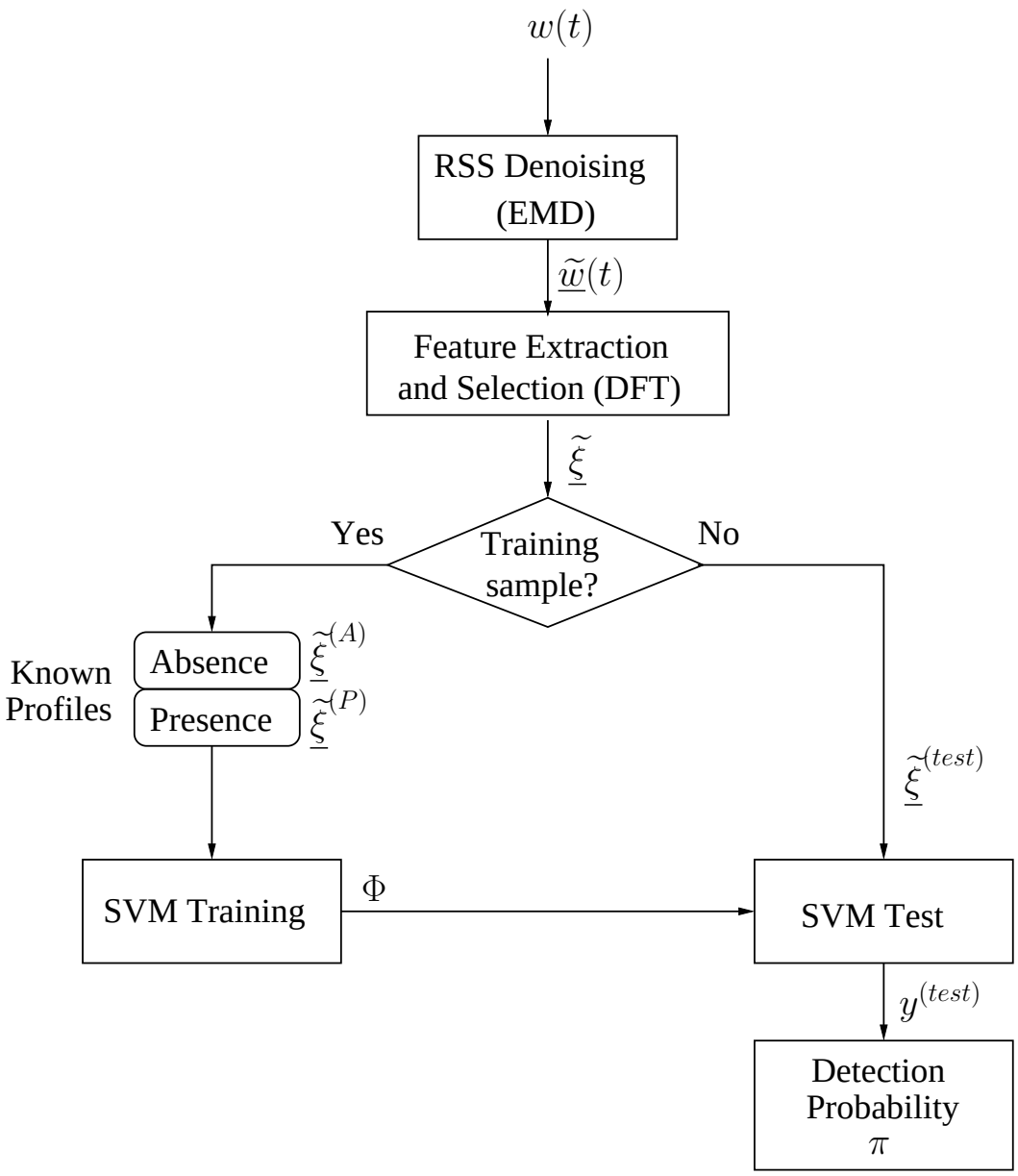

Figure 3.1: *RSS Presence Detection.* Block scheme of the passive wireless detection approach.

3.1.2.1 Empirical Mode Decomposition for RSS Denoising

The *RSS* stream is decomposed in a finite number of intrinsic mode functions (*IMFs*), which represent the oscillatory modes embedded in the signal, adopting the so-called *sifting* process [129] summarized in the following main steps:

1. identify the local maxima and minima of the considered time-windowed data $\underline{\omega}(t)$;

2. evaluate the upper and lower envelopes by interpolating the local maxima and minima identified at step 1;

3. estimate the local trend as the average between the upper and lower envelopes;

4. calculate the difference between the original signal and the local trend. The difference is the first *IMF* if (i) the number of extrema and the number of zero-crossing differs by one, and (ii) it is zero-mean. If such conditions are not satisfied, iterate steps 1-4 on the calculated difference;

5. once the highest frequency (i.e., the first *IMF*) is extracted from the signal, the same procedure is applied on the residue to identify the next highest frequency. Finally, the original signal is decomposed as follows

$$\underline{\omega}(t) = \sum_{i=1}^{I} \underline{c}_i(t) + \underline{\vartheta}(t) \tag{3.1}$$

   where $\underline{c}_i(t)$, $i = 1, ..., I$, are the *IMFs* and $\underline{\vartheta}(t)$ is the final negligible residual. The *IMFs* are narrowband components with decreasing frequency [the first *IMF* $\underline{c}_i(t)$, $i = 1$, is composed of faster oscillations than the second $(i = 2)$, which in its turn has faster fluctuations than the third $(i = 3)$, and so on].

The reconstruction of the denoised signal is obtained combining only a subset of *IMFs* in order to remove the undesired frequency components. The proper selection of the significant *IMFs* is performed considering the Hurst exponent $H \in]0 \div 1[$, which is a measure of long-term memory of a time series [133]. Higher values indicate a persistent behavior of the time series and long-term autocorrelation, while lower values refer to fast changes between adjacent pairs of the series (i.e., lower autocorrelation). According to this rule, high Hurst exponents are more related to the signal components while lower values are representative of the noise. The reconstructed time window obtained with the selected *IMFs* is

$$\underline{\tilde{\omega}}(t) = \sum_{g=1}^{G} \underline{\varsigma}_g(t) \tag{3.2}$$

where $\underline{\varsigma}_g(t)$, $g = 1, ..., G$, $G \leq I$, are the *IMFs* selected according to the following rule

$$\underline{\varsigma}_g(t) = \begin{cases} \underline{c}_i(t) & if\ \mathcal{H}(\underline{c}_i(t)) \geq H_{th} \\ 0 & if\ \mathcal{H}(\underline{c}_i(t)) < H_{th} \end{cases} \quad g = 1, ..., G \tag{3.3}$$

$\mathcal{H}(\cdot)$ being the function devoted to the computation of the Hurst exponent, and $H_{th} \in]0 \div 1[$ a user-defined threshold.

3.1.2.2 RSS Features Extraction in the Frequency Domain

The Euclidean distance between two *RSS* time series acquired in absence and in presence of targets has been adopted as similarity measure in order to analyze the effects on the *RSS* stream caused by the target presence. In particular, the distance has been formulated as

$$\delta\left(\underline{\tilde{\omega}}^{(A)}(t), \underline{\tilde{\omega}}^{(P)}(t)\right) = \sqrt{\sum_{u=0}^{U-1}\left(\tilde{\omega}_u^{(A)}(t) - \tilde{\omega}_u^{(P)}(t)\right)^2} \tag{3.4}$$

where $\underline{\tilde{\omega}}^{(A)}(t)$ and $\underline{\tilde{\omega}}^{(P)}(t)$ are the denoised time windows acquired in absence and in presence of targets, respectively. In order to extract few and representative features of such difference, the time sequences are mapped in the frequency domain to isolate the frequencies of interest for the detection problem at hand. The *DFT* provides a mathematical tool to represent the denoised time window $\underline{\tilde{\omega}}(t)$ into periodic Fourier series. The sequence of coefficients $\underline{\xi} = [\xi_f;\ f = 0, ..., U-1]$ is given by

$$\xi_f = \frac{1}{U}\sum_{u=0}^{U-1} \underline{\tilde{\omega}}_u(t)\ e^{-\frac{j2\pi f u}{U}} \quad f = 0, ..., U-1 \tag{3.5}$$

where $j = \sqrt{-1}$ is the imaginary unit, and ξ_f, $f = 1, ..., U-1$, are complex numbers (ξ_0 is real since the input signal $\underline{\tilde{\omega}}(t)$ is real). According to the Parseval theorem [134], the energy of the signal in the time domain is the same as the energy in the frequency domain as follows

$$\sum_{u=0}^{U-1}\left|\tilde{\omega}_u^{(A)}(t)\right|^2 = \sum_{f=0}^{U-1}|\xi_f|^2 \tag{3.6}$$

and this implies that the Euclidean distance between two sequences in the time domain is the same as their distance in the frequency domain, formulated as [135]

$$\hat{\delta}\left(\underline{\xi}^{(A)}, \underline{\xi}^{(P)}\right) = \sqrt{\sum_{f=0}^{U-1}\left(\xi_f^{(A)} - \xi_f^{(P)}\right)^2} \tag{3.7}$$

where $\underline{\xi}^{(A)}$ and $\underline{\xi}^{(P)}$ are the *DFT* coefficients computed in absence and in presence of targets, respectively.

In order to further enhance the effects of the target presence on the Euclidean distance computed in the frequency domain, a band-pass filtering procedure is applied to the *DFT* coefficients. The bandwidth of the filter is calibrated to discard the frequency contributions not affected by the target absence/presence. The Euclidean distance computed with the filtered coefficients is formulated as

$$\Delta\left(\underline{\tilde{\xi}}^{(A)}, \underline{\tilde{\xi}}^{(P)}\right) = \sqrt{\sum_{f=f_{min}}^{f_{max}} \left(\xi_f^{(A)} - \xi_f^{(P)}\right)^2} \tag{3.8}$$

where $\underline{\tilde{\xi}}^{(A)} \subset \underline{\xi}^{(A)}$ and $\underline{\tilde{\xi}}^{(P)} \subset \underline{\xi}^{(P)}$ are the subset of filtered *DFT* coefficients, and f_{min} and f_{max} are the corresponding lower and upper coefficients indexes, respectively. The number of filtered *DFT* coefficients is $F = f_{max} - f_{min}$.

3.1.2.3 SVM-based Target Detector

The automatic estimation of the target absence/presence from the *RSS* data stream is based on a *SVM*-based classifier trained with a finite set of $m = 1, ..., M$ known input-output samples $\{\underline{x}_m, y_m;\ m = 1, ..., M\}$, where $\underline{x}_m$ is the m-th vector of input features, and $y_m \in \{-1, +1\}$ indicates the target absence (i.e., $y_m = -1$) and presence (i.e., $y_m = +1$). More in details, the input vectors include the Euclidean distance Δ_m, $m = 1, ..., M$, (defined in Sect. 3.1.2.2) calculated between a reference configuration in absence of targets (the corresponding *DFT* coefficients are $\underline{\tilde{\xi}}_m^{(A)}$) and a training configuration $\underline{\tilde{\xi}}_m^{(train)}$, $m = 1, ..., M$, which includes both the absence of targets (for the training samples $m = 1, ..., M/2$) and the presence of targets (for the remaining samples $m = M/2 + 1, ..., M$). Moreover, in order to also consider the trend of the *DFT* coefficients during the learning process, the input vector includes the statistical indicators of the coefficients, as follows

$$\underline{x}_m = \left[\Delta_m, \overline{\xi}_m^{(A)}, var\left(\underline{\xi}_m^{(A)}\right), \overline{\xi}_m^{(train)}, var\left(\underline{\xi}_m^{(train)}\right)\right];\ m = 1, ..., M \tag{3.9}$$

where $\overline{\xi}$ and $var\left(\underline{\xi}\right)$ are the mean and the variance of the considered *DFT* coefficients.

A linear *SVM*-based learning method is devoted to separate the training data set with the function

$$y = sign\left[w^T \varphi\left(\underline{x}\right) + w_0\right] \tag{3.10}$$

where $sign\left(\cdot\right)$ is the binary sign function, w and w_0 are weight parameters computed during the training phase [136], and $\varphi\left(\cdot\right)$ is the linear function mapping the data from the input space to the feature space. However, since the *RSS* data

acquired in the two absence/presence status are not linearly separable, a non-linear radial basis function (RBF) has been adopted for the features mapping

$$k\left(\underline{x},\underline{x}_m\right)=\varphi\left(\underline{x}\right)^T\cdot\varphi\left(\underline{x}_m\right)=e^{-\gamma\|\underline{x}-\underline{x}_m\|^2} \tag{3.11}$$

where $\gamma>0$ is the RBF parameter learned during the training phase. The learning process requires the solution of the following optimization problem

$$\min_{(w,w_0,\epsilon)}\left[\frac{1}{2}w^Tw+C\sum_{m=1}^{M}\epsilon_m\right] \tag{3.12}$$

subject to

$$y_m\left(w^T\varphi\left(\underline{x}_m\right)+w_0\right)\geq 1-\epsilon_m;\;\; m=1,...,M \tag{3.13}$$

where C is the penalty parameter of the error terms ϵ_m, $m=1,...,M$, calibrated to control the trade-off between the model complexity and the training error [137]. The optimization problem can be solved with its Lagrangian dual and the Karush-Kuhn-Tucker conditions [138].

Once the training phase is done and the model parameters are estimated, the SVM prediction computed during the online test phase is given by

$$y^{(test)}=sign\left[\Phi\left(\underline{x}\right)\right]=sign\left[\sum_{m=1}^{M}\lambda_m y_m k\left(\underline{x},\underline{x}_m\right)+w_0\right] \tag{3.14}$$

λ_m, $m=1,...,M$ being the Lagrange multipliers and $\Phi\left(\cdot\right)$ the decision function. Moreover, instead of only predicting the binary labels of the test data, the proposed approach approximates the a-posterior class probability

$$\Pi=Pr\left(y^{(test)}=1\middle|\,\underline{x}\right)=\frac{1}{1+\exp\left(\alpha\Phi\left(\underline{x}\right)+\beta\right)} \tag{3.15}$$

where α and β are the parameters of the Sigmoid function estimated according to the Platt algorithm [139]. Besides the estimation of the target absence/presence, such a probability represents an additional information about the confidence level of the detection estimation.

3.1.3 Experimental Validation

The effectiveness and the robustness of the proposed detection method are assessed in the following by considering a set of experimental configurations in a real indoor scenario. The test field is within the laboratories of the ELEDIA Research Center at the University of Trento (*ELEDIA@UniTN*).

The whole building floor covers an area of $X_\Omega=80$ $[m]$, $Y_\Omega=46$ $[m]$, and $Z_\Omega=2.8$ $[m]$ organized in offices and laboratories, with different and heterogeneous obstacles such as furniture and lab equipment [Fig. 3.2(a)]. A single

wireless link between two *IEEE802.11b/g* Wi-Fi access points has been considered. The *APs* belong to the existing Wi-Fi network, they are installed at the ceiling level and configured to operate at the working frequency $\phi = 2.4\ [GHz]$ with transmitting power $P_{TX} = 18\ [dBm]$.

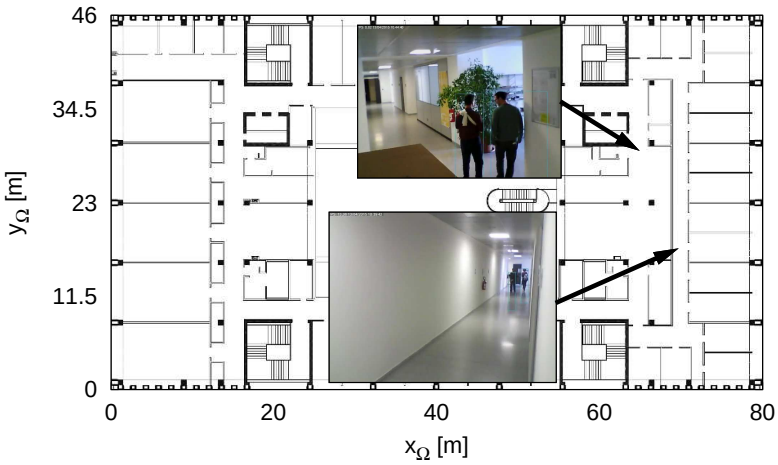

(*a*)

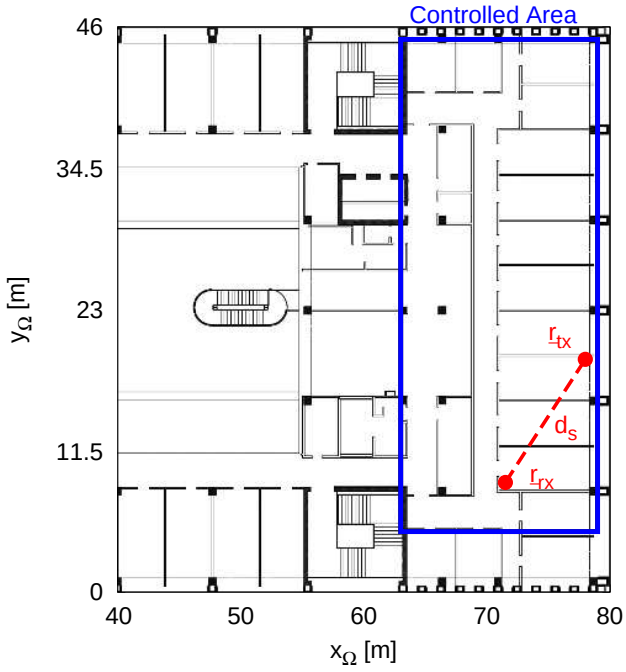

(*b*)

Figure 3.2: *RSS Presence Detection* - Indoor test site for experimental validation. (*a*) Blueprint of the building floor with snapshots of ground truth acquisition, (*b*) test area with the wireless link of *Experiment 1*, $d_S = 11.9\ [m]$.

The proposed system stores the *RSS* readings in the vector $\mathbf{S}(t)$ with a constant sampling rate $\Delta t = 0.6$ $[sec]$ [1]. The *APs* have been chosen in order to center the wireless link respect to the area monitored by the video-surveillance system, which has been deployed for the acquisition of the actual target presence. Figure 3.2(a) shows two sample snapshots of the camera views, while Fig. 3.2(b) the boundary of the area controlled by the surveillance system. A set of 2 surveillance cameras has been used to obtain the occupancy ground truth. The occupancy information (i.e., the number of occupants inside the detection area and their position) has been inferred from the video recordings and used for the manual labeling of the dataset.

Let us define the status of "target presence" when $P \geq 1$ humans occupy such sub-domain of the considered test site. The focus of this work is to estimate the binary status of target presence and target absence, while the impact of the number of humans on the detection probability will be investigated in future studies.

The detection performance of the proposed strategy has been evaluated in terms of false positive rate ρ_{FP} [%] , which refers to the wrong detections generated in absence of targets, false negative rate ρ_{FN} [%] pointing out how much the method fails to detect the target presence, and finally of failure rate ρ [%], which is the total error rate considering both false positives and false negatives. More in detail, the performance metrics have been formulated as follows

$$\rho_{FP} = \frac{100}{K-U} \sum_{q=1}^{K-U} \left(\chi_q^{(+)} \Big|_{y_q^{(test)}=-1} \right) \tag{3.16}$$

$$\rho_{FN} = \frac{100}{K-U} \sum_{q=1}^{K-U} \left(\chi_q^{(-)} \Big|_{y_q^{(test)}=+1} \right) \tag{3.17}$$

$$\rho = \frac{100}{K-U} \sum_{q=1}^{K-U} \left(\chi_q^{(-)} \Big|_{y_q^{(test)}=+1} + \chi_q^{(+)} \Big|_{y_q^{(test)}=-1} \right) \tag{3.18}$$

where

$$\chi_q^{(+)} = \begin{cases} 1 & if\ Pr\left(y_q^{(test)} = 1 \Big| \underline{x} \right) > 0.5 \\ 0 & otherwise \end{cases} \tag{3.19}$$

and

$$\chi_q^{(-)} = \begin{cases} 1 & if\ Pr\left(y_q^{(test)} = 1 \Big| \underline{x} \right) \leq 0.5 \\ 0 & otherwise\,. \end{cases} \tag{3.20}$$

[1] The sampling rate depends by the adopted hardware platform. The well-known Linksys WRT54GL has been adopted for validation. The standard scanning procedure provided by the OpenWRT operating system (v. 8.09, r14511, Kamikaze) has been used for the acquisition of the *RSS*.

All the experiments have been performed using test dataset not belonging to the training dataset. More in details, the testing periods are temporally shifted respect to the training periods (the reference configuration assumes the test period with one week delay after the training).

3.1.3.1 Experiment 1 - Detection Performance

In the first experiment (*Experiment 1*), the detection methodology has been configured with the optimal parameters set in order to point out the performance in the reference working conditions. The considered *APs* are located in $\underline{r}_{TX} = (78.0, 19.0, 2.6)$ $[m]$ and $\underline{r}_{RX} = (71.5, 9.0, 2.6)$ $[m]$ and the arising wireless link with line-of-sight (LOS) length $d_S = 11.9$ $[m]$ shown in Fig. 3.2(b) has been taken into account for the acquisition of the *RSS* time series. A *3*-days measurement campaign has been carried out during working days (Thursday and Friday) and during the weekend (Saturday) in order to consider different user presence patterns. The area has been occupied by a variable number of targets $0 \leq p \leq 25$ during the measurements. A total number of $K = 442 \times 10^3$ *RSS* readings have been stored in $\mathbf{S}(t)$ and successively processed applying a sliding window $\underline{\omega}(t)$ of size $U = 500$. It has to be noticed that the detection algorithm is executed every $\Delta t = 0.6$ $[sec]$ and that each estimation has a "memory" of $U \times \Delta t = 300$ $[sec]$. The *EMD* denoising has been performed with a threshold $H_{th} = 0.6$ applied to the Hurst exponent for the selection of the most informative *IMFs*. The band-pass filtering procedure has been applied and the *DFT* coefficients between the lower index $f_{min} = 1$ and the upper index $f_{max} = 10$ have been selected, pointing out a significant reduction of the most important features, from $U/2 = 250$ (only half coefficients are considered by the method due to the symmetry of the Fourier spectrum) to $F = 9$. The *SVM*-based classifier has been trained with $M = 200$ samples well balanced between the absence and presence classes ($m = 1, ..., 100|_{y_m=+1}$ and $m = 101, ..., 200|_{y_m=-1}$ acquired one week before the testing period), and calibrated with the *RBF* parameter $\gamma = 1$ and the penalty parameter $C = 100$.

The detection probability Π has been computed for the whole *3*-days test period and the obtained results have been compared with the ground truth acquired by means of the video-surveillance system. The comparison shown in Fig. 3.3 points out a good matching of the estimated probability with the actual target presence, as also confirmed by the performance indicators reported in Tab. 3.1.

The values ρ_{FP} [%], ρ_{FN} [%], and ρ [%] have been calculated for each day of the measurement campaign in order to analyze the detection performance during the different daily user activity patterns. As it can be seen, the higher false detection rate has been obtained during the second day ($\rho = 8.37$ [%]), mainly due to the high value of the false negative estimations ($\rho_{FN} = 12.53$ [%]) obtained during the Friday afternoon. It has to be noticed that, even if the ground truth declares the target presence during the whole afternoon, lower activity has been

recorded by the surveillance system (less than 20 target movements have been detected from 2:30 PM to 7:00 PM). As expected, this result points out that the presence of still targets within the domain makes the passive detection from *RSS* perturbations much more complex, but the failure rate is still lower than 10 [%].

Test Period	Performance Metrics		
	ρ_{FP} [%]	ρ_{FN} [%]	ρ [%]
Day 1 (*Thursday*)	1.02	7.09	6.73
Day 2 (*Friday*)	0.00	12.53	8.37
Day 3 (*Saturday*)	1.04	0.01	1.16
Total	0.69	6.54	5.42

Table 3.1: *RSS Presence Detection - Experiment 1* (short link, $U = 500$, $H_{th} = 0.6$, $f_{min} = 1$, $f_{max} = 10$, $M = 200$). Performance metrics of the *3*-days measurement campaign.

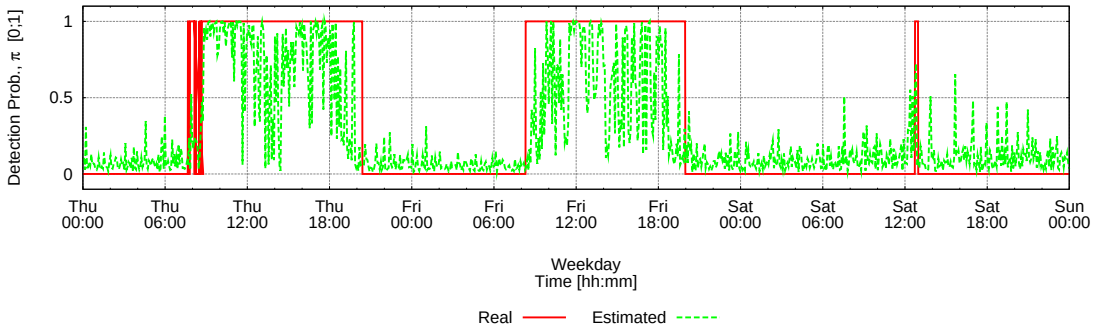

Figure 3.3: *RSS Presence Detection - Experiment 1* ($U = 500$, $H_{th} = 0.6$, $f_{min} = 1$, $f_{max} = 10$, $M = 200$). Time evolution of the real and estimated detection probability Π.

Besides the temporal analysis of the target absence/presence, the same experiment has been also exploited to estimate the spatial extension of the passive detection capability with a single wireless link. Figure 3.4 shows the spatial representation of the detection probability inferred from the comparison between the timestamp of the detection estimations and the actual movements of the targets extracted from the video recordings. Also predefined and controlled target paths have been deliberately scheduled during the *3*-days measurement campaign in order to cover most of the test area. As it can be noticed, the area where the target presence is detected differs from the predefined boundary adopted for the computation of the ground truth. The shape of the "detection coverage" is

strictly related to the geometrical and electrical properties of the scenario. This analysis points out that the detection area is not geometrically limited to the transmitter-receiver *LOS*, but extends beyond with satisfactory detection probability over than 10 meters far from the devices. Such a behavior is related to the very complex indoor propagation and to the unpredictable effects of the objects and obstacles, which alter the *EM* propagation generating *NLOS* reflections, diffractions, and scattering phenomena. Such effects extend the impact of the target to a wider area respect to the commonly considered *LOS* shadowing.

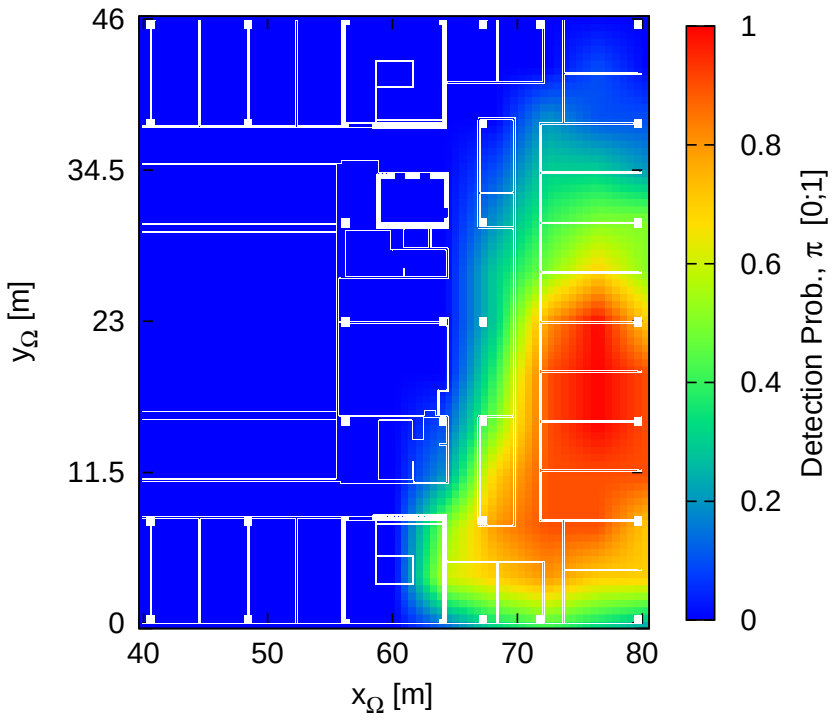

Figure 3.4: *RSS Presence Detection - Experiment 1* ($U = 500$, $H_{th} = 0.6$, $f_{min} = 1$, $f_{max} = 10$, $M = 200$). Target detection coverage map of the short link $d_S = 11.9$ $[m]$.

3.1.3.2 Experiment 2 - Parameters Calibration

The second experiment (*Experiment 2*) deals with the calibration of the input parameters in order to study the effect of changing the system configuration on the detection performance. The failure rate ρ [%] has been used as the main performance metric. The first calibration test has been carried out on the length U of the sliding time window $\underline{\omega}(t)$. Such a parameter highly affects the overall performance of the proposed method, as clearly shown in Fig. 3.5. Longer time windows (e.g., $U = 1500$) enable higher performance since much more information is available, but at the cost of a higher time delay and a lower

time resolution of the detections. As an example, the failure rate decreases to $\rho = 2.31$ [%] with $U = 1500$, but each estimation is based on a time window of $U \times \Delta t = 900$ [sec]. The optimal value $U = 500$ has been adopted as the best trade-off between accuracy and real-time performance.

The *EMD* denoising strategy has been calibrated computing the failure rate for different values of the Hurst exponent threshold $H_{th} \in [0.1 \div 0.9]$. The results of the threshold calibration are shown in Fig. 3.6. As it can be seen, the trend of the failure rate presents an unstable behavior but with a minimum at $H_{th} = 0.6$, and such value has been selected for the optimal parameter set.

The calibration of the feature extraction procedure by means of the *DFT* is devoted to identify the best f_{min} and f_{max} indexes for the selection of the most significant *DFT* coefficients ξ_f, $f = f_{min}, ..., f_{max}$. The results shown in Fig. 3.7 point out that most of the information useful for the target detection is contained in the first set of coefficients at the lower frequencies. In particular, the first coefficient ξ_0 related to the *DC* component, which is simply the average value of the signal itself, has been filtered setting $f_{min} = 1$, while the upper coefficient index has been set to $f_{max} = 10$. The failure rate decreased from $\rho = 15.53$ [%] to the minimum value $\rho = 5.42$ [%] using this configuration of the band-pass filtering strategy.

The last calibration refers to the training set size and to the hyper-parameters setting of the *SVM* classifier. The number of training samples has been varied in the range $10 \leq M \leq 360$ to identify the minimum value that guarantees a satisfactory failure rate. Figure 3.8 shows a decreasing trend of the failure rate that stabilizes when $M > 150$. According to this result, the *SVM* classifier has been trained with $M = 200$ samples, which represents a good trade-off between low training complexity and estimation accuracy. The parameter $C = 100$ and the *RBF* parameter $\gamma = 1$ have been calibrated using the well known cross-validation procedure [136].

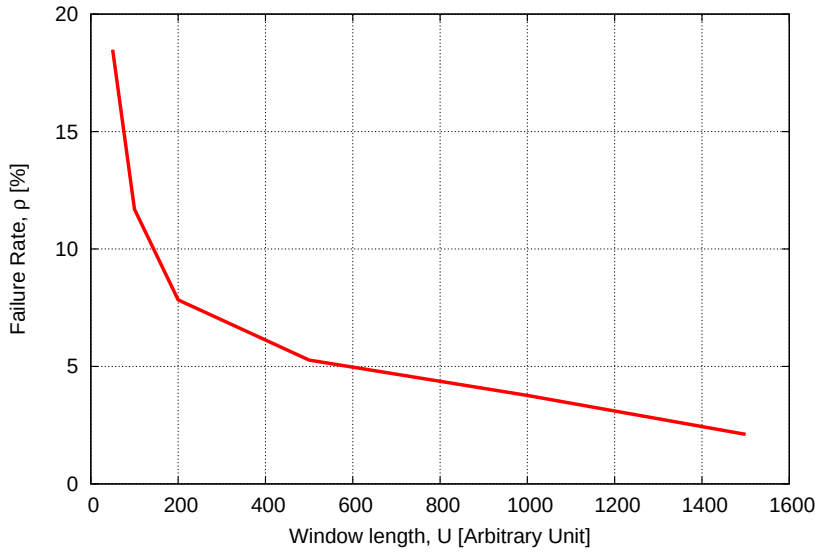

Figure 3.5: *RSS Presence Detection - Experiment 2* ($50 \leq U \leq 1500$). Failure rate analysis vs the length U of the sliding window.

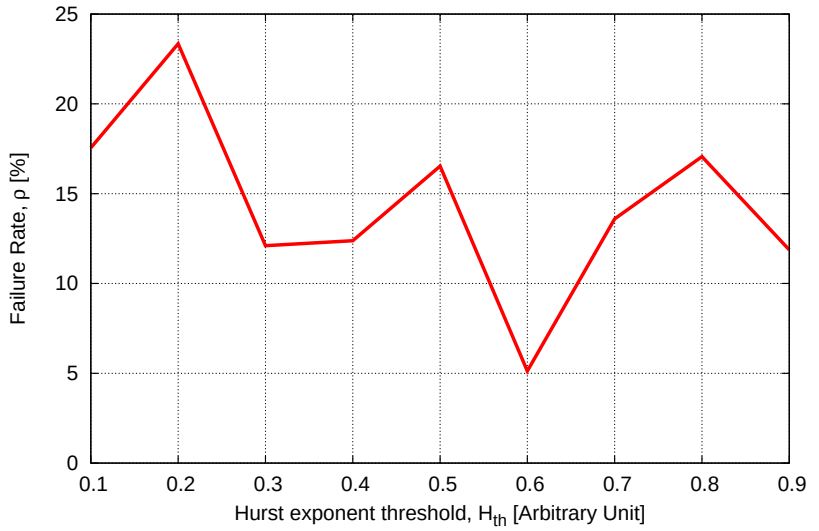

Figure 3.6: *RSS Presence Detection - Experiment 2* ($0.1 \leq H_{th} \leq 0.9$). Failure rate analysis vs the Hurst exponent threshold H_{th} for *EMD* denoising.

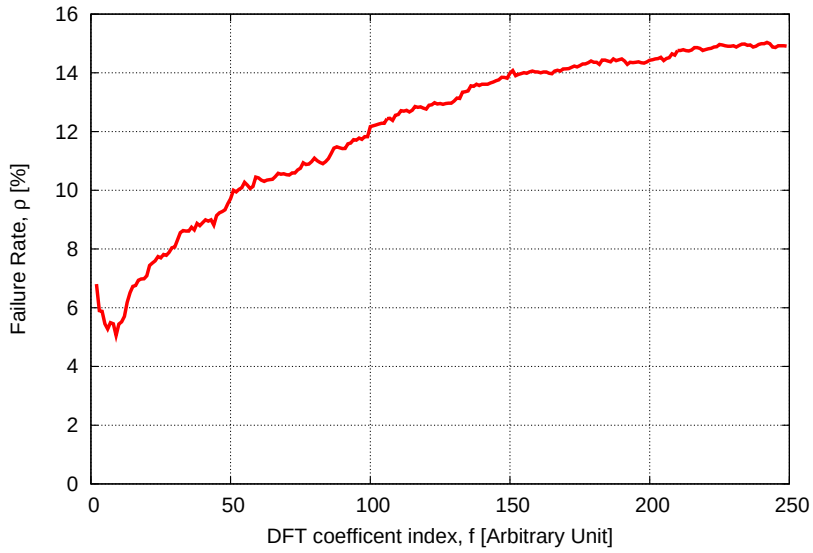

Figure 3.7: *RSS Presence Detection - Experiment 2* ($0.1 \leq H_{th} \leq 0.9$). Failure rate analysis vs the Hurst exponent threshold H_{th} for *EMD* denoising.

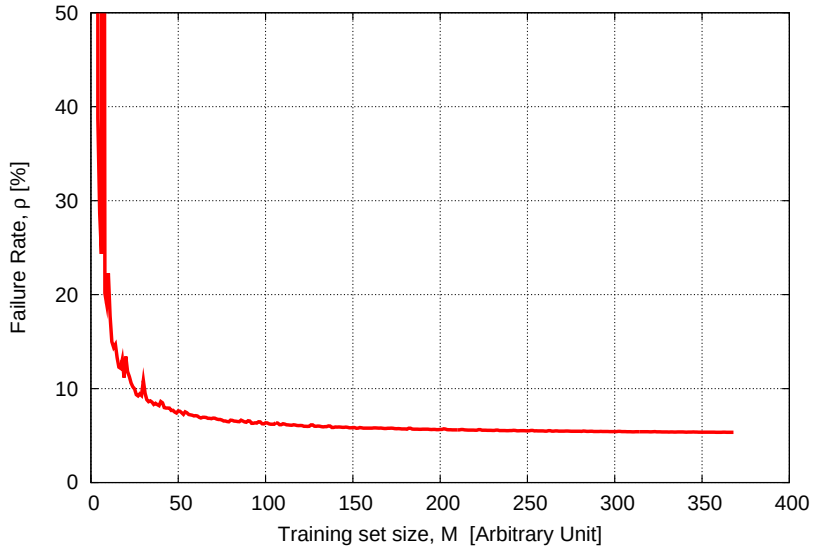

Figure 3.8: *RSS Presence Detection - Experiment 2* ($2 \leq f \leq 250$). Failure rate analysis vs the bandwidth of the band-pass filtering for *DFT* coefficients selection.

3.1.3.3 Experiment 3 - Detection in Large-scale Complex Scenario

The third experiment (*Experiment 3*) is aimed at assessing the detection performance in a more complex system configuration. Toward this end, a second measurement campaign has been performed in the same week days of the previous one (Thursday, Friday, and Saturday, with a variable number of target $0 \leq p \leq 21$) but a different transmitting AP has been selected among the available ones (the new position is $\underline{r}_{TX} = (71.5, 43.1, 2.6)$ $[m]$) already installed in the domain in order to increase the LOS length of the wireless link from $d_S = 11.9$ $[m]$ to $d_L = 34.1$ $[m]$, as graphically shown in Fig. 3.9(a).

The transmitting power is unchanged respect to the previous experiments ($P_{TX} = 18$ $[dBm]$), and the RSS values are close to the sensitivity threshold of the receiver ($s(t) = -90$ $[dBm]$). It is expected that an higher distance between the transmitter and the receiver causes noisier RSS with direct consequences on the detection performance. Compared to the previous results reported in Fig. 3.4, the detection coverage is wider as it can be clearly observed in Fig. 3.9(b), but the values of the detection probability are lower and the failure rates are increased (the daily values of ρ_{FP} [%], ρ_{FN} [%] and ρ [%] are reported in Tab. 3.2).

As it can be noticed, the extension of the link length has caused an increase of the average failure rate from $\rho = 5.42$ [%] to $\rho = 9.94$ [%], with a significant increase of the false negatives (up to $\rho_{FN} = 24.81$ [%] during the second day). This means that longer links may detect the target presence in wider areas but with a lower reliability. The time evolution of the detection probability is shown in Fig. 3.10. Even if the probability values point out a more unstable trend compared to the previous results shown in Fig. 3.3, the detection is still satisfactory except for the false negatives estimated during the second day.

Test Period	Performance Metrics		
	ρ_{FP} [%]	ρ_{FN} [%]	ρ [%]
Day 1 (*Thursday*)	2.43	18.32	12.57
Day 2 (*Friday*)	2.01	24.81	16.89
Day 3 (*Saturday*)	0.05	0.01	0.38
Total	1.50	14.38	9.94

Table 3.2: *RSS Presence Detection - Experiment 3* (long link, $d_L = 34.1$ $[m]$). Performance metrics of the *3*-days measurement campaign.

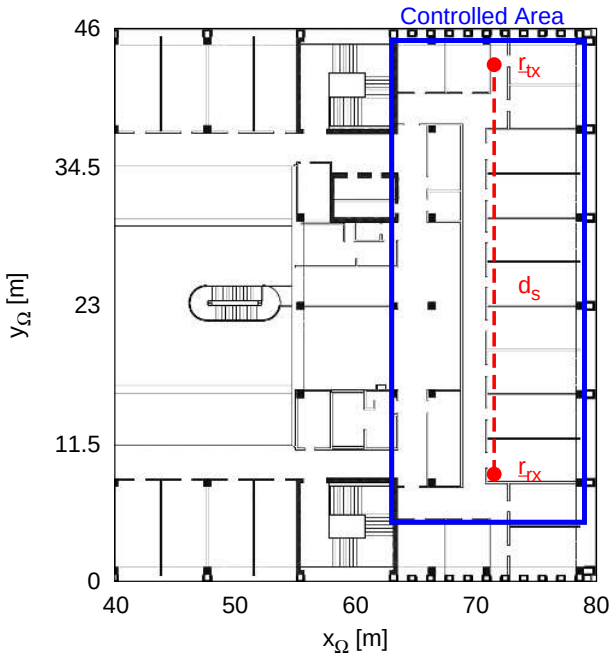

(*a*)

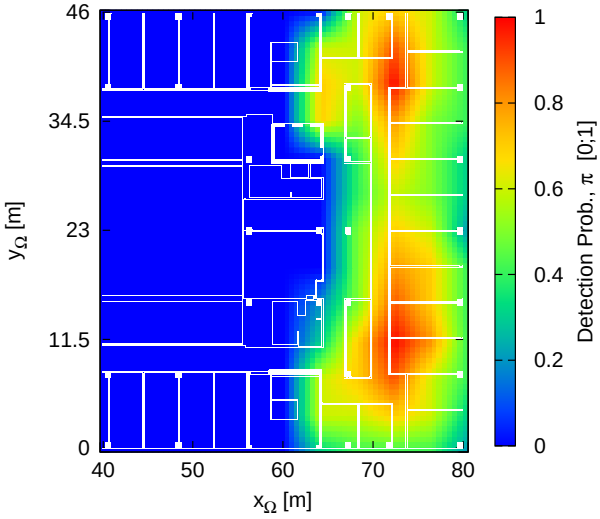

(*b*)

Figure 3.9: *RSS Presence Detection - Experiment 3* (long link, $d_L = 34.1$ $[m]$). (a) Geometry of the scenario with the longer wireless link, (b) target detection coverage map of the long link.

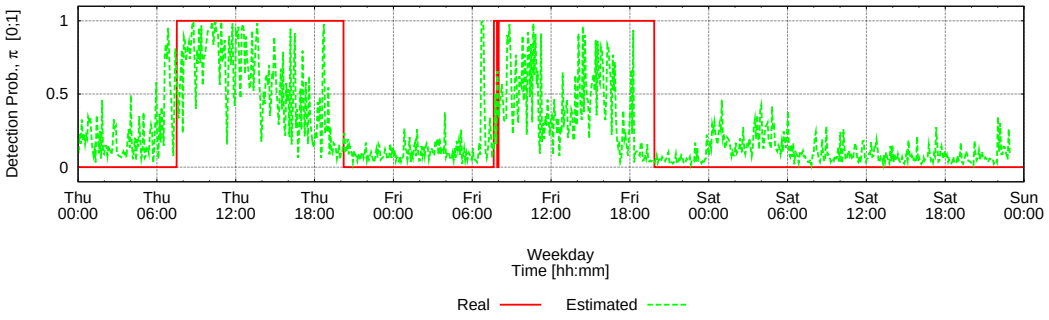

Figure 3.10: *RSS Presence Detection - Experiment 3* (long link, $d_L = 34.1$ $[m]$). Time evolution of the real and estimated detection probability Π.

3.1.3.4 Experiment 4 - Comparison with the State of the Art

In the fourth experiment (*Experiment 4*), the proposed methodology is compared to different detection methods available in the state of the art. As a first comparison, a variance-based method for the detection of anomalies in the time evolution of *RSS* stream has been considered. The *RSS* variance is a statistical indicator commonly adopted by many passive wireless localization methods available in the state of the art. The variance of the *RSS* readings stored in the sliding time window $\underline{\omega}(t)$ has been computed and considered anomalous if above a predefined silence threshold. More in detail, the target detection is verified when $var(\underline{\omega}(t)) > s_{th}$, where s_{th} has been computed according to the method in [107], using the same time window length as above ($U = 500$). The comparison has been performed on the same *3*-days data set and in the same test field of the *Experiment 1*. The obtained performance is reported in Tab. 3.3.

The failure metrics point out that the proposed method outperforms the time-domain analysis, especially in the reduction of the false positive detections (the time-domain analysis shows $\rho_{FP} = 17.51$ [%] respect to the false positive rate $\rho_{FP} = 0.69$ [%] obtained with the proposed detection strategy).

In order to further compare the proposed method with the state of the art on device-free target detection, the *RASID* approach presented in [81] has been considered as a robust WLAN motion detection system, that outperforms other state of the art solutions based on the moving average (*MA*) and the moving variance (*MV*) proposed in [95], and on the maximum likelihood estimation (*MLE*) proposed in [96]. *RASID* considers multiple wireless links but since each stream is analyzed independently, the comparison has been fairly performed using the single wireless link adopted also in the previous *Experiment 1* (with the sliding window length $U = 500$).

The anomaly score has been computed according to the formulation of the *Basic Detection Module* [81] based on the sample variance of the time window and assuming the significance parameter $\alpha = 0.01$. The performance of *RASID*

are reported in Tab. 3.4. The obtained results point out detection capabilities in line with the false negative and false positive rates declared by Kosba *et al.* in [81]. Such failure metrics show that the method proposed in this work strongly outperforms RASID in terms of false positive (average $\rho_{FP} = 0.69$ [%] obtained in *Experiment 1* respect to the *RASID* false positive rate $\rho_{FP} = 17.51$ [%]) as well as false negative rates (average $\rho_{FN} = 6.54$ [%] obtained in *Experiment 1* respect to the *RASID* false negative rate $\rho_{FN} = 15.03$ [%]). It has also to be noticed that the performance of the proposed solution is still comparable to RASID even if the test field of *Experiment 3* (i.e., with the longer wireless link of LOS length $d_L = 34.1$ $[m]$) is considered.

Test Period	Performance Metrics		
	ρ_{FP} [%]	ρ_{FN} [%]	ρ [%]
Day 1 (*Thursday*)	34.67	19.32	29.37
Day 2 (*Friday*)	16.51	25.03	22.39
Day 3 (*Saturday*)	1.36	0.81	2.35
Total	17.51	15.03	18.03

Table 3.3: *RSS Presence Detection - Experiment 4* (state-of-the-art comparison). Performance metrics of the variance-based time domain analysis [107].

Test Period	Performance Metrics		
	ρ_{FP} [%]	ρ_{FN} [%]	ρ [%]
Day 1 (*Thursday*)	19.55	12.22	17.87
Day 2 (*Friday*)	13.23	21.51	19.11
Day 3 (*Saturday*)	0.98	0.73	1.29
Total	11.25	11.48	12.75

Table 3.4: *RSS Presence Detection - Experiment 4* (state-of-the-art comparison). Performance metrics of the *RASID* detection method [81].

The methodology presented in [83] has been also considered to compare the performance of the proposed method with the state of the art. Zhao *et al.* exploit the kernel distance quantifying the difference between two histograms of signal strength measurements in order to detect the presence of a person on the wireless link line. The receiver operating characteristic (ROC) curve has been calculated in order to assess and compare the detection performance of the proposed method with *RASID* and with the kernel-based solution. The results shown in Fig. 3.11 point out that the proposed solution outperforms the state of the art methods based on the sample variance (*RASID* in [81]) and on the kernel distance [83].

In particular, the proposed solution provides higher detection performance (up to 80 [%]) even with very low false positive rates (lower than 10 [%]).

The detection of a person crossing wireless links between transceivers deployed linearly along a border has been addressed in [82]. The classifiers proposed by Hillyard *et al.* have been considered for comparison as valuable detection methods in the state of the art. Their performance has been analyzed assuming the reference wireless architecture considered in this work and composed by a single wireless link. It has been verified that, as also declared by the authors in [82], none of the classifiers worked well when a reduced number of wireless devices are deployed, since the basic working principle is to leverage the redundancy of multiple and overlapping links to mitigate the detection errors. Accordingly, the obtained probability of correct classification turned out to be in line with the results shown in [82], and much lower that the ones obtained with the previous state of the art approaches. Detection probabilities lower than 10 [%] have been obtained with a single wireless link (the authors declared an average classification probability of 7.6 [%] when 3 nodes are adopted).

The system *Nuzzer* [86] has been also considered as a powerful state of the art method providing satisfactory performance to be compared with the proposed solution. Instead of detecting the target presence, *Nuzzer* aims to localize it exploiting a fingerprinting strategy. In order to guarantee a fair comparison, the discrete space estimator of *Nuzzer* has been adapted to provide the probability of target presence (using the same dataset of the *Experiment 1*) assuming that all the samples acquired in presence of the target have been collected in a single spatial position. This modification has been introduced because the comparison is about the target detection instead of the localization. It has been verified that the probability of correct estimation obtained by the discrete space estimator with a single wireless link is lower than 40 [%] and with an average false positive rate $\rho_{FP} = 22.3$ [%] (it has to be noticed that *Seifeldin et al.* declares a probability of correct estimation lower than 50 [%] using four wireless links).

Summarizing, the proposed solution outperforms four different state of the art approaches in the binary detection of passive targets when a single wireless link is adopted. The obtained performance is higher in terms of both detection capability as well as false positive rate.

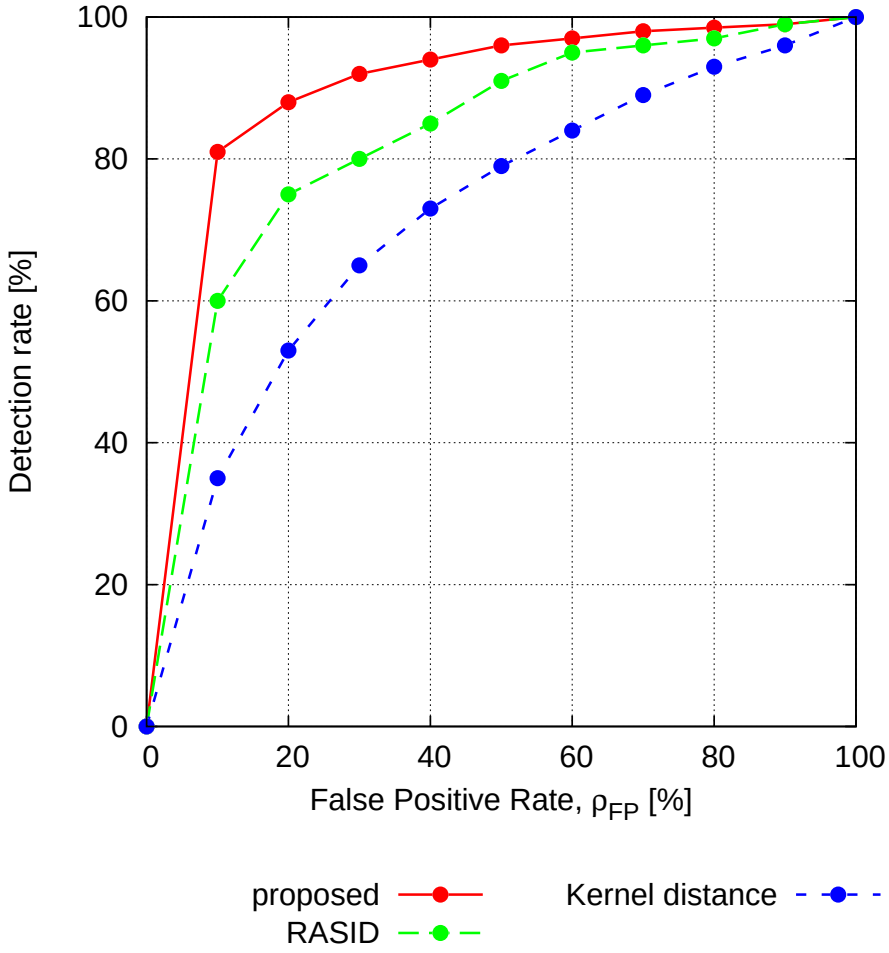

Figure 3.11: *RSS Presence Detection - Experiment 4* (state-of-the-art comparison). ROC curve of the *proposed* method compared to *RASID* [81] and *kernel distance* [83] methods.

3.2 *CSI*-based Localization and Human Monitoring

The received signal strength information (*RSSI*) has been widely used to enable detection, localization, and monitoring of targets in indoor areas [62, 61, 78] . However, the *RSSI* suffers from a significant quantization error and is a rough indicator of the amplitude of the electromagnetic field on the antenna. Furthermore, it does not allow to take advantage of the phase of the measured field, that is a quantity highly sensible to the variations of the environment. In the last decade, a great effort has been devoted to assure a better use of the available frequency and spatial resources for high-rate wireless connectivity. To this end, the knowledge of the wireless channel response, known as Channel State Information (*CSI*), is required [141]. This opens new possibilities for localization systems, taking advantage of the *CSI* to obtain much more detailed information about the effects of the humans on the electromagnetic fields [142]. However, the *CSI* has been partially exploited in the current state of the art. For example, many approaches avoid to use the phase information, which is considered unstable and difficult to be calibrated [143].

In this Section, an innovative approach to analyze the *CSI* available in Wi-Fi based systems for the estimation of the presence, position, and posture of a device-free target is addressed through a multi-resolution strategy that applies a virtual zoom on the information content of the *CSI* measured by a single Wi-Fi link. The method is based on the representation of the *CSI* data as "strings" and on the analysis of their distance in the complex domain in order to identify different human behaviour and actions. The scattering of the human body is exploited to solve the inverse problem of human behavior reconstruction from the electromagnetic field measurement. A preliminary experiment using a couple of IEEE 802.11 wireless devices in a non-controlled indoor scenario is reported.

3.2.1 Multi-resolution Wireless Sensing Strategy

In this work, multiple target features characterized by different resolution levels are estimated simultaneously by applying a multi-resolution strategy, which iteratively exploits the large amount of information content of the channel state information [140] of a multiple-input multiple-output (*MIMO*) Wi-Fi link. Three different target features are considered, namely the *presence* (low-resolution), the *position* (medium-resolution), and the *posture* (high-resolution). Accordingly, three customized support vector machine (*SVM*) classifiers [60] are trained using the complex-valued constellations of the *CSI* measured at multiple carrier frequencies of the 5 $[GHz]$ Wi-Fi band.

Let us consider an indoor three-dimensional investigation domain Ω where a couple of Wi-Fi transmitter and receiver equipped with N_{tx} and N_{rx} antennas are located in known and fixed positions $\underline{r}_{tx}$ and $\underline{r}_{rx}$, $\underline{r} = (x, y, z)$ being the

position vector, and generate an *IEEE 802.11ac MIMO* connection based on the orthogonal frequency division multiplexing (*OFDM*) technique. The complex terms of the CSI vector $\underline{H}_u(t,f) = [h_u(t,f_c)\,;\, c = 1,...,C]$, where $h_u(t,f_c) = |h_u(t,f_c)|\, e^{j\angle h_u(t,f_c)}$, $u = 1,...,U$, are measured at multiple sub-carrier frequencies f_c, $c = 1,...,C$, at the time instant t, and for each orthogonal spatial sub-channel $u = 1,...,U$, $U = N_{tx} \times N_{rx}$. Let us consider the *CSI* vectors $\underline{H}_u(t,f) \in \mathbb{C}$, $u = 1,...,U$, as the complex representation of the channel frequency response (CFR) determined by the adopted OFDM constellation scheme, and subject to the perturbations of the electromagnetic propagation from the transmitter to the receiver. Such perturbations reflect on the changes of $\underline{H}_u(t,f)$, $u = 1,...,U$, which are exploited by the communication standard to maximize the link robustness. Accordingly, a strict relation exists between the target activities within Ω and the time-varying shapes of $\underline{H}_u(t,f)$, $u = 1,...,U$, which can be represented as "*CSI strings*" on the complex plane. The goal of the proposed multi-resolution technique is to learn such a relation and to make it usable for the reconstruction of the underlying target activities. Unlike most of the contribution in the state of the art, all the available CSI information has been considered since the *strings* are generated by the complex-valued measurement [expressed in the form of magnitude $|h_u(t,f_c)|$ and phase $\angle h_u(t,f_c)$] at the sub-carrier frequencies f_c, $c = 1,...,C$ and the *MIMO* sub-channels $u = 1,...,U$. In order to profitably use such a large amount of information on the communication channel, the fine-grained *CSI* is pre-processed as follows.

Phase correction: the linear phase shift due to the transmission at different frequencies is removed, and a common phase reference is introduced, which is not used in *IEEE 802.11ac* to avoid the complex process of phase synchronization.

Outlier removal: an Hampel filter is applied to remove the isolated and short-time changes of the *CSI strings* that are not related to the target activities but to the unpredictable adaptive schemes of the physical layer management.

Features extraction: the phase-corrected and time-filtered *strings* $\underline{\widetilde{H}}_u(t,f)$, $u = 1,...,U$, are approximated by a set of least-squared splines in order to represent the shapes of the *strings* in the complex plane by using a number of uniformly spaced control points K lower than the number of carrier frequencies (i.e., $K < C$) for features selection. More in detail, the whole set of *CSI* data is represented by a set of features $\underline{\phi}(t) = [|\mathcal{H}_{u,k}(t)|\,;\, \angle\mathcal{H}_{u,k}(t)\,;\, u = 1,...,U;\, k = 1,...,K]$, where $\mathcal{H}_{u,k}$ is the spline-based interpolated value of $\underline{\widetilde{H}}_u(t,f)$ evaluated at the k-th control point in the complex plane.

The features $\underline{\phi}(t_m)$, computed at successive time instants $t_m = t_0 + m\Delta t$, Δt being the acquisition sampling time, are used to train a set of *SVM* binary classifiers devoted to learn the unknown relations between the *CSI strings* and the target presence, position, and posture. The learning process is organized in a multi-step procedure in order to iteratively focus on the *strings'* shapes that are effectively related to the addressed target feature. The synthetic zoom applied by the proposed multi-resolution strategy fully exploits the very high sensitivity of

the *CSI* using the proper amount of information according to the spatial accuracy required at each sensing step. The target detection is applied to the whole domain Ω, the localization is focused on the target position within Ω', while the desired posture is recognized within the smallest domain Ω'', as pictorially shown in Fig. 3.12. The three *SVM* binary classifiers aim to maximize the margin (i) between the background in absence of targets and any other target presence pattern in Ω, (ii) between whatever target position and the positions within Ω', and (iii) between whatever posture in Ω' and the posture in Ω''. During the test phase, the trained classifiers are triggered one after the other according to the following simple rule: *the localization in* Ω' *is activated only if a target is detected in* Ω, *and the posture is estimated in* Ω'' *only if a target is localized in* Ω'.

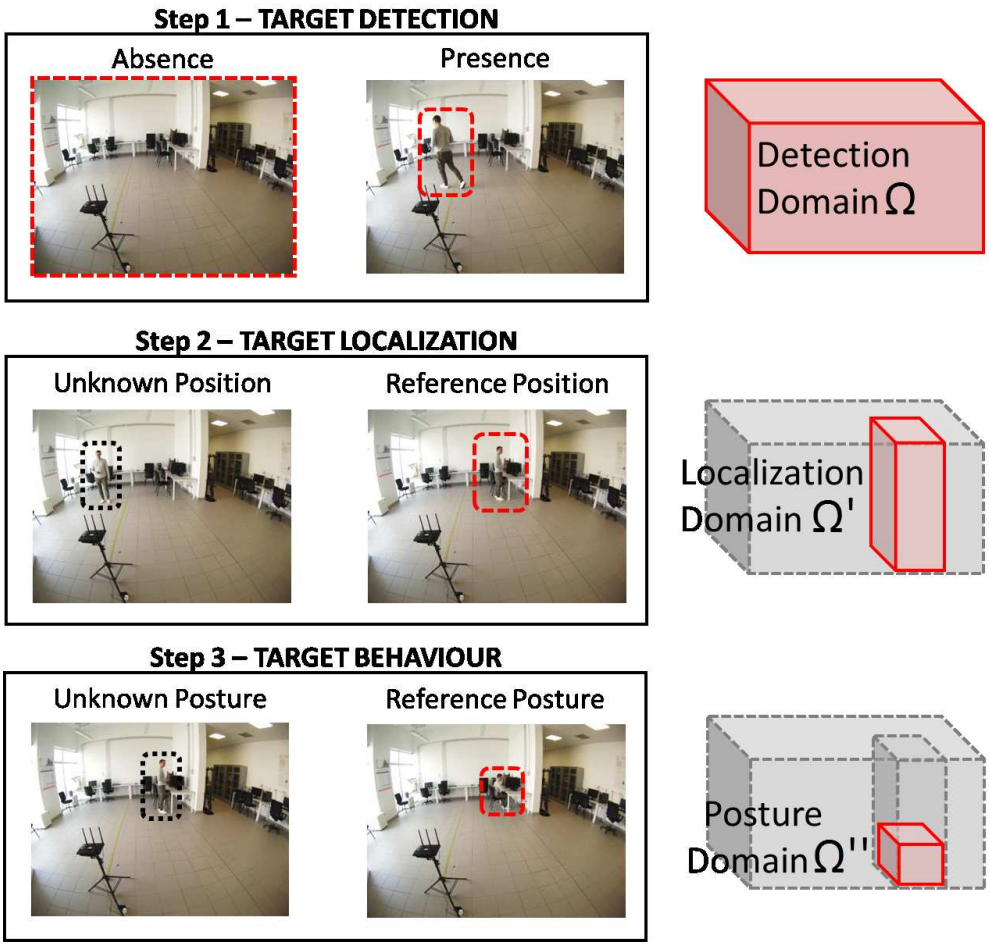

Figure 3.12: *CSI Multi-Resolution Strategy.* Iterative procedure for the estimation of multiple location-based target features.

3.2.1.1 Experimental Validation

The proposed multi-resolution sensing strategy has been experimentally validated in a non-controlled indoor area of size $X = 8.4\,[m]$, $Y = 9.6\,[m]$, $Z = 4.2\,[m]$. An *IEEE 802.11ac* Wi-Fi access point has been deployed in position $\underline{r}_{tx} = (3.0\,[m]\,,\, 2.0\,[m]\,,\, 0.9\,[m])$ as transmitter, while the receiver equipped with the Intel Link 5300 network interface card (NIC) has been located in $\underline{r}_{rx} = (3.0\,[m]\,,\, 9.0\,[m]\,,\, 0.9\,[m])$, with a tx-rx line-of-sight distance $d = 7\,[m]$. A set of $U = 6$ wireless sub-channels have been generated by using $N_{tx} = 2$ and $N_{rx} = 3$ antennas. The transmitter has been configured with the working frequency $f = 5.18\,[GHz]$ (i.e., the Wi-Fi channel 36) and the CSI is provided by the receiver at $C = 30$ frequency sub-carriers with the sampling interval $\Delta t = 0.05\,[s]$. The number of control points has been set to $K = 10$, leading to a features selection rate of $\frac{K}{C} = \frac{1}{3}$. A measurement campaign has been performed to collect the training data set in different scenario conditions including the empty domain, the target presence and movement in random positions within Ω, the target in the reference position $\underline{r}_T$ within Ω', and the target in the reference posture shown in Fig. 3.12 (i.e., sit down in the spatial position $\underline{r}_T$ and within Ω''). Three different training subsets composed by $M = 1600$ well-balanced samples have been generated according to the binary classification task of each SVM classifier. For example, $M|_{\Gamma=0} = 800$ and $M|_{\Gamma=1} = 800$ samples have been labeled with class index $\Gamma = 0$ (i.e., target absence) and $\Gamma = 1$ (i.e., target presence) for the target detection task. The radial basis function (RBF) kernel has been selected, the training hyperparameter $C_{SVM} = 10^4$ and the RBF parameter $\gamma_{SVM} = 10^{-1}$ have been calibrated through a 5-fold cross-validation strategy.

The representative test case is concerned with a target entering the domain Ω for a duration of 1 minute (i.e., for a total number of test samples $M \simeq 1200$ with $\Delta t = 0.05\,[s]$). During this presence period, the target has changed position frequently and has stopped twice in the reference position $\underline{r}_T$, each time for 15 $[s]$. When the target was in position $\underline{r}_T$, the reference "sit down" posture has been assumed for 5 $[s]$ two times. As an illustrative example, Fig. 3.13 shows the output probability given by the three SVM classifiers. The grey backgrounds represent the activation time periods of the classifiers, which are triggered according to the estimations of the previous and lower-resolution classification step. As can be observed, the target presence [Fig. 3.13(a)], position [Fig. 3.13(b)], and posture [Fig. 3.13(c)] have been correctly estimated by comparing the actual and the estimated target behaviour. The classification performance have been quantified in terms of false detection, false localization, and false posture rates (defined as the ratio between the number of wrong and total classifications, with probability threshold set to 0.5), which turned out $\rho_D = 1.3$ [%], $\rho_L = 2.1$ [%], $\rho_P = 3.4$ [%], respectively.

Preliminary experiments point out the feasibility to estimate high-resolution features such as the target posture even in very large investigation domains,

passing through the estimation of the target presence and position. A robust and ubiquitous wireless sensing is obtained with failure rates lower than 2.5% $\rho = 2.5$ [%] in the three considered resolution steps.

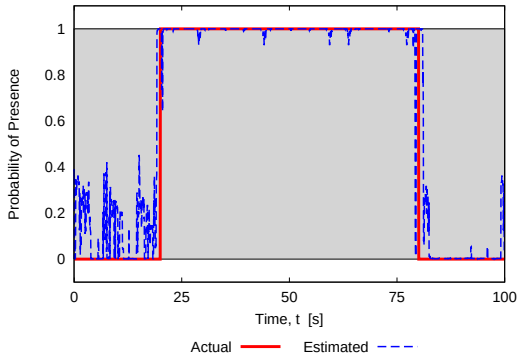

(a)

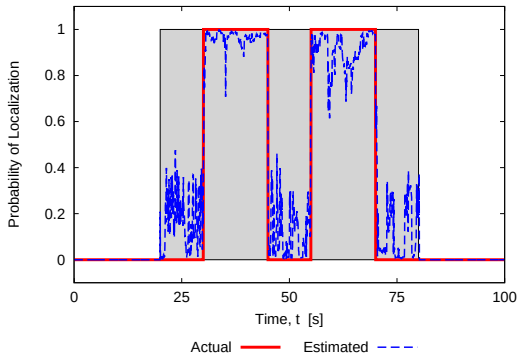

(b)

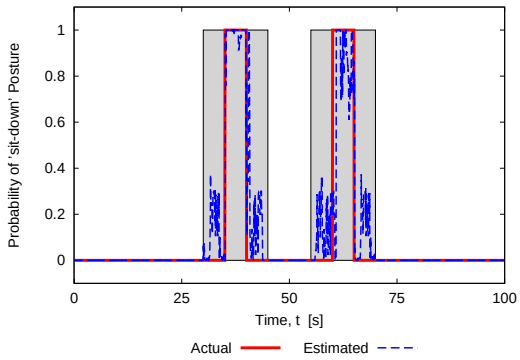

(c)

Figure 3.13: *CSI Multi-Resolution Strategy.* Probability of target presence (a), of target localization in the reference position (b), and of target behaviour in the reference "sit down" posture (c).

3.2.2 *CSI* Data Interpretation for Human Monitoring

In this Section, an intuitive approach to understand and quantify the degree of reliability of the whole *CSI* data, both magnitude and phase across all the frequency subcarriers, to enable indoor accurate location-based services is proposed. The results of a preliminary experiment for human posture recognition are presented to assess the advantages and the limitation of the investigated method.

The aim of this Section is twofold. On a side, a way to quantify the amount of human information associated to the *CSI* is described. On the other hand, a method to extract such information is proposed. In order to quantify the amount of information conveyed by *CSI*, the number of distinguishable *CSI* configurations has to be identified. The method adopted in this paper is based on the Kolmogorov approach to information theory. The Kolmogorov approach [144]-[146] is intuitive, simple, and general. The basic idea is that, given a continuous set of data X, two elements of the set give different information when they are distinguishable. To be more specific, given a continuous set X of elements x, affected by an uncertainty ϵ, we consider an ϵ-packing of the set a group of open balls having ϵ radius (called ϵ-balls) whose centers are at least $(2 \times \epsilon)$ far each to the others. Kolmogorov proposed to identify the maximum number of balls of any ϵ-packing of the set as the amount of information associated to the set. This is equivalent to identify the maximum number of elements of X having at least $(2 \times \epsilon)$ distance. This number is known as the Kolmogorov ϵ-capacity of the set.

Let us consider the *CSI* information collected using an orthogonal frequency division multiplexing (*OFDM*) multiple-input multiple output (*MIMO*) system with N_t transmitting elements ad N_r receiving elements, on N_f subcarriers, and during N_T time instants [145]. For the sake of simplicity, let us consider a static environment. We collect the real and imaginary part of the N_f signals received on the N_f subcarriers of the (h, l) link, in a complex vector $\mathbf{a}^{(h,l)}(t_k) \in C^{N_f}$, wherein t_k is the k-th time instant, and h and l are the h-th and l-th receiving and transmitting elements. Consequently, the value of the n-th entry of the $\mathbf{a}^{(h,l)}(t_k)$ vector for a given t_k represents the data transmitted by the h-th antenna at time t_k on the n-th subcarrier and received by the l-th antenna.

After subtracting the linear phase shift associated to different sucarriers and normalizing to the mean phase, let $\hat{\mathbf{a}}^{(h,l)}(t_k)$ be a vector whose *shape* is a function of the frequency and is a specific fingerprint of the environment. Consequently, also the information on the human in the environment is encoded in the shape and position of the 3D *strings* representing the $\hat{\mathbf{a}}^{(h,l)}(t_k)$ vectors.

Using the Kolmogorov approach, the points of the set X are the configurations of the strings associated to the $\hat{\mathbf{a}}(t_k)$ vectors. Two strings give different information when their distance is larger than the uncertainty ϵ. In the following, the standard deviation of the strings is adopted as uncertainty level ϵ. In the Kolmogorov approach, the signal $\hat{\mathbf{a}}(t_k)$ is an element in a $N_f \times N_t \times N_r$ complex space. In order to give a pictorial view, the signal for a fixed (h, l) *TX-RX* path

in a 3D space is represented, where (x, y) are the real and imaginary parts of the signal, and z is the index of the subcarrier.

Let us consider the following numerical example. A single-input single-output (*SISO*) system consisting of two short dipole elements is placed in $(x = 0, y = 0, z = 0)$ and $(x = 0, y = 30\lambda, z = 0)$, and a point-like metallic scatterer with unit reflection coefficient is placed in 3 different positions $(x = 5\lambda, y = 15\lambda, z = 0)$, $(x = 7\lambda, y = 15\lambda, z = 0)$, $(x = 5\lambda, y = 9\lambda, z = 0)$. A number of 100 data samples affected by a noise level of -20 [dB] are collected for each position of the scatterer. The mean value of the received signal and the standard deviation have been evaluated for each subcarrier and for each data set. The uncertainty circle is plotted in the $x - y$ plane for each *OFDM* subcarrier. The circles are centered in the mean value of the *CSI* and have radius equal to the standard deviation. The data at different frequencies are plotted at different z values. As an example, the results obtained from the vector $\tilde{\mathbf{a}}^{(1,1)}(t_k)$ considering the three different positions of the scatters are plotted in Fig. 3.14 (first position: blue, second position: red, third position: green). A slight superposition between the uncertainty circles associated to the first and second positions can be noted. The degree of superposition is an indication of the probability that the positions can not be distinguished. Such a probability is proportional to the intersection area. Figure 3.14 gives an intuitive idea of the information content of the *CSI* data, and also suggests a practical way to elaborate such information in terms of *strings*. Two different configurations of the scenario are distinguishable if the distance between the strings is larger than the sphere of uncertainty ϵ affecting the data.

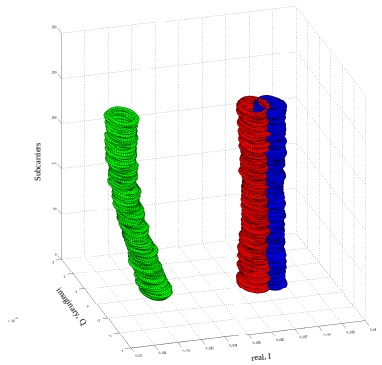

Figure 3.14: *CSI Analysis.* Pictorial view of the CSI strings. The colors represent different positions of the scattering object. The OFDM frequency subcarriers are along the vertical axis. The circles in the horizontal complex I-Q plane are centered in the mean value of the CSI and the radius is equal to the standard deviation.

3.2.2.1 Experimental Validation of Human Posture Monitoring

The *CSI* data collected in three different configuration of the scenario shown in Fig. 3.15 are considered. The uncertainty circles of the received signal in the three cases are plotted respectively in blue [Fig. 3.15(a), configuration 1 - empty environment], red [Fig. 3.15(b), configuration 2 - standing man], and black [Fig. 3.15(c), configuration 3 - crouched man] in Fig. 3.16. Non-intersecting circles of the three configurations are shown, confirming that the three sets of strings carry different information on the environment.

(a) (b) (c)

Figure 3.15: *CSI Analysis.* Indoor scenario for experimental validation. Empty environment (a), standing man (b), and crouched man (c).

According to the concept of Kolmogorov capacity, a distance among the received signals can be introduced. In the following, the Euclidean distance $\|\hat{\mathbf{a}}^{(h,l)}(t_k) - \hat{\mathbf{b}}^{(h,l)}(t_k)|_2$ will be adopted, where $\hat{\mathbf{a}}$ and $\hat{\mathbf{b}}$ are two different strings. The distance is evaluated for the three environmental configurations considered above and reported in Fig. 3.16. The temporal sequence of configurations reproduced in the measurement campaign is 1-2-3-2-3-1 (i.e., empty, standing, crouched, standing, crouched, empty). A reference signal has been acquired for each configuration and let R_1, R_2, R_3 be the strings of the reference signals.

The *CSI* data have been acquired using an *Intel Wi-Fi Wireless Link 5300* (*IWL5300*) *IEEE 802.11a/b/n* network card using a 3×2 *MIMO* system, obtaining a total of 6 spatial channels and 30 frequency subcarriers. The measurements have been performed at 2.4 [GHz]. The distance between the point associated to the *CSI* data and the reference signals R_1, R_2, R_3 are reported on a polar plot at angles $\theta \in 0, 2\pi$ proportional to the acquisition time. The angle $\theta = 0$ corresponds to the starting time instant. The results are reported in Fig. 3.17 showing that the proper sequence of the minimum distance has been obtained. The estimated sequence is: 1 (blue), 2 (red), 3 (green), 2 (red), 3 (green), 1 (blue), as expected. The obtained results have been obtained using a single spatial channel. As an additional example, the six *CSI* data strings acquired using the 3×2 *MIMO* system have been elaborated adopting a simple "choice by majority", obtaining the results shown in Fig. 3.18. The reliability of the choice is

plotted as blue curve and the time evolution of the estimated configuration is reported with the red curve. As it can be noticed, the estimated sequence properly reproduced the actual target posture (i.e., configuration sequence: 1-2-3-2-3-1).

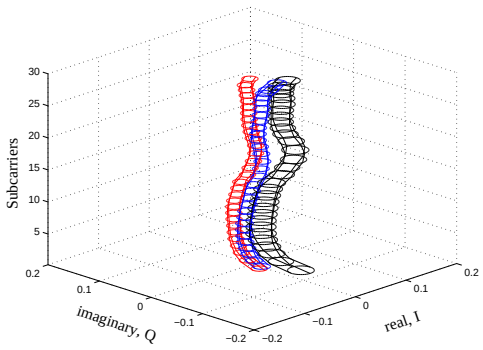

Figure 3.16: *CSI Analysis.* CSI strings of empty environment (black), standing man (red), and crouched man (blue).

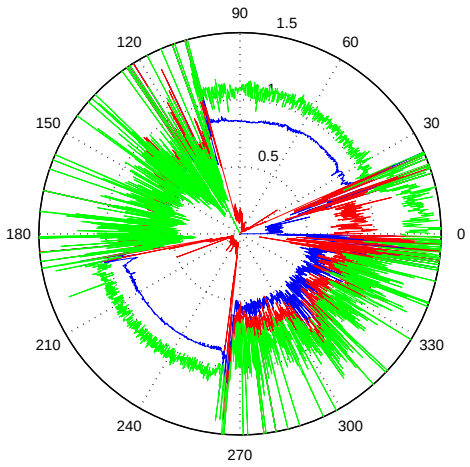

Figure 3.17: *CSI Analysis* - SISO system. Polar representation of the distance among the reference and measured CSI strings. Blue (1 - empty), red (2 - standing), green (3 - crouched). The estimated sequence of minimum distance is: 1-2-3-2-3-1, as expected.

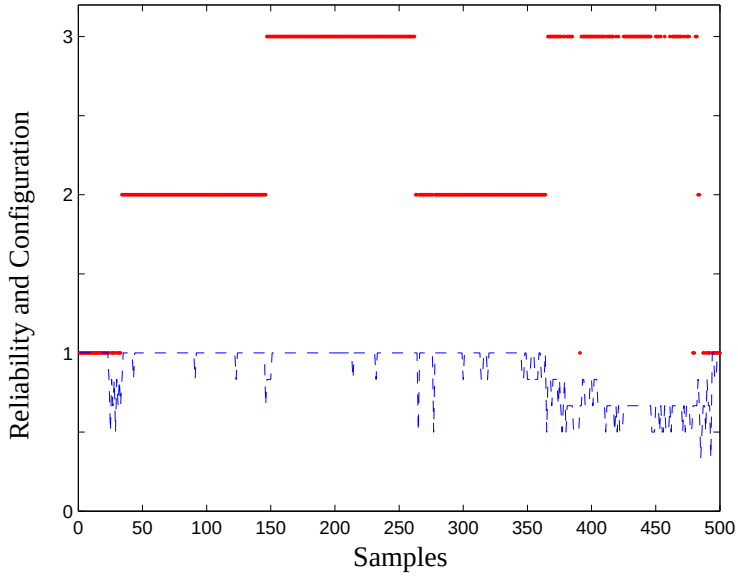

Figure 3.18: *CSI Analysis* - MIMO system (6 spatial links). Temporal evolution of the estimated scenario configuration (red), and of the degree of estimation confidence (blue). The estimated sequence is: 1-2-3-2-3-1, as expected.

3.3 Conclusions

In this Chapter, methodologies for the presence detection, the localization and the posture recognition of device-free passive targets in indoor scenarios have been presented. Both approaches, *(i) RSS*-based presence detection and *(ii) CSI*-based posture recognition, rely on the electromagnetic channel analysis of a single wireless link communication between two commodity devices without any hardware modification as they have been designed work in real-world scenarios where simple wireless architectures already exist for standard communications.

In particular, *(i)* exploits received signal strength *(RSS)* measurements by means of a Learn-by-Example *(LBE)* strategy for the extraction of the components in the frequency domain that are more affected by the target presence. The proposed method has shown being able to:

- detect humans approaching the monitored area exploiting a single wireless link between commercial wireless devices. The detection capability has been verified with different link lengths, up to the maximum wireless coverage (with *RSS* values close to the receiver sensitivity);
- cover a detection area ($\pi > 0.5$) of 250 $[m^2]$ (*Experiment 1*) using a wireless link of length $d_S = 11.9$ $[m]$, and up to 450 $[m^2]$ with a link length $d_L = 34.1$ $[m]$ (*Experiment 3*);

- estimate the target absence/presence with failure rates lower than 10 [%], even with the longer wireless link (*Experiment 3*);
- provide target detection in real-time (every $\Delta t = 0.6$ [*sec*]) processing the *RSS* data stored in a sliding time window of length $U \times \Delta t = 300$ [*sec*].

Further analyses are required to explore whether the proposed strategy can perform in different and more complex configurations. For example, the following points are currently under study to extend the potentialities of the method:

- the complex relation between the detection probability and the number of targets occupying the area is currently under investigation in order to better understand and formulate the detection sensitivity in presence of single or multiple targets;
- the detection area of a single wireless link strictly depends by the environment characteristics and by the complex indoor *EM* propagation. Current activities are focused on the estimation of the minimum number of links required to provide a robust detection in a desired area;
- further studies are aimed at understanding the relation between the coverage requirements for standard wireless communication and for the target detection in order to understand a-priori the detection capabilities of an existing wireless networks composed by multiple *APs.*

In Section *3.2 (ii)* the more accurate channel state information *(CSI)* is considered. This information is required by new high-speed MIMO communication standards (e.g., *IEEE 802.11n/ac/ax*) and can be exploited for real-time localization and posture recognition. In particular the *CSI* of a single *IEEE 802.11ac* Wi-Fi link acquired by commercial *OFDM-MIMO* Wi-Fi devices has been exploited in the form of interpolated *CSI strings* changing in the complex plane according to the channel frequency response. The huge information content of the *CSI* has been fully exploited focusing on the changes effectively related to the target presence, position, and posture accordingly to the proposed multi-resolution strategy. The feasibility to estimate multiple target features at different resolutions using a single *TX-RX* couple of Wi-Fi devices has been assessed by considering an experimental test case in a large indoor test area, the obtained re-sults have shown a satisfactory robustness of the *SVM*-based classification method, with an average failure rate lower than $\rho = 2.5$ [%]. In order to improve the reliability and the accuracy of the human posture recognition among a set of reference *CSI* configuration, a "choice of majority" strategy has been adopted. The Kolmogorov principle has been exploited to quantify the separability among the *CSI* strings and to estimate the temporal behavior of the passive human moving in proximity of the *MIMO* wireless links. A preliminary measurement campaign has shown the feasibility to use the key-concept of the Kolmogorov ϵ-capacity to extract the human information from the highly sensitive *CSI* data.

Chapter 4

Location-Aware Decision Support Systems

In this Chapter, the field of decision support systems (*DSS*) based on location information is considered.

In particular, a *DSS* tool for the environmental monitoring and the fleet management in the field of emergency response and assets coordination is illustrated. The system is interconnected with the assets on the field - vehicles and rescue teams by means of civilian and military communication networks, such as 3G,4G and *TETRA* respectively. Distributed wireless sensor networks and online data-sources feed the system with real-time information, such as road traffic and weather information, for providing situation awareness to the decision makers and the situation room operators. Finally, a novel method for supporting the selection of assets to be deployed for rescuing emergencies is proposed. The illustrated DSS has been experimentally validated by domain experts in real scenarios for more than two years.

4.1 Fleet and Emergency Management

The fleet and emergency management scenario deals with a highly dynamic, uncertain, and dangerous environment where the exchange of information and the coordination between civil defense actors are essential for mission accomplishment. The situation room operators have to take quick and proper decisions according to their interpretation of the situational picture. This is possible only when professional managers and first responders have access to the required information, and when the assets are ready to intervene with low latency [58] and supported by the situation room personnel and technologies during the operations on the field.

4.1.1 Decision Support System

The term Decision Support System (*DSS)* has been coined before the computer invention and was usually referred to hard copy documents and collections of experience-based best practices. Over the years, *DSSs* have been implemented and applied in a variety of scenarios [147]. With advances in information and communication technologies, advanced systems have been developed to improve the activity of decision-makers at different levels of the command chain.

Modern *DSS*s are able to rapidly gain the situation awareness thanks to the massive amount of data acquired by systems distributed on the territory, such as wireless sensors and wireless communication systems. The key characteristics of a *DSS* [148] are:

- assistance and improvement of human reasoning without replacing the human final control;
- adaptability to context changes and to the availability of new information;
- combination of analytical models that provide synthetic information automatically gathered from heterogeneous and distributed sources;
- user-friendly interactivity/interfaces;
- alleviation of efforts to amplify decision making capability of the operators.

One of the main factors affecting the decision-making process is that multiple groups (e.g., different kind of employers and stakeholders such as firefighters, policeman, medical first responders, volunteers, etc.) have often to cooperate in the same mission. The combination of different viewpoints (even if a common final objective exists), different internal organizations, heterogeneous resources including personnel, facilities, and equipment make the mission management difficult to be accomplished by standalone operators. The main role of a fleet and emergency management *DSS* is to provide situation awareness to the control

room and to support the selection and the activation of the best resources for the efficient accomplishment of each mission [59, 150]. Decision support tools based on this research do not aim to replace the operators, but to provide updated, reliable, punctual information and propose candidate solutions in order to support the process and reduce the risk of taking wrong choices, for example due to the emotional involvement. In the following, the main features and functional aspects that characterize decision support systems in the field of fleet management and emergency response are introduced.

4.1.2 Real-time Wireless Communication and Localization

Modern organizations and civil defense agencies exchange information and coordinate teams on the field by means of wireless technologies. In last decade, legacy voice communications relying on analog radio-frequency protocols are being replaced by digital systems that also provide real-time messaging, asset status notifications, localization, and the ability to share rich information about the mission among actors and the situation room [59]. In particular, real-time communication and messaging services for mission control can be provided by civilian technologies such as the global system for mobile communications (*GSM*), 3G, 4G long-term evolution (*LTE*) as well as more reliable and secure military telecommunication networks such as the terrestrial trunked radio (*TETRA*) [54]. The current status and the location of these assets is known thanks to more and more diffused location technologies such as global positioning system (*NAVSTAR GPS*) and newer technologies such as *GALILEO*. In particular, *TETRA* terminals and the communication system itself integrates the *GPS* positioning service. The *DSS* tool can exploit online mapping and routing services (e.g., Google Maps, Microsoft Bing, TomTom, etc.) for estimating the real distance on the road and for predicting the travelling time between asset location and mission destination at run-time by considering real-time road and traffic conditions.

4.1.3 Distributed Sensing for Situation Awareness

The ability to gather precise real-time information on the mission scenario is a key requirement for decision-makers. In smart cities, the spread of wireless sensors, interconnected devices (i.e., IoT) and online data-sources available on the Internet offers many advantages to the *DSS*. Some relevant examples are road-traffic information, weather conditions, river and floods level status, and high resolution video streams of strategic locations. The information, once normalized and aggregated by custom adapter software modules (as these data-sources are hosted by different organizations and available in different formats and protocols), can be exploited by the engine algorithms and directly offered to the

operators through the interactive front-end. All these data put the decision maker in the position of understanding the mission scenario characteristics from a practical and physical point of view.

4.1.4 Knowledge Base and Inference Engine

In order to provide useful information to operators and assist best practices such as the selection of assets to be deployed for accomplishing a given action, the *DSS* must be aware of a-priori information about available assets, supported missions taxonomy and their correlations. For example, the transportation of a good might require special vehicles supporting its weight and volume, therefore the characteristics of each vehicle must be available. In the emergency management scenario, more constraints are typically related to given mission kind with respect to personnel skills and on-board vehicles equipment.

4.1.5 System Security and Accessibility

In the fleet management scenario and in particular when dealing with emergency mission control, the assets location and mission information are strictly confidential and cannot be accessed by all users. Therefore the system must embed security mechanisms based on the organizational role assigned to the user.

4.1.6 Front-end Interface

In order to interact with emergency managers and situation room operators, the system shall provide an interactive user-friendly interface for having users access to information of interest including the setup of new missions and the output representation. Moreover the system shall provide useful information related to the fleet, such as the currently active missions and environmental information describing the target scenario.

4.2 Assets Selection for Emergency Response

In this Section, one of the most relevant problem in the field of emergency response - the selection of assets to be deployed for a given emergency event is addressed. For example, in order to put out a fire emergency, the situation room shall deploy specific fleet assets depending on the kind of fire, its context (i.e., location) and considering assets availability in real-time. The selection requires the simultaneous optimization of different objectives, for example taking into account the utility of selected assets with respect to mission accomplishment, the estimated time of arrival, cost, the risk of moving assets from their current location, the skills of personnel. In the following, the use of evolutionary metaheuristic is adopted for estimating the best set of assets to be selected for a given task.

4.2.1 Proposed Approach

The classical approach consists in reducing the multi-objective problem into a single-objective one by combining (usually linearly) the objectives [47], although in this kind of problems objectives are typically non-commensurable (i.e., in different units) and conflicting (i.e., the improvement of one leads to another objective degradation). As result, those classical techniques have serious drawbacks, in particular the functional definition requires a-priori information about the problem dynamics in order to balance the contribution of each objective by means of empirical weights and thresholds. In last years, multi-objective evolutionary algorithms (*MOEA*) have been applied in many fields where optimal decisions are taken in presence of trade-offs among multiple conflicting objectives [149]. Unlike single objective optimization, multi-objective optimization does not provide a single solution, but rather a set of idempotent solutions (i.e., the Pareto front), that eventually can be ordered by considering one objective at time. Hence, the term "optimize" means finding such solutions that would give the values of all the objective functions acceptable to the decision maker.

In the problem at hand, the solution defines how many and which assets shall be deployed for the given mission. The knowledge base of the system, which represents the features of entities (e.g., vehicle taxonomy and characteristics, requirements for handling emergency events, missions best practices) and the relationships between candidate asset and target mission features can be very complex to be fully represented and handled at run-time by an autonomous software system, in this work we propose a very simple feature mapping approach based on scalar weights that define the cross-correlations between such features. Given a target mission, the system selects from the knowledge base the set of suitable mappings (i.e., matrixes).

4.2.1.1 Features Definition

The system supports an extensible taxonomy of domain entities like vehicles and events, as well as standardized and user-defined features defined as key-value properties. Each property provides some granular information (e.g., classification label) that might be exploited in the decision process. For example, the vehicles are classified into five major categories *Aerial*-Vehicle, *Road*-Vehicle, *OffRoad*-Vehicle, *Amphibious*-Vehicle, *Water*-Vehicle and latter with a more specialized taxonomy defined by classes such as *Fire-Engine*, *Pick-Up*, *Police-Car*, *Ambulance* and so on. This approach has two major advantages: it's simple, human friendly, and easy to be obtained. Secondly, it synthetizes in a single high-level indicator many features related to the capabilities and the utility of the asset. Each event is classified and decorated with information that are usually acquired by emergency operators such as the location, the typology (e.g., *Fire*, *Landslide*, *Medical* or *Road* emergency), the number of injured people. Moreover some information are inferred from event meta data, such as the environmental characteristics of the event location that can be latter used for selecting the best suitable rescue vehicles (e.g., urban road, forest, on mountain, near a lake).

4.2.1.2 Features Mapping

Emergency operators and fleet managers plan asset deployment basing decisions on best practices and their experience, but a computerized system usually evaluates only mathematical rules such as the balance between utility and costs for a given *asset - event* tuple. Given an emergency, domain experts might define the knowledge base as the collection of relationships between assets features with respect to emergency event features. For example, we can assume that fire events require the early deployment of fire-engines rather than ambulances. These relationships can be represented as a set of matrices where each one refers to a mapping between one asset feature and one event feature, eventually under given conditions or filtered by some event properties. This simple approach brings some relevant advantages: it can be easily understood and edited by humans, and secondly it's fast, scalable and dynamic in terms of values, features mappings extension and pre-condition evaluation. The weights are typically initialized with empirical values assigned with the support of domain experts, but they also might be updated and tuned with respect to best practices by analyzing historical missions statistics, enabling the *DSS* to be self-adaptive.

At run time, the inference engine searches the whole knowledge base for each specific mapping query and retrieves the matching columns. For example, given a *Fire* emergency event, the Table 4.1 would be considered for estimating the utility of vehicle type given the event location. The vehicle type is mapped to the place (*Place-Type*) where a given fire event occurred (i.e., *Event-Type* set to *Fire* is the implied condition). Each cell element of the matrix defines the utility of a specific feature mapping tuple (e.g., *Off-Road* and *Urban*). An higher weight

implies that the related mapping is more suitable for the given context. In this case, we are instructing the *DSS* to prefer the selection of some vehicle types depending on target location, in particular the assumption is that the vehicle type *Off-Road* is more useful in sub-urban or extra-urban environment rather than in urban one.

Vehicle Type	*Place-Type* feature mapping of Fire Event			
	Urban	*Industrial*	*Forest*	*Mountain*
Normal Car	0.97	0.89	0.01	0.02
Off-Road Vehicle	0.20	0.25	0.85	0.78
Helicopter	0.01	0.20	0.78	0.95

Table 4.1: *Fleet Asset Selection*. A sample feature mapping matrix that define relationship between the type of place when the emergency (*Fire*) event occurred and the kind of vehicles that are suitable for deployment.

4.2.1.3 Decision Engine

The decision engine is responsible of preparing the problem context for a given input emergency event and running the solver algorithm that outputs the selection of assets to be deployed. First, the event and all available assets are loaded into problem context. Parameters which are constant with respect to problem scope are estimated only once during initialization, such as the matrix of routes and estimated time of arrival for each candidate asset. Secondly, the engine queries the inference engine for all available features mappings. All the matrices which validate pre-conditions (e.g., event type is *Fire*) and describe mappings related to any existing event feature are loaded. During optimization, the utility of each asset is evaluated by considering the weight of matching features. The cost of asset selection is estimated by considering the distance of the asset to event location, as well as the asset activation and travelling time.

4.2.2 Mathematical Formulation

In the problem at hand, a solution describes how many and which assets shall be deployed for the given event and takes into account three objectives: *(i)* the utility of selected assets shall be maximized, *(ii)* the dispatch time shall be minimized, and *(iii)* the cost of moving assets from its currently assigned location shall be also minimized. In practice, the solution can be represented as an ordered string of bits having length equal to the number of all candidate assets and where each bit enables the selection of one asset. For example, given a set $K = 10$ of available assets, one solution could be represented as the bit-string: $\{0\ 1\ 0\ 1\ 0\ 0\ 1\ 0\ 0\ 0\}$. Note that the cardinality (i.e., number of bits set to 1) of a

solution, that is the number of selected assets, is a variable in the optimization process.

For a given emergency event to be handled, the multi-objective optimization problem can be stated as follows:

$$\hat{\underline{r}}_{opt} = \min_{\underline{r} \in \Omega} \Theta\left(\underline{r}\right) \left(\frac{1}{U\left(\underline{r}\right)}, T\left(\underline{r}\right), C\left(\underline{r}\right) \right) \tag{4.1}$$

where a $\Theta\left(\underline{r}\right) : \Omega \rightarrow R^m$ consists of $m = 3$ real-values objective functions and R^m is called the objective space. A candidate solution $\underline{r} = [r_k;\, k = 1, ..., K]$ is defined as the set of $K \leq N$ assets selected from all available assets N. Since the objectives in 4.1 contradict each other, no point in Ω minimize all the objectives simultaneously. One has to balance them, the best tradeoff among the objectives can be represented in terms of Pareto front optimality. The definition of each objective term follows.

1. Maximize the utility of selected assets for the considered mission in terms of required personnel, vehicle features such as the typology, equipment and tools. The utility function $U\left(\underline{r}\right)$ is defined as the sum of selected assets utility:

$$U\left(\underline{r}\right) = \sum_{k=1}^{K} U\left(r_k\right) \tag{4.2}$$

   where the utility of each selected asset $U\left(r_k\right)$ is estimated by means of the inference engine taking into account the characteristic of the k-th asset with respect to given mission features and requirements and can be formulated as follows:

$$U\left(r_k\right) = \frac{1}{M} \sum_{m=1}^{M} \alpha_m \cdot H_m\left(r_k\right) \tag{4.3}$$

   where M is the total number of feature mappings $m = 1, ..., M$ found in knowledge base, in particular each mapping refer to one correlation matrix as the example shown in Tab. 4.1. The factor $0 \leq \alpha_m \leq 1$ represents an user configurable constant weight to balance feature relevance, the weight default value is set to $\alpha_m = 1$. H_m is the transfer function that selects the normalized weight of the specific asset-mission tuple of the m-th feature mapping from the knowledge base. In other words, the transfer function selects the weight of the m-th matrix that describes the correlation between input mission feature and m-th asset feature.

2. Minimize the dispatch time in terms of asset activation and traveling time, including also the route feasibility for selected asset as constraint (e.g.,

some arduous locations not reachable by road vehicles require the use of helicopters or drones). Formally, we define the objective $T(\underline{r})$ as follows:

$$T(\underline{r}) = \max_{r_k} [AT_k + RT(d_k)] \;\; for\, k = 1, ..., K \tag{4.4}$$

where the estimated time of arrival of k-th asset is the sum of the time activation time AT required to setup the asset for deployment (including personnel) and the vehicle travel time RT required to cover the distance d_k between the k-th asset and mission target location. Accordingly to domain experts, the K assets selected for the mission are considered as a monolithic group, therefore the maximum deployment time is considered (e.g., all assets must be at target location for mission accomplishment).

3. Minimize the cost of moving an asset away from assigned area. The idea behind this objective is that the deployment of some assets implies not only an economic cost (i.e., related to the consumption of resources, such as fuel) but also a risk of compromising the default behaviour of the fleet. In fact, under normal conditions, the fleet is distributed and moves on the field with some rational scheme defined by the organization logistic protocol. For example, a good transportation truck (and its driver) might usually travel forward and back along similar routes or in the same territory; in the emergency management scenario, an ambulance might be assigned to a reference parking location in order to guarantee an upper-bound rescue time in the nearby area. Formally, we define the objective $C(\underline{r})$ as the sum of selected assets cost contribution:

$$C(\underline{r}) = \sum_{k=1}^{K} C(r_k) \tag{4.5}$$

where the cost of each selected asset $C(r_k)$ is defined as:

$$C(r_k) = d_k \cdot [1 - \rho(x, y\,|r_k)] \tag{4.6}$$

where d_k is the estimated route length between the current position of k-th asset and mission target location (x, y), and $\rho(x, y\,|r_k)$ models the a-priori spatial correlation between the area usually covered by k-th asset and target mission location. In particular, the probability ρ is estimated against the recent history of the asset routes (e.g., one month of interpolated location samples). The more an asset is near and at ease with target location, the more is suitable for mission accomplishment.

4.2.3 Preliminary Assessment

The experimental assessment of DSS applied to emergency response field is not trivial as the civil defense agencies must follow well-known and consolidated practices and system when handling real situations. Actually we are still collecting data and logs from state-of-the-art methodologies (which are mostly based on personnel experience) in order to validate the solutions proposed by the DSS. In the meanwhile, we focused on the study and validation of the multi-objective evolutionary optimization approach itself in a small scale scenario. In particular, we are interested in evaluating which optimization algorithm is suitable and in comparing the performances of most used algorithms. The assets database has been populated with 10 fully featured vehicles of different kinds. The target emergency event is a fire in a carpenter's shop occurring in an industrial (suburban) zone. The multi-objective optimization process quality shall be evaluated in terms of two proprieties: convergence and uniform diversity. Many indicators for measuring these criteria have been proposed in literature, the most common metrics were considered:

- generational distance [153] is a metric representing how "far" the non-dominated solution set found at a given iteration is from a reference set (i.e., the Pareto front);
- hyper-volume [154] represents the n-dimensional (i.e., 3) space "contained" by a set of points and measures the spread of the solutions along the Pareto front as well as the closeness of the solution set to the optimal front;
- maximum spread [155] takes into account the proximity to the true Pareto front in terms of the objective functions range (i.e., min/max).

It should be noted that most interesting performance metrics require the Pareto optimal set, when the true optimal set is not defined (as in this case), the best known approximation might be used. In the proposed example, the reference set shown in Fig. 4.1 were generated merging results of all the algorithms using a very high number of iterations (i.e., 5000), population size (i.e., 100) and seeds (i.e., 50). The following algorithms have been considered: Duplicate Elimination Non-domination Sorting Evolutionary Algorithm (DENSEA) [156], Multiobjective Optimization Evolutionary Algorithm Based on Parameter ϵ (ϵ-MOEA) [157], Nondominated Sorted Genetic Algorithm II Based on Parameter ϵ (ϵ-NSGAII) [158], Fast Pareto Genetic Algorithm (FastPGA) [159], (General) Indicator Based Evolutionary Algorithm (IBEA) [160], Multi Objective Version of a Cellular Genetic Algorithm (MOCell) [161], Multi Objective Version of Convex Hull Contribution (MOCHC) [162], Nondominated Sorted Genetic Algorithm II (NSGA-II) [163], Nondominated Sorted Genetic Algorithm III (NSGA-III) [164], Pareto Archived Evolution Strategy (PAES) [165], Second Version of Pareto Envelope Based Selection (PESA-II) [166], Multiobjective selection based on

dominated hyper-volume (SMSEMOA) [167], Second Version of Strength Pareto Evolutionary Algorithm (SPEA-II) [168]. All algorithms were configured with a population size set to 20; the optimization is limited to 500 iterations. Run-time metrics have been collected and aggregated for each algorithm using 10 random seeds.

The results of most interesting indicators, including processing time are listed in Tab. 4.2. Algorithms have been compared by means of standard optimization metrics and with respect to Random search which proved to be much slower even in such small-scale scenario taking into account a limited domain space (i.e., any possible combination set of the 10 candidate assets). We can notice that ϵ-MOEA and IBEA methods have a zero generational distance, meaning they perfectly match the approximation set used as reference set (assumed as the true Pareto front) and shown in Fig. 4.1. The Hyper-volume indicator is stable for all algorithms, as rule of thumb the higher value the better computed front. The spread takes zero value for an ideal distribution, pointing out a perfect spread of the solutions in the Pareto front, such as in the DENSEA case. We expect that as the problem complexity grows (i.e., considering more candidate assets and more features), the gap between considered strategies will grow. Future work will focus on the extension and the validation of the knowledge base and the assets database, also analyzing statistical effects of weights value distribution on results. We will also introduce equipment entries (e.g., water, CO2 detector, hydraulic clamp) and their relationships with vehicles and events both.

	Performance Metrics			
Algorithm	*Generational Distance*	*Hyper-volume*	*Spread*	*Time [ms]*
Random Search	$7.06693 \cdot 10^{-3}$	0.74794	6.11135	125.284
DENSEA	$0.09374 \cdot 10^{-3}$	0.41656	0	40.54
eMOEA	0	0.76876	4.4115	60.935
eNSGAII	$0.13795 \cdot 10^{-3}$	0.7865	5.99173	44.834
FastPGA	$0.96136 \cdot 10^{-3}$	0.78582	5.98473	73.856
IBEA	0	0.77759	12.8435	50.358
MOCell	$0.53598 \cdot 10^{-3}$	0.78741	5.69376	56.463
MOCHC	$0.85239 \cdot 10^{-3}$	0.77102	6.41539	50.183
NSGAII	$0.78629 \cdot 10^{-3}$	0.78081	6.55847	19.331
NSGAIII	$0.14822 \cdot 10^{-3}$	0.77052	6.13967	21.852
PAES	$0.26930 \cdot 10^{-3}$	0.78699	6.19187	34.538
PESA2	$0.62066 \cdot 10^{-3}$	0.78808	5.6668	43.421
SMSEMOA	$0.30632 \cdot 10^{-3}$	0.78729	6.13085	87.838
SPEA2	$1.41677 \cdot 10^{-3}$	0.78584	5.93479	70.969

Table 4.2: *Fleet Asset Selection.* Key Performance Indicators of the multi-objective optimization process with respect to different algorithms.

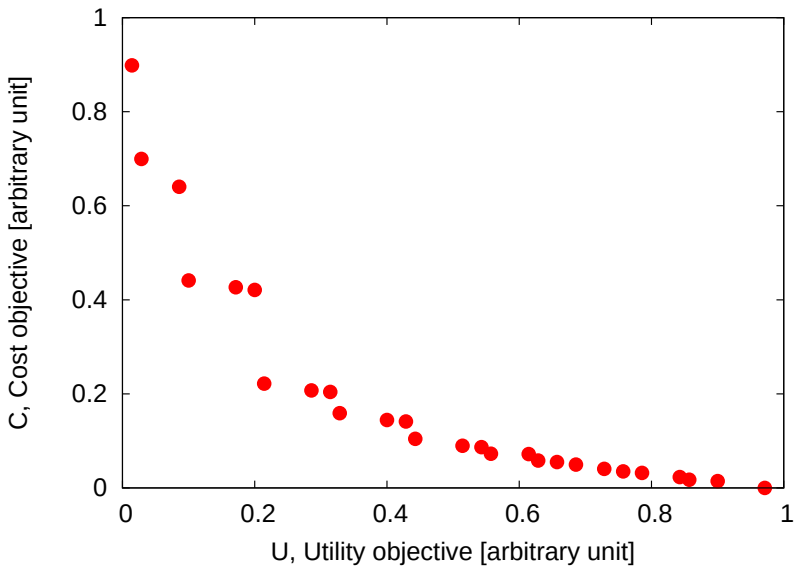

Figure 4.1: *Fleet Asset Selection.* The approximation set used as reference set (Pareto Front) for computing performance metrics of the Utility and Cost objectives.

4.3 System Architecture and Features

This Section introduces the system architecture, components and the main features of the proposed *DSS* tool for the fleet and emergency management scenario. Civil defense units exchange information and often coordinate the rescue teams interventions by means of wireless technologies. Namely, *INSPECTOR* is a geographic informative system (*GIS*) that supports operators in the situation rooms and on the field for monitoring the environment, tracking assets (e.g., vehicles, helicopters, drones) and that assists decision makers for mission planning and coordination.

The proposed system is based on a modular architecture distributed across different networks and infrastructures. This approach is not only required for interacting with external software, hardware and telecommunication systems located in different physical facilities, but also to support the redundancy requirements and to simplify the maintenance operations. The system modules, including user front-ends, device firmware, mobile applications, databases and bindings with external systems, are interconnected by means of highly secured wireless channels, including the *TETRA* standard (Fig. 4.2). Accordingly, the platform is usually installed in a redundant clustered environment as shown in Figure 4.3 rather than as a single instance (Fig. 4.4).

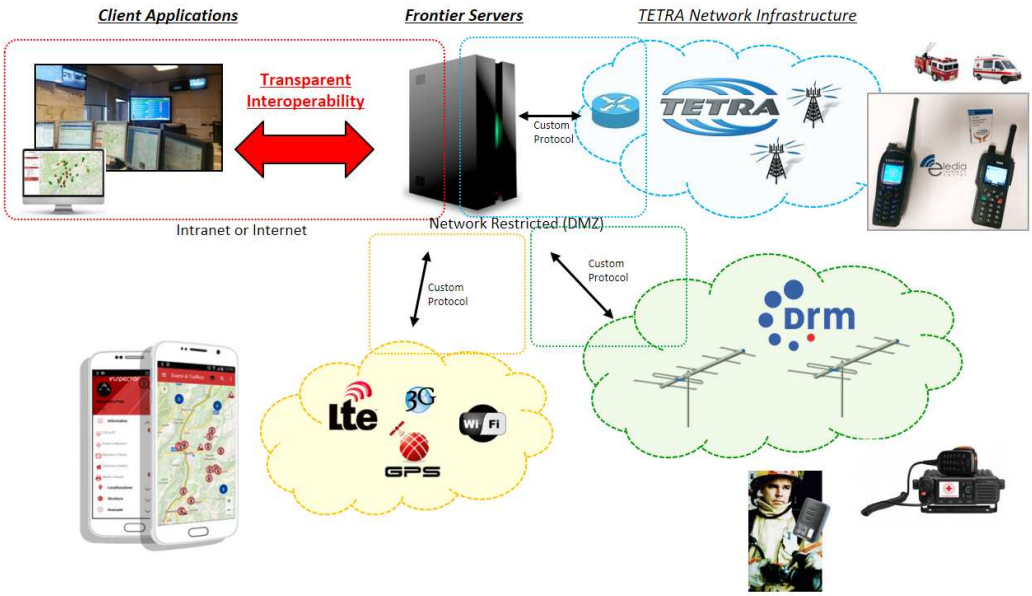

Figure 4.2: *INSPECTOR* - Network Architecture. The application clients are connected to the frontier servers that provides access to other networks and information.

The system can be transparently extended by means of remote hooks and adaption layers, in order to support more communication protocols, information data sources, and actuators. Modules, such as data-sources (i.e., adapters), services and database drivers have been designed in a modular manner and requiring minimal dependencies in order to be easily maintained. Components interact by means of a well-defined Application Programming Interface (*API*) and the system provides a wide set of built-in implementations of real-world entities, such as radio devices, vehicles, events, professionals, teams, and missions.

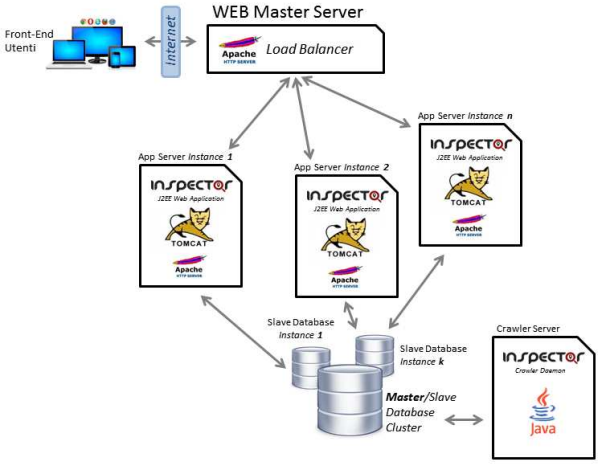

Figure 4.3: *INSPECTOR* - Production Platform. The standard architecture based on replicated instances in terms of front-end and database. The approach grants high reliability and supports many simultaneous users.

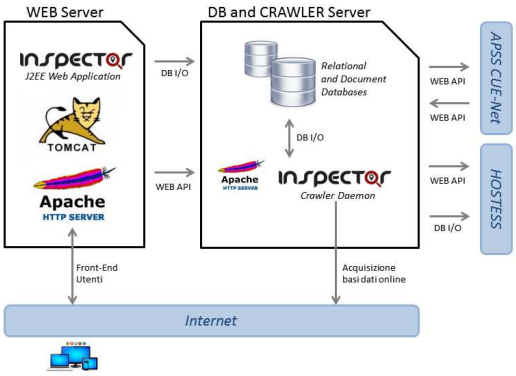

Figure 4.4: *INSPECTOR* - Minimal Platform. The architecture in a non-clustered environment, ideal for development, beta testing and backup installations.

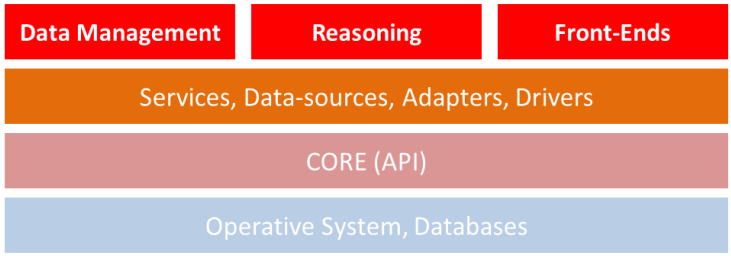

Figure 4.5: *INSPECTOR* - Framework Architecture. The framework is based on modular packages, the core API provides all interfaces used by modules.

On top of Figure 4.5 the three major aspects of the system are shown: data-management, reasoning, and front-end. They have been split in different daemons and applications, designed to cooperate across multiple servers through RESTful services and eventually and enterprise messaging bus (*AMQP*). Due to the high confidentiality level of the treated data (i.e., location history or emergency events) and the access by users with different levels of privilege, the system is required to support multi-user and multi-group security policies. The decision support modules exploit the integration of different data like traffic and viability, meteorological real-time indicators and forecasts as well. In this sense, the proposed system is a collector of heterogeneous information acquired periodically and in real-time from distributed monitoring systems and professional telecommunication networks such as *TETRA*. This complex task is accomplished by the data-management modules. The location module is responsible of acquiring positioning information from external data-sources, such as the terminals of the *TETRA* network, mobile devices, or *GPS* modules. In fact, the *TETRA* standard enables not only voice calls but also advanced data and positioning services. The real-time locations are stored in the central databases and analyzed in runtime for monitoring the lifecycle of planned operations, eventually triggering alerts and reactions. The reasoning engine takes care of solving the problems proposed by the user (e.g., planning a mission), it performs classification and data mining tasks to extract useful information from available knowledge base and live data streams. For example, traffic and viability events can be exploited to improve suggested routes and selection of roads to vehicles, while weather and wind statistics and forecasts can be used to predict the flight conditions of helicopters and drones.

The system provides multiple front-end clients, summarized in next sub Sections, that are customized for web and mobile platforms. The user interface for situation room exploits state-of-the-art *HTML5* web technologies and it is accessible through standard Internet browsers (Fig. 4.6). Applications for mobile devices (e.g., smartphones and tablets) have been designed to provide real-time bidirectional communication with the headquarters(Fig. 4.7). For example, the synchronization of the mission information and the navigation routes, the loca-

tion and the state of the assets, as well as the multimedia content are constantly shared with the situation room. Toward this end, the geo-referenced information are accessible through an interactive geographic map with thematic layers (e.g., assets, events, sensing stations, points of interest, etc.) and grouped in a hierarchical tree, each layer can be activated as it is required. Data is stored in relational (*SQL*) and *NO-SQL* databases.

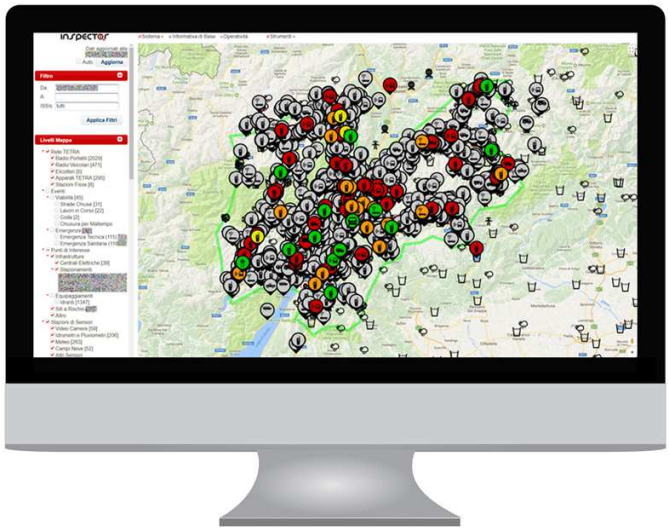

Figure 4.6: *INSPECTOR* - Screenshot. The web interface based on HTML5 technologies showing the location of the fleet and distributed sensors.

Figure 4.7: *INSPECTOR* - Screenshot. App optimized for Mobile devices.

4.3.1 Fleet Positioning and Tracking

The operators in the control room monitor the movements of assets on the interactive map. Therefore, operators are constantly aware of fleet movements and they can support the on-field navigation by sending suggestions about the best route and providing reference points to the drivers. The system is connected in real-time with fleet and external data sources by means of pluggable module adapters. The client application for mobile devices (i.e., *Android 4.1* or later) has been designed to support location features similar to the *TETRA LIP* technology, including asynchronous location requests and real-time reconfiguration. The system is also able to reconfigure the settings of remote terminals in real-time (e.g., the transmission frequency of terminal position can be adaptively controlled to manage the power supply according to the risk level of the operation). As a matter of fact, any positioning technology such as low-cost global positioning system (*GPS*) is transparently managed by the system. The system exploits online mapping and routing services (i.e., Google Maps *API*) for estimating the real distance, the route and the travelling time between two locations.

The real-time fleet monitoring interface (Fig. 4.8) shows the current location and recent movements of each asset. The kind of asset is graphically identified by a custom icon (e.g., vehicle, handheld radio, helicopter), the asset status with respect to active missions is highlighted by using different background colors (e.g., the green background means that the asset is available). Finally, the recent track of each asset is shown using different pseudo-random colors (aligned to icon border). In the left panel, the operator can apply filters on time and asset type, configure advanced display options, and export data.

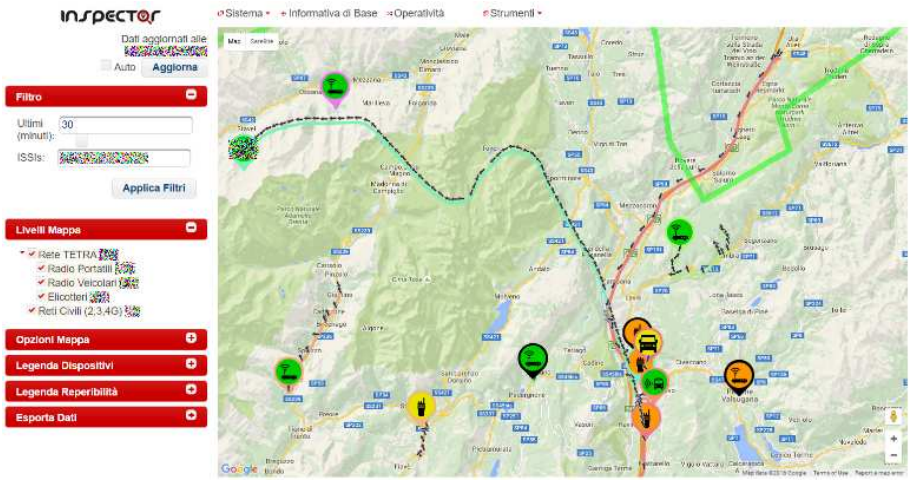

Figure 4.8: *INSPECTOR* - Screenshot. The map showing typology (icon symbol), position, recent route, and status (color) of assets on the field.

4.3.2 Interoperability with Military Network (TETRA)

TETRA is a digital trunked mobile radio standard developed by the European Telecommunications Standards Institute (*ETSI*) and designed for providing professional data, voice and positioning services in critical applications such as military and civil defense missions. Since 1995, *TETRA* has been spread to traditional professional mobile radio user organizations such as public safety, transportation, oil and gas utilities. In fact, *TETRA* is the only wireless network that was approved in Schengen agreement to serve as public safety and security (*PSS*) network in Europe. Modern *TETRA* hardware, such as base-stations and terminals, is deployed by international manufactures (e.g., *Motorola*, *DAMM*) and is available in more than 114 countries.

The interoperability with vehicles and helicopters as well as with personnel equipped with *TETRA* terminals in terms of real-time positioning, tracking and exchange of information (e.g., asset status and textual messaging) is implemented by another standalone software system which acts as smart gateway between the *TETRA* network and high-level external clients - applications such as the proposed *DSS* tool. The system enables the seamless access and interaction with remote *TETRA* terminals.

The network architecture, shown in Figure 4.9, allows to overcome some important practical limitations of the *TETRA* terminals (e.g., vehicular and hand-held radio) that typically allow only a single entry (*ISSI* address) for the central *TETRA* application server that is allowed to perform actions on the radio and that is the recipient address of positioning datagram (*LIP* protocol). The software gateway allows multiple remote applications to interact with the networks and to receive asynchronous updates from remote *TETRA* devices, such as their status and location.

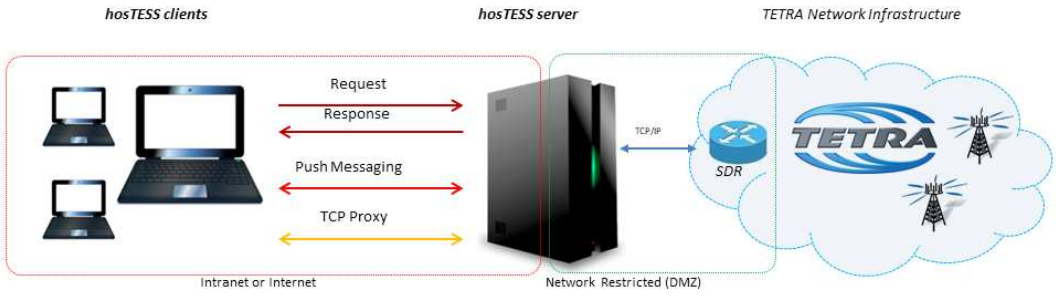

Figure 4.9: *HOSTESS* - Network Architecture. Client requests and asynchronous data from the TETRA network are stored, translated and forwarded to/from TETRA on-air protocol used by the TETRA SDR network component by means of TCP/IP channel.

The key features of the framework follows:

- it enables the seamless interaction with remote *TETRA* terminals;
- it extends many *TETRA* functionalities in terms of status management, textual messaging, real-time localization and tracking (spontaneous and on demand), on-air reconfiguration of remote terminals (e.g., how and when a terminal acquires its location), batch operations of many devices at once;
- it implements the most used part of *ETSI* (on-air) *TETRA* protocol, and in particular the full stack of the Location Information Protocol (*LIP*);
- it support granular security to each feature on the basis of account (or access token) permissions and roles;
- it stores every information to the persistent database (e.g., locations, messages, terminal configuration);
- it is a modular, extendible software framework;
- it supports most used communication protocols (*HTTP REST*, *AMQP*, *SQL*, Web interface);
- it is connected to *TETRA* network through *TCP/IP* communication (with the Short Data Router component);
- the framework Application Programming Interface and the Software Developer Kit (e.g., including a fully-featured network simulator) are well documented, the whole software is written in Java;

The system architecture consists of a central server component that communicates on *TCP/IP* with the Short Data Router (*SDR*) of the *TETRA* network and a second server that supports the database and interconnects the remote software applications - clients offering well-known communication protocols such as *HTTP REST*, *AMQP* Messaging and *SQL* database accessibility (Fig. 4.10). The embedded web administration of the gateway allows authorized users to monitor the system, browse and search data (e.g., statuses, messages, locations), interact with remote terminals and apply new configurations of the air (e.g., increase the frequency at which a terminals transmit its location). In Figure 4.11, the dashboard of the gateway shows the some overall statistics, the status of the *TETRA* connection link and recent information on interest.

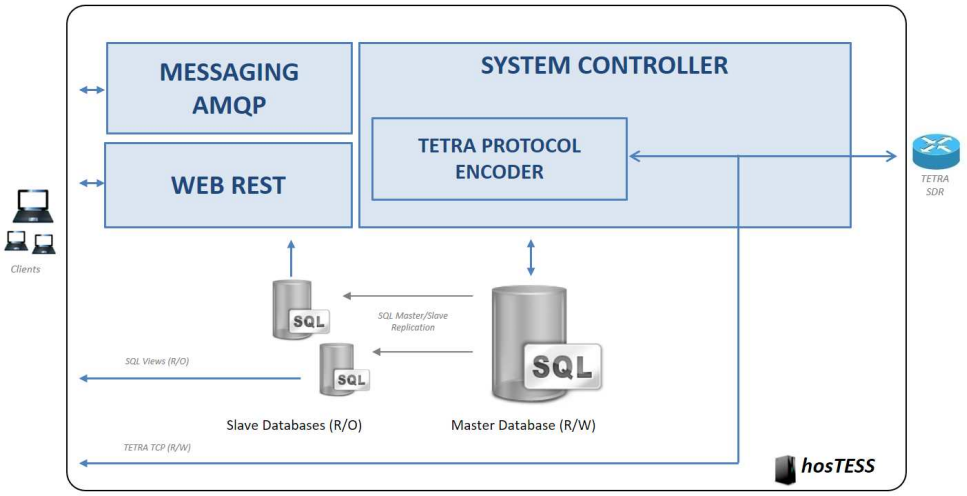

Figure 4.10: *HOSTESS* - I/O Flow scheme. The TETRA protocol channel is (de)coded to higher level communication standards (Push messaging, HTTP REST) and reliable databases for data persistence.

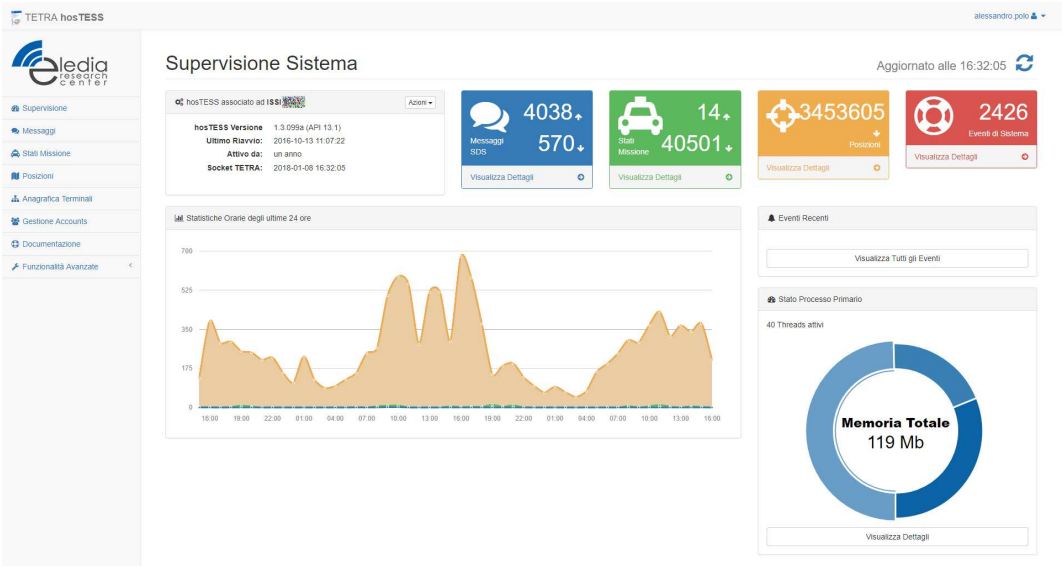

Figure 4.11: *HOSTESS* - Web Interface for Administrators. It allows users to monitor system status and interact with remote TETRA terminals.

4.3.3 Interoperability with Civil Networks (3G,4G)

The web front-end is accessible on the Internet from any device equipped with a standard web browser, including smart-phones and tablets, although a native mobile application for Android platform has been implemented in order to improve the usability of the most used features, such as map navigation, for operators and decision makers on the field (Figure 4.12). The *INSPECTOR* Mobile application is particularly interesting as it provides also remote sensing and actuation functionalities through the user device by means of a secure bidirectional communication channel with the central architecture. The communication channel, based on *Google Cloud Messaging* technology, allows the device to post on the server acquired information as well to execute locally some actions requested by the server. In particular, most interesting features follows:

- Access to all information in a modern hierarchical card-view layout
- User Positioning using Android Location services (*GPS*, Wi-Fi)
- Remote Reconfiguration of localization settings (e.g., push location modalities and frequency)
- Push Textual Notifications and Map-routes (e.g., a target location to be reached sent by control room)

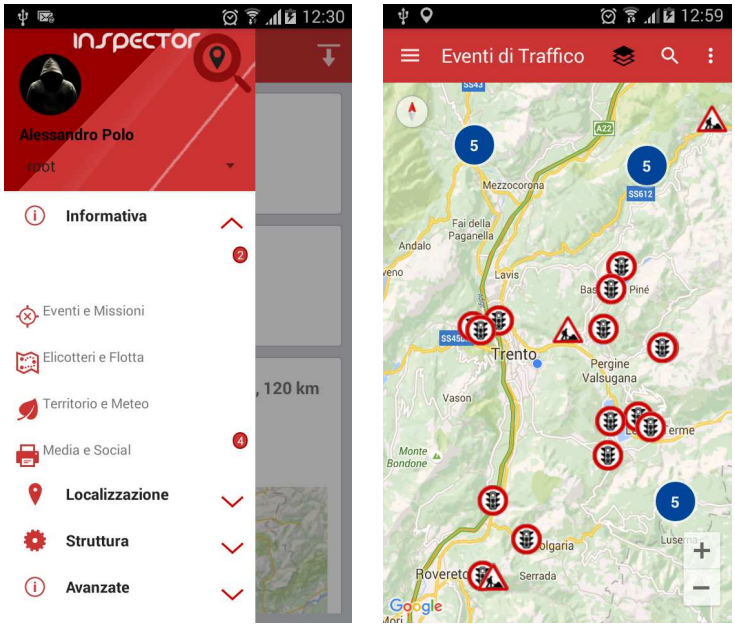

Figure 4.12: *INSPECTOR* - Screenshot of Mobile App for Android devices. On the left, the main menu; on the right, the map of road-traffic events.

4.3.4 Routes Analysis and Fleet Statistics

In order to improve the efficiency assessment of the situation room response and the coordination of rescue teams as well as to enforce the best practices, past missions are periodically evaluated by quality managers. The proposed *DSS* provides visualization and reporting tools for the statistical analysis of historical locations of the assets. Figure 4.13 shows an example of a vehicle track (i.e., a set of location samples acquired in a given time period) that has been automatically segmented in chronological itineraries and associated to the intervention missions. In particular, the system automatically analyzes space-time correlation between location samples and related missions, when the distance in term of time or space of two sequential locations is not statistically coherent with the samples distribution (i.e., 2nd and 3rd order statistics), a new path is assumed.

The user can generate mission reports, which describe the assets involvement, also aggregated according to predefined key performance indicators (e.g., asset typology, owner unit, distances, paths, etc.). Finally, the system can export data in most common format to be imported in third-party *GIS* tools for further analysis.

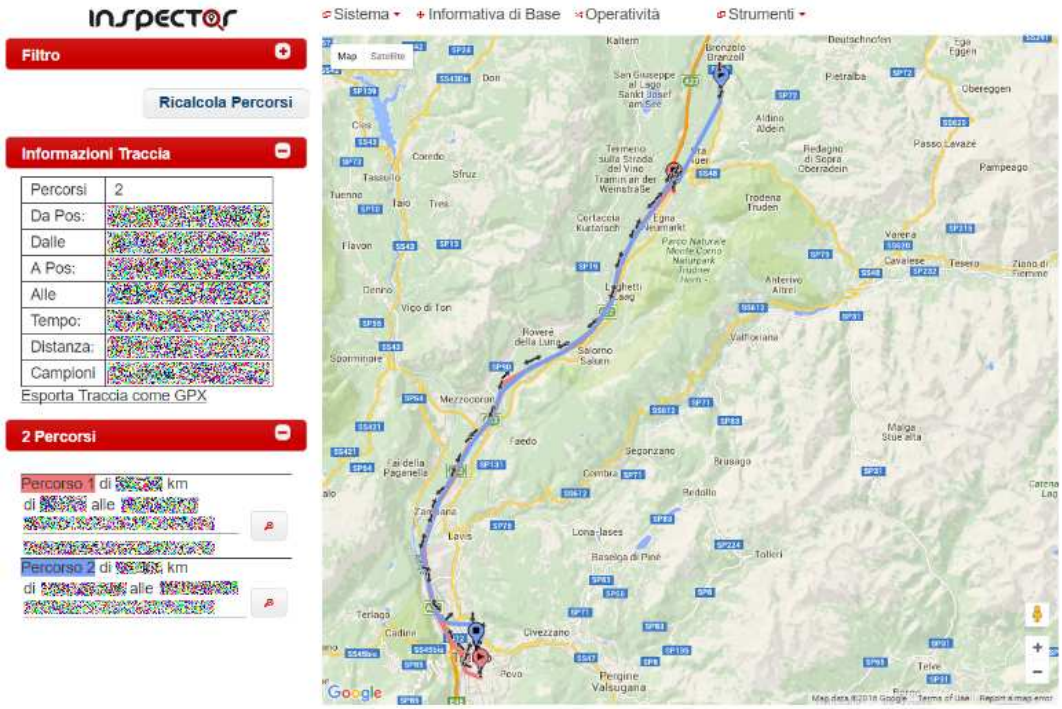

Figure 4.13: *INSPECTOR* - Screenshot of Asset Tracking front-end showing the route of a vehicle in a given period. Two different itineraries ('Percorso 1' and 'Percorso 2') of the considered route are highlighted (i.e., forward and backward travel). On the left panel, overall statistics and details about each path are shown.

4.3.5 Distributed Wireless Monitoring

The ability to gather precise information about the target environment during an emergency is a key requirement for decision-makers. The spread of low-cost wireless sensors as real-time data sources offers many advantages to *DSS*s, although such information is typically hosted by different organizations and made available in custom formats and third-party applications. A key feature of the proposed solution is the seamless integration and the aggregation of heterogeneous sensing sources in the same user interface. Decision-makers in the situation room and operators working on the field can easily access real-time information such as road-traffic, weather conditions, river and floods level status, and high resolution video streams of strategic locations. In fact, the system has been designed to support the integration of any kind of data stream coming from distributed networks of sensors by means of a modular plugin-based architecture that can be easily extended as the needs and the availability of information grows.

The environmental monitoring interface shows acquired information in the same map for providing situation awareness to the operator. In particular, environmental monitoring data-sources are organized in the layers tree shown in the left panel and includes:

- road events - the traffic status and the presence of works on the roads
- emergency events - the current events handled by civil defense agencies (i.e., medial rescue, fire-fighters)
- weather conditions - the live data acquired by weather stations installed on the field
- hydrometers - the level of rivers and lakes
- video-cameras - for monitoring roads and places of interest
- point of interest and localized equipment - such as critical infrastructures and hydrants for fire-fighters

The user can access to real-time data by clicking on each asset icon. The latest status of each sensor data-stream and the recent history (up to 12 hours) are cached locally by the system and information is exploited within the assisted procedures such as the select of asset to be deployed to an emergency event. For example, at the time of writing the installation of the tool counts more than 59 video-cameras installed at strategic urban locations and along the highways (Figure 4.14), 263 weather stations measuring air temperature, precipitations and wind (Figure 4.15), 206 hydrometers monitoring main rivers and floods are monitored (Figure 4.16), 52 snow sensor stations for monitoring and preventing avalanches during the winter period. Points of interest includes road events

(Figure 4.17), 39 critical infrastructures, 1347 hydrants of the city of Trento (Figure 4.18), and 17 sites at risk (i.e., seismic monitored areas).

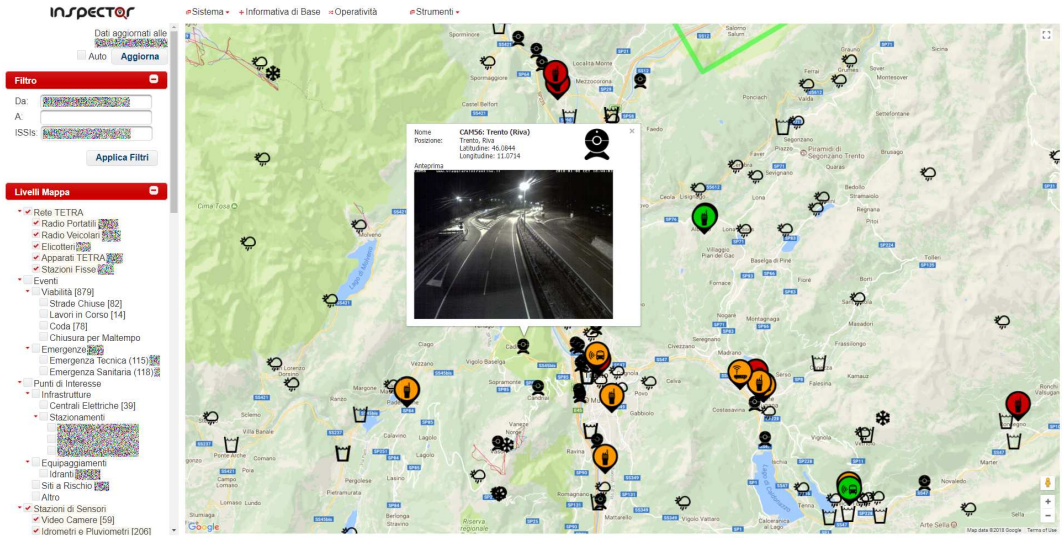

Figure 4.14: *INSPECTOR* - Screenshot of Environmental monitoring front-end showing Video cameras. The real-time snapshot of the video stream is shown in the embedded popup window.

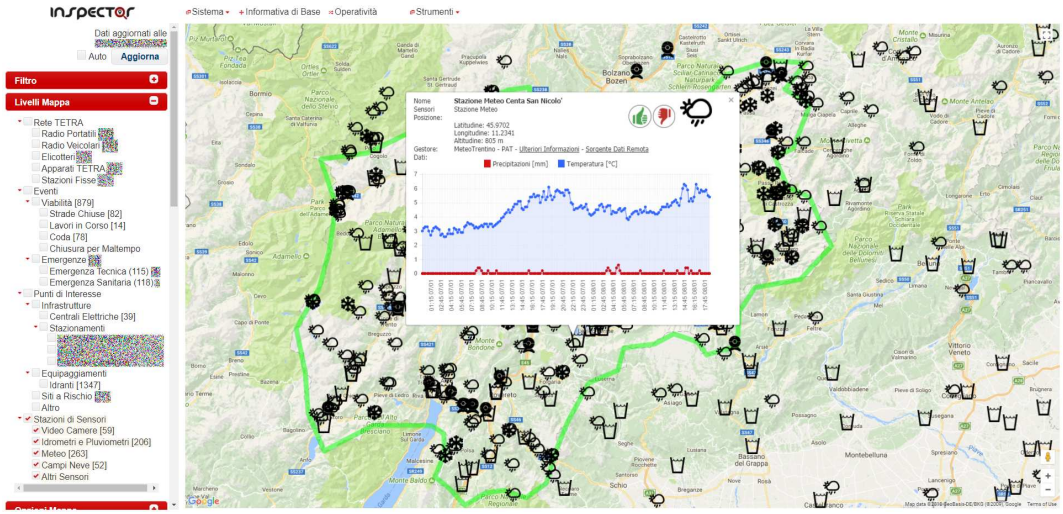

Figure 4.15: *INSPECTOR* - Screenshot of Environmental monitoring front-end showing Weather Stations and Hydrometers. The information and the recent history of data (e.g. air temperature and precipitations series) acquired by selected weather station are shown in the embedded popup window.

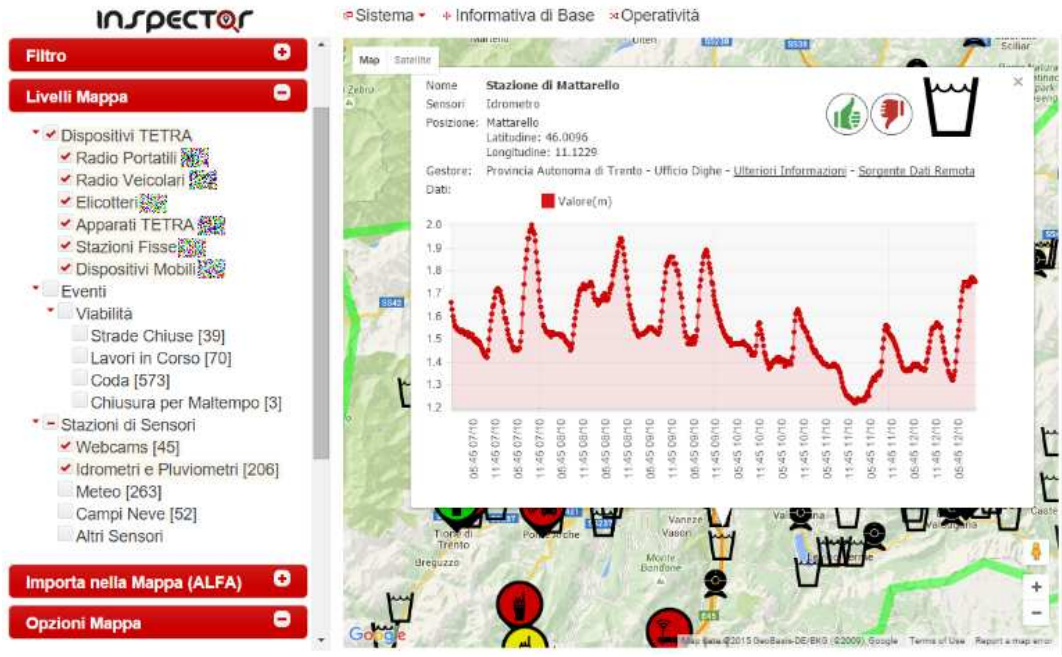

Figure 4.16: *INSPECTOR* - Screenshot of Environmental monitoring front-end showing Weather Stations and Hydrometers. The information and the recent history of water level (and/or flow) acquired by selected Hydrometer is shown in the embedded popup window.

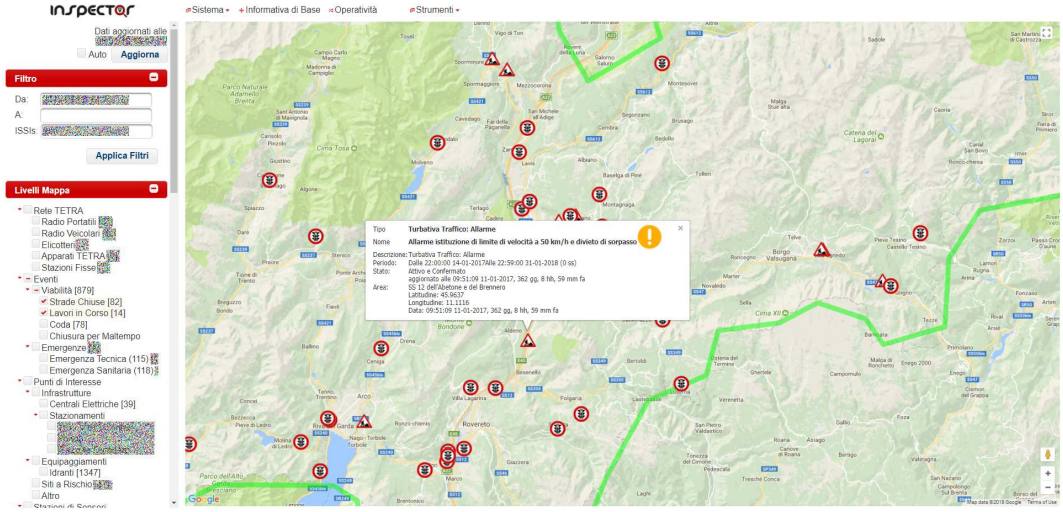

Figure 4.17: *INSPECTOR* - Screenshot of Environmental monitoring front-end showing Road Events layers (only). The information and metadata of interest about selected event are shown in the popup window (event type, description, duration, last update).

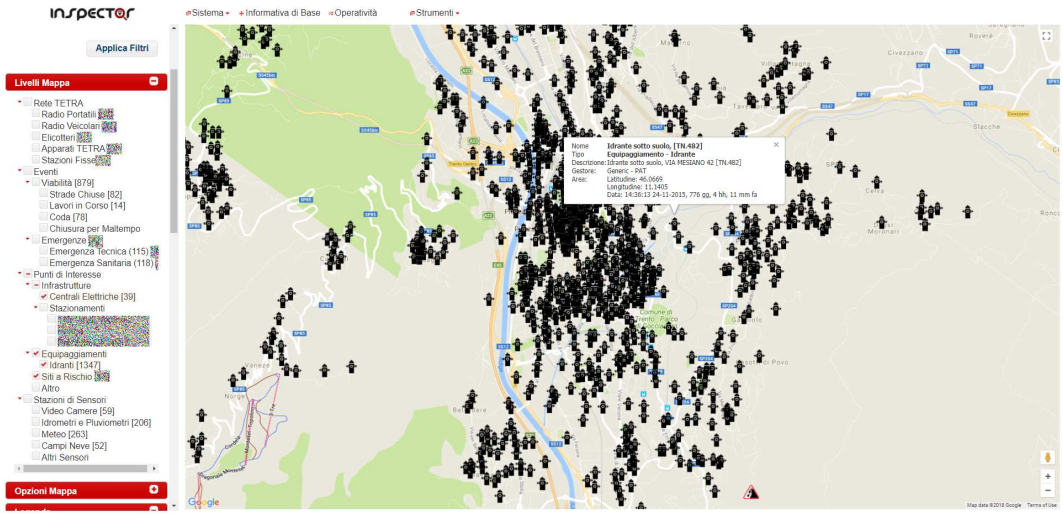

Figure 4.18: *INSPECTOR* - Screenshot of Environmental monitoring front-end showing Points of interest. In particular, hydrants of the city of Trento are useful information to fire-fighters for mission planning and fire-engines routing.

4.3.6 User Accounting and Security Management

The *DSS* tool implements advanced mechanisms for enforcing security and restricting the operations accordingly to the organization and the roles of the user. Any operation on the system requires the user to be recognized - authenticated for security and privacy issues. The access to information and system features is authorized by considering explicit permissions as well as privileges inherited from user roles and memberships. In fact, the system might be accessible not only by the situation rooms of central emergency agencies but also by operators and decision makers on the field by means of Internet connection and a compatible device (i.e., any web browser).

In particular, the system security is based on *Apache Shiro* framework which is a powerful Java security framework that performs authentication, authorization, cryptography, and session management. The *Shiro* framework has been extended for matching the system requirements including account definition, the support of fine permissions granularity and the application of user privileges on changes in real-time (i.e., not requiring the target user to logout and login again). An account defines the information necessary to uniquely identify and authorize the access to system features and data. The system administration might grant to each single user the access to high-level functionalities (e.g., ability to view a map-layer) as well as specific operations to each system entity (e.g., a device, an event, a point-of-interest). A typical example is granting the visibility of assets location, and the possibility to request and obtain the real-time location of a remote terminal on demand.

An account is typically associated with an individual, but it is possible to define virtual accounts that are shared by multiple people, such as in the case of operators in situation rooms and emergency call center. The account holds login credentials (username and encrypted password), roles (that implies privileges), relationships with organization, explicit permissions, network access limitations, the account status and scheme- free metadata. The logical states of an account are listed in chronological order as follows:

1. Created. The account was set up by the administration that validates the essential information: name, surname, email and defines the granted permissions, such as which assets share which information (e.g., location tracking). The account is in a transient state and is not yet usable;

2. Enabled. During the creation or at a later time, the administration enables the account for access and eventually defines a time period in which the account is valid. It is not possible to access the system by a not-enabled account. As enabled, the account can be activated by the user autonomously; (at this point, the administration notifies the user of the availability of the account through the system mailer)

3. Activated. The user completes the automated activation procedure described in the mail my accessing to the Account management application. Once the identity is confirmed and the user accepts the terms of use (license), the account is activated and accessible (even if a password has not yet been set);

4. Accessible. The account can access to granted features. After the activation procedure or at any time (i.e., in the case of lost password), the user can restore the access and reset the password through the automated procedure based on two-way secret links sent to the private user email.

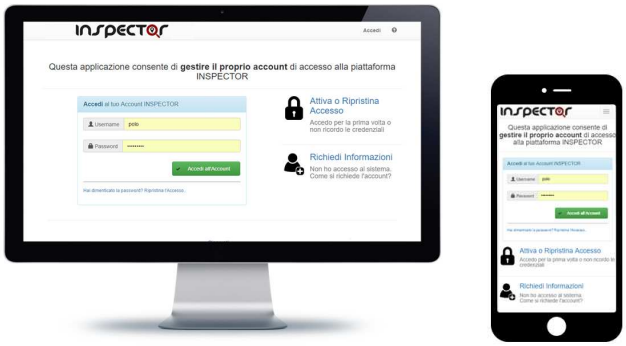

Figure 4.19: *INSPECTOR* - Screenshot of Account Management front-end on desktop (on the left) and on mobile (on the right).

In terms of user interaction, all aspects are managed by a custom web-based tool (Figure 4.19) that *(i)* allows standard users to activate and ti restore the account (Fig. 4.20), to edit profile details and to review events related to the account activity (Figure 4.21), and *(ii)* supports system administrators with most common operations such as creating, searching and updating existing accounts details (Figure 4.22) and privileges (Figure 4.23). Batch operations on multiple accounts and the sending of massive emails are also supported (Figure 4.24).

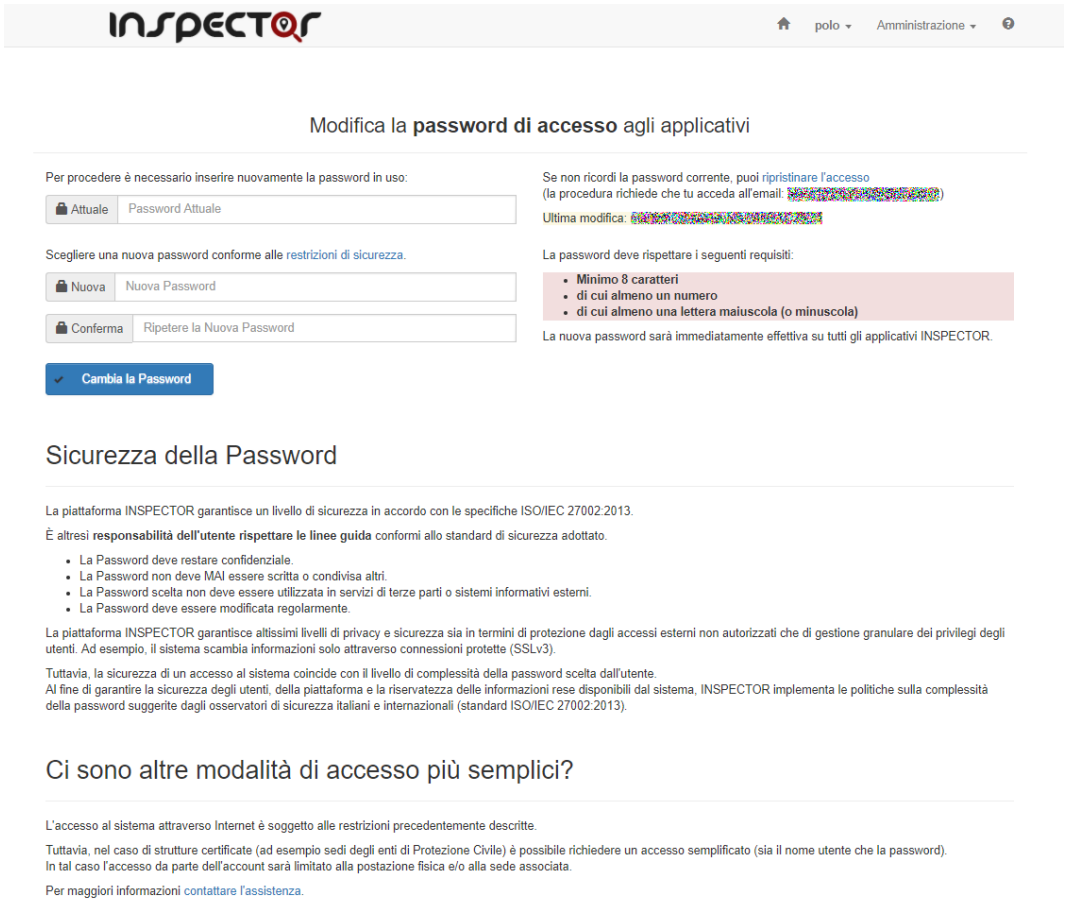

Figure 4.20: *INSPECTOR* - Screenshot of Account Password Reset. The front-end prompts the procedure for resetting the password (user identity has been verified through the email by sending secret temporary web link).

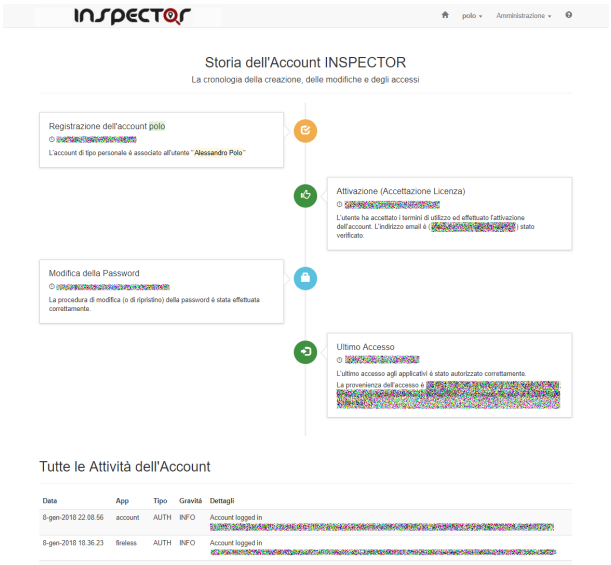

Figure 4.21: *INSPECTOR* - Screenshot of the Timeline of an Account. The table at bottom page lists all activities for security checks.

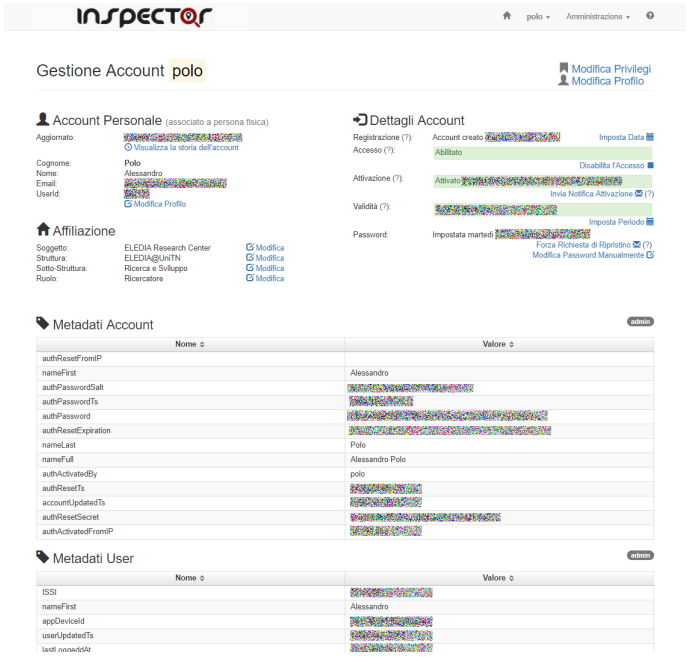

Figure 4.22: *INSPECTOR* - Screenshot of Account Management. The panels at the top let administrators to edit details inline and to execute most common actions such as (de)activation, password restore.

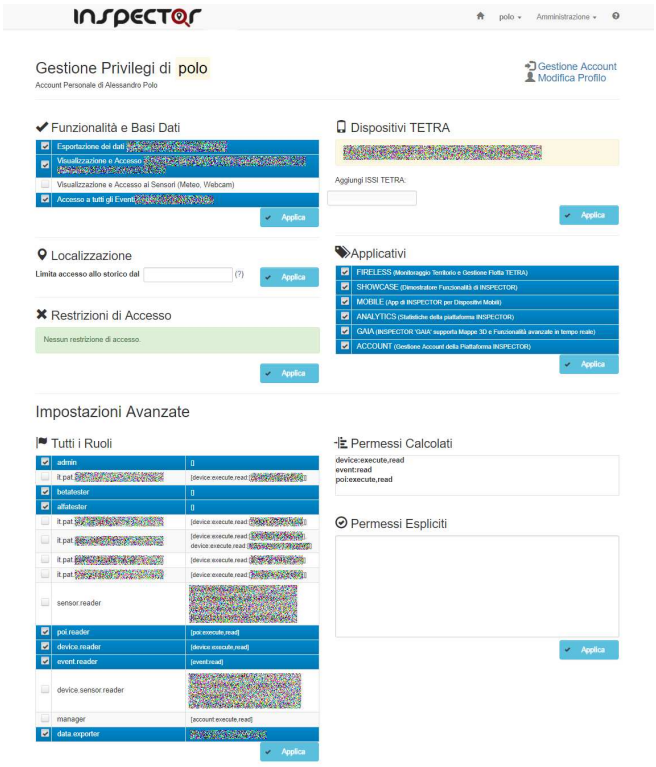

Figure 4.23: *INSPECTOR* - Screenshot of Account Privileges Management. The interactive interface allows administrators to apply security templates, predefined roles and explicit permissions.

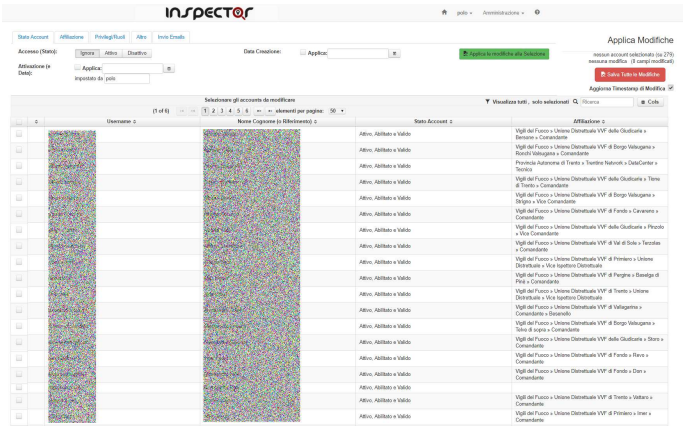

Figure 4.24: *INSPECTOR* - Screenshot of Batch Operations on Accounts. The front-end supports administrators for modifying many accounts at once, for importing accounts from external data-sources and for sending communications to the users.

4.3.7 Assisted Mission Planning

The selection of assets to be deployed toward an emergency event for the rescue operation is mainly related to aspects related to localization information, such as the resource-event distance, the time of arrival on the event, the vehicle characteristics, such as the available equipment and the personnel skills. The optimization strategy proposed in Sect. 4.2 has been preliminary integrated into the *DSS* tool. The implementation exploits the real-time information from the fleet (i.e., location, status, assets metadata) and embeds the well-known Non-dominated Sorting Genetic Algorithm-II (NSGA-II) [151] that proven good results in the optimization performance assessment. The experience of situation room operators has been integrated as the set scalar matrixes that describe most relevant mappings which defines features correlation between considered emergency mission and the assets suitable for the deployment.

The system assists the operator in the asset selection process by means of the interactive visual interface shown in Fig. 4.25. The operator typically pre-filter assets to be considered nearby the target location (e.g., 50 Km) by editing the mask on the map which display the real-time position of candidate assets. This step is not required by the proposed approach and it has been introduced only to reduce the process computational time and the number of proposed solutions, accordingly to operators best practices. On the left panel, selection criteria (i.e., objectives) can be deactivated and ordered by priority, the order affects the default proposed solution and the ranking of candidate assets list. The travel time depends on the current location and the kind of the asset, in the case of road vehicles it is estimated using online navigation services (i.e., *Google Maps API*). The system computes the solutions front in few seconds, the best solution (e.g., dispatching the second and forth asset in Fig. 4.25) is pre-selected accordingly to current criteria ordering, and the full listing of all candidate assets, that is the union of assets included in all solutions sets, is shown in the bottom panel. The estimated route including time of arrival and path length are shown in the output table and on the map.

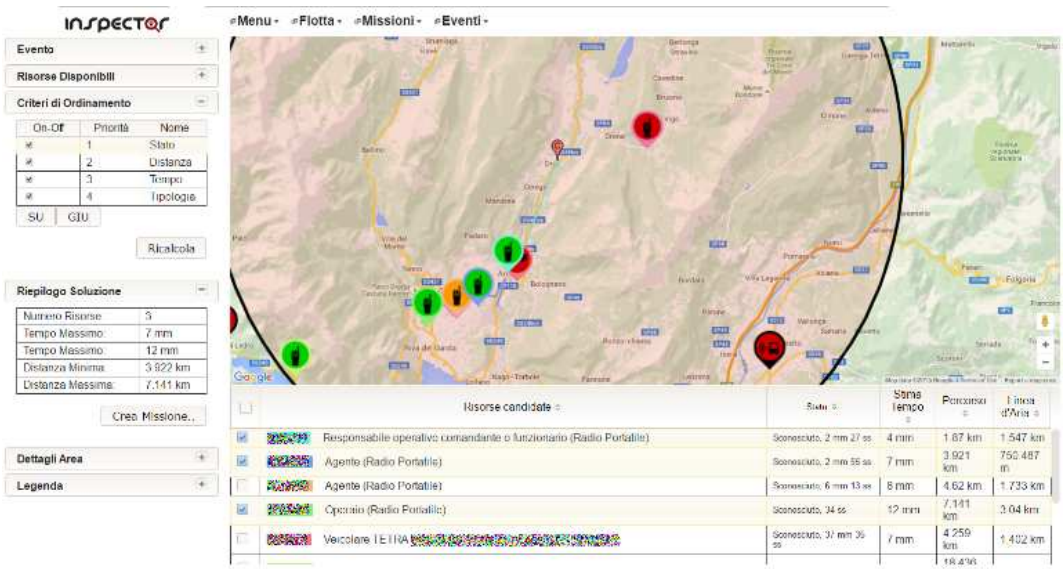

Figure 4.25: *INSPECTOR* - Screenshot of the Fleet Assets Selection Wizard. The operator configures objectives and refine the proposed selection of assets to be deployed for the emergency event.

4.4 Experimental Validation in Trentino

The research activities including the development and the experimental validation of the proposed work has been carried out within the framework of the *"MoU* between Centrale Unica Emergenza (*CUE*) and ELEDIA Research Center" and has been experimentally validated in real cases by Civil Defense agencies of the Autonomous Province of Trento since 2015. At the time of writing, the proposed systems are still active. The illustrated *DSS* tool has been implemented and customized with the support of the domain experts who have supported the definition of requirements, objectives and the main features of the system. A lot of work has been done for importing external data-sources, for enabling interoperability with *TETRA* network and for modeling the knowledge base. Finally, situation rooms (e.g., fire-fighter station shown in Fig. 4.26) and more than 270 professionals have been added as end-users. Among the experimental test cases and scenarios, the most relevant case of success of the system in terms of usage and users satisfaction are related to the support given during inter-forces emergency missions and during the search and rescue of missing people (Fig. 4.27).

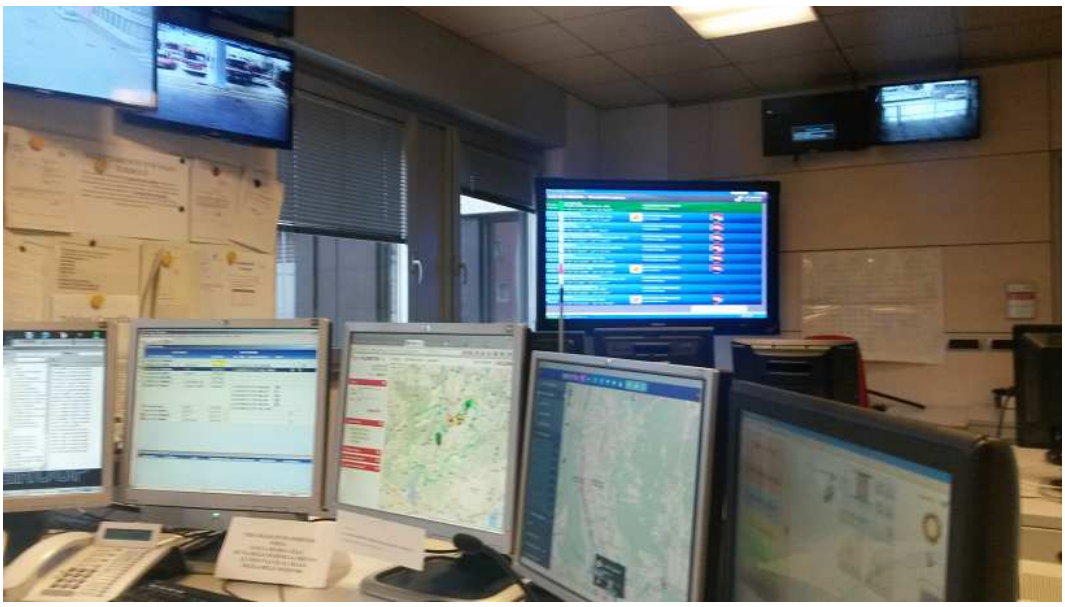

Figure 4.26: *INSPECTOR* - Picture. The tool running on one of the monitors of the emergency call-taking center of fire-fighters, Trentino - Italy.

The institutional *TETRA* network covers more than 87% of the whole region ($157\,km^2$) by means of 78 base stations that serve about 3900 radio terminals (hand-held radios, vehicles, helicopters) on the field. After an accurate trial, briefly summarized in next Section, the *HOSTESS* gateway has been installed

in civil defense data-center and connected to the *TETRA* network for enabling interoperability with *INSPECTOR* and other software tools supporting operators and decision makers in the situation rooms. At the time of writing, the spatial database of the DSS tool stored more than 9 million of positions, with a rate of about half million new entries per month.

Figure 4.27: *INSPECTOR* - Picture. The tool on the main monitor of the situation room of fire-fighters, Trentino - Italy.

4.4.1 TETRA HOSTESS: Trial and Stress Tests

The official activation of *HOSTESS* gateway within the *TETRA* core network in date 13 October 2016 at 11:07. At the time of writing the system is still running continuously without any failure. In date 23 June 2016, an extensive validation-trial of system functionalities and reliability, including stress tests of the software and the hardware components (i.e., the Mobile Switching Office, base station, terminals), has been done. In fact, the reliability is a key point as the *TETRA* network is used for emergency communications and coordination by civil defense organizations and police.

In particular, all features supported by *HOSTESS* relevant for the users of the network have been validated for hand-held and vehicular radio terminals, as shown in Fig. 4.28. The base station used within the experiment, a *Motorola MTS2*, is shown in Figure 4.29. It should ne noted that the *TETRA ETSI* standard includes many non-mandatory features and supports advanced mechanism

for extending the protocol itself. The support of such features depends on the device and typically the manufacturer. Features of interest can be grouped in three categories:

- Localization functionalities (Location Information Protocol - *LIP*). *TETRA* terminals embed a *GPS* device and can be programmed, even over the air, to push the location periodically or on specific triggers. The supported features are listed in Tab. 4.3.
- Status Communication. States are used the emergency management to identify the status of an asset, namely: 'Ready', 'Outgoing', 'On Place', 'Returning'. The states are associated with textual and numeric codes that are encoded as *SDS* and in other custom *TETRA* protocols, such as *PID 200* implemented by *Sepura*. *HOSTESS* provides to applications clients a transparent abstraction of the encoding used for each kind of terminal, functions related to states are summarized in Tab. 4.4;
- Textual Messaging (Short Data Service - *SDS*). The transmission and the reception of textual messages from *HOSTESS* application client to remote *TETRA* terminals, results are summarized in Tab. 4.5;

	Hand-held Terminals		Vehicular Terminals	
Localization Function	*STP9000*	*MTH800*	*SRG3009*	*MTM800*
Receive Location (short)	OK	OK	OK	OK
Receive Location (long)	OK	OK	OK	OK
Request location (short)	OK	OK	OK	OK
Request location (long)	Unavailable	OK	Unavailable	OK
Read Triggers	Unavailable	OK	Unavailable	OK
Toggle Triggers	OK	OK	OK	OK
Add/Edit/Remove Trigger	OK	OK	OK	OK

Table 4.3: *HOSTESS* Localization features supported by different TETRA terminals.

	Hand-held Terminals		Vehicular Terminals	
States Function	*STP9000*	*MTH800*	*SRG3009*	*MTM800*
Send as Text	OK	OK	OK	OK
Send as Code (Protocol 200)	OK	Unavailable	OK	Unavailable
Receive Text	OK	OK	OK	OK
Receive (Protocol 200)	OK	Unavailable	OK	Unavailable
Send on Emergency button	OK	Unavailable	OK	Unavailable

Table 4.4: *HOSTESS* States features supported by different TETRA terminals.

	Hand-held Terminals		Vehicular Terminals	
Messaging Function	*STP9000*	*MTH800*	*SRG3009*	*MTM800*
Send SDS (Standard)	OK	OK	OK	OK
Receive SDS (Standard)	OK	OK	OK	OK
Send SDS (Protocol 200)	OK	Unavailable	OK	Unavailable
Send SDS (Fake Sender)	OK	Unavailable	OK	Unavailable

Table 4.5: *HOSTESS* Messaging features supported by different TETRA terminals.

(a)

(b)

(c)

Figure 4.28: The TETRA hand-held and vehicular radio terminals used within HOSTESS validation: *(a)* on the left a *Sepura STP9000* and on the right a *Motorola MTH800-HL, (b) Motorola MTM800-E, (c) Sepura SRG3009.*

Figure 4.29: The TETRA base station (*Motorola MTS2*) used within HOSTESS validation.

After the validation of the end-user operational functions, the second part of the trial concerns the analysis of the whole system of *TETRA* infrastructure and information systems under heavy and critical network traffic conditions. In particular, we considered the scenario in which a large number of *TETRA* radios are associated with a single base station and interact massively with the network. This kind of scenario may happen during big events and large emergencies in rural locations. In particular, the objectives of the qualitative experiment are:

- estimate the limits of the base station and the *TETRA* network, with respect to the number of associated devices (e.g., the saturation state of the *TETRA* control channel, the stability of the association between the base station and terminals);
- evaluate the features and the conditions that lead to a degradation of voice services;
- estimate the impact of having many terminals transmit the location at the maximum frequency (every 30 seconds) on the quality of other services and the control channel;
- reach the conditions in which the voice service is subject to a degradation perceivable by end users.

The experimental analysis has been divided into eight sequential scenarios as the stress conditions, in terms of number of involved terminals and concurrent networks operations, are progressively increased toward the limits of the infrastructure. In *TETRA* network protocol, both the short data service (*SDS* textual messaging) and location service (LIP protocol) are transmitted on the control channel that is responsible of basic network operations including voice service

management. The saturation of control channel lead to degradation of all services and finally to communications failure (i.e., the terminal is disconnected). During the experiment, the state of the base station and of the control channel was constantly monitored by the technical staff of the *TETRA* operation center.

The 136 hand-held radio terminals of different brands (Fig. 4.30) were initially switched off and were configured to be associated to a single Base Station dedicated for the test (i.e., *Motorola MTS2*) which was connected to *HOSTESS* gateway through the Short Data Router (i.e., *Motorola DIMETRA v. 8.1*). Terminals were placed in line of sight with the base station (antenna was replaced with a dummy load) and under sky visibility for ensuring GPS service availability. The simulation of the massive use of network was performed through an ad-hoc (*AMQP*) client application connected to the *HOSTESS* system that enables the execution of concurrent batch procedures on a given range of recipient devices. Each operation, such as the transmission of a text message, is performed in parallel on four processes and sequentially on all recipient terminals having a maximum delay of 100ms between invocations.

Figure 4.30: The TETRA terminals (136) used within the stress tests during HOSTESS trial.

During the experiment (about four hours), *HOSTESS* and the *TETRA* network correctly managed 15760 location reports (i.e., with peaks of 15 reports per second), 965 textual messages, 43 states, 534 location requests, 376 reconfigurations of *GPS* triggers settings of involved terminals. The statistics of textual messages and location reports sent during the test are shown in Fig. 4.31 and Fig 4.32, respectively.

At time of writing, *HOSTESS* gateway is still running without failures. In about 14 months, the system handled 4600 messages, 40000 states and 3.4 million

of location reports, as shown in Figure 4.11.

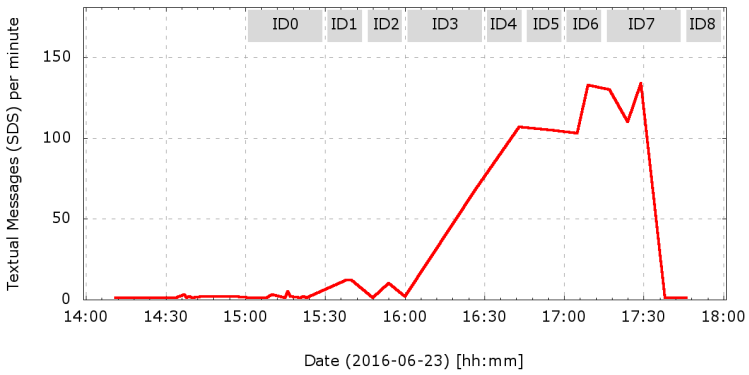

Figure 4.31: *HOSTESS* - Trial. The number of textual messages sent during HOSTESS stress tests.

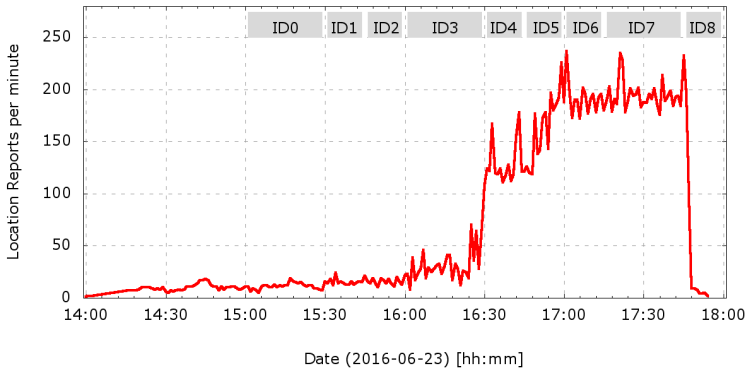

Figure 4.32: *HOSTESS* - Trial. The number of location reports received during HOSTESS stress tests. During the experiment, terminals were re-configured to progressively increase the push rate.

4.4.2 INSPECTOR: Facts and Numbers

After eight months of internal validation, in October 2015 the application *INSPECTOR* was made available as an official tool to the fire-fighters central station of Trento which handles the call-taking and the management of technical emergencies occurring in the whole province (Fig. 4.26).

Since 2016, together with the distribution of *TETRA* equipment to all 13 district unions of the fire-fighters volunteers (counting many thousands of personnel), the access to the system was granted to the heads of the organization and to the commanders in charge of all corps. Of course the privileges of each user reflect his roles in the organization, for example a commander is allowed to track and interact only with the assets in charge. In many occasions, the privileges of users have been elevated for supporting inter-corps and inter-force rescue missions (e.g., security of big events, search of missing persons) through the *INSPECTOR* Account tool (Fig. 4.23). In the period between the end of 2016 and May 2017, the access was progressively granted to all corps of fire-fighters, as shown in Figure 4.33. At the time of writing, 279 users are registered and allowed to use the tool, 210 users (about 75%) have used the tool at least one time, the number of monthly accesses is shown in Figure 4.34. The distribution of per-user accesses to the system shows that most users have used the system between 4 and 15 times, as shown in Figure 4.35. Accordingly to users feedback, INSPECTOR has been proven to be an useful *DSS* tool in many real world scenario (Fig. 4.36).

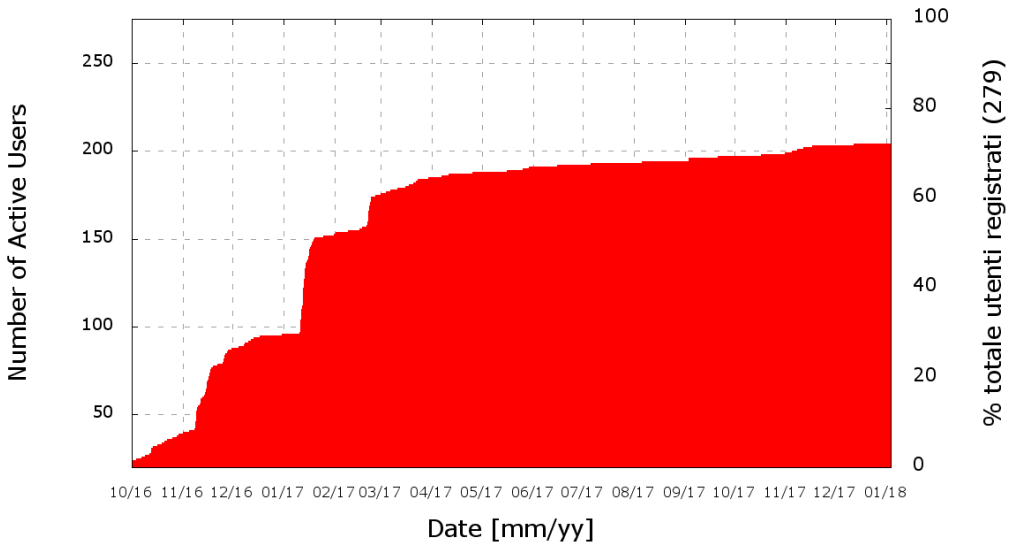

Figure 4.33: *INSPECTOR* - Statistics. The number of active users since October 2016.

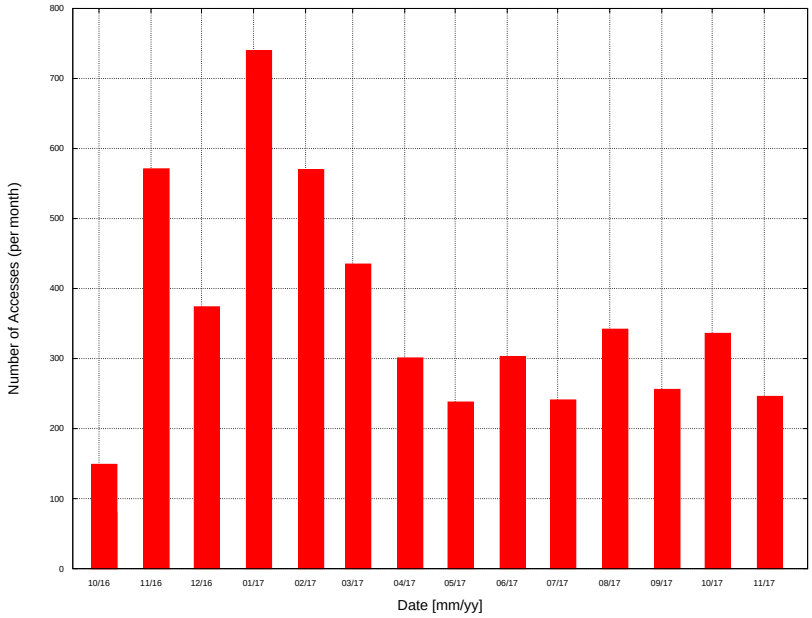

Figure 4.34: *INSPECTOR* - Statistics. The number of monthly accesses to the tool since October 2016.

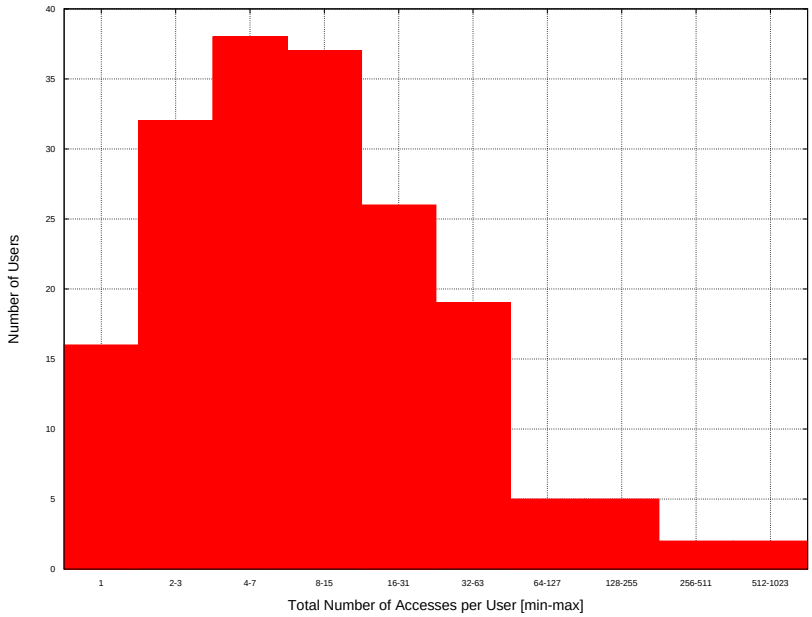

Figure 4.35: *INSPECTOR* - Statistics. The number of active users with respect to the total number of accesses of each user since October 2016.

l'Adige — Lavis e Rotaliana — venerdì 26 agosto 2016 43

SOCCORSI

Ogni comandante dei 16 Corpi sul territorio del Distretto con un account personale avrà accesso, tra le altre informazioni, a tutti i dati delle webcam installate lungo strade e punti strategici

Le grandi potenzialità del sistema sono state testate di recente sulla Paganella, nelle ricerche di un turista scomparso L'ispettore Cattani: «Più agevole coordinare gli uomini»

Radio Tetra e Inspector ai pompieri della Rotaliana

MARIANO MARINOLLI

ROTALIANA - Nelle prossime settimane, oltre ai 150 apparati già consegnati, saranno recapitati ai sedici corpi dei vigili del Fuoco racchiusi nel distretto della Protezione civile di Mezzolombardo altri nuovi apparecchi radio portatili connessi alla rete Tetra, alla quale sono collegate tutte le Forze dell'ordine e gli operatori (come Soccorso Alpino, Trentino Emergenza, ecc.) che affiancano nelle situazioni di emergenza i vigili del Fuoco.

Inoltre, ogni comandante delle sedici caserme sparse sul territorio della Rotaliana, Paganella e bassa val di Non, sarà autorizzato, con un account personale, ad accedere all'applicativo Inspector, il sistema gestionale che raccoglie tutti i dati delle webcam installate lungo le strade e nei punti strategici, oltre alle informazioni provenienti dai sensori meteo e di pericolo disseminati sul territorio. In un colpo d'occhio, tramite segnale Gps a cui sono connessi gli apparati Tetra, si può conoscere la posizione precisa delle singole squadre e dei mezzi di soccorso, visionando online le immagini e provvedendo, in tempo reale, a coordinare dalla sala operativa gli interventi d'emergenza. In sintesi, saranno facilitati e velocizzati tutti gli interventi d'emergenza, a beneficio dell'intera collettività.

Questo sistema gestionale è stato sperimentato, per la prima volta, in Paganella quando un anziano turista si era perso il mese scorso tra i boschi ed è stato ritrovato dopo due settimane, purtroppo privo di vita.

«In quella circostanza - ricorda l'ispettore del distretto, Matteo Cattani - furono coinvolti nelle ricerche, tra vigili del Fuoco, Soccorso Alpino, Unità cinofile, Guardia di Finanza, Carabinieri e Polizia di Stato, più di cento soccorritori. Era la prima volta che usavamo le radio Tetra e, fin da subito, ci eravamo accorti dell'enorme vantaggio di poter dialogare tra interforze; alcune radio le abbiamo prestate a chi non le possedeva, in modo da poter interagire con la sala operativa senza alcuna difficoltà».

Durante le ricerche, l'ispettore Cattani ricorda che la dirigente della centrale unica 112 di Trento, Luisa Zappini, gli aveva accennato tempo addietro di uno studio avviato con l'Università di Trento del software Inspector. E proprio per agevolare le ricerche dell'uomo disperso in Paganella era stato attivato un account per consentire all'ispettore Cattani di coordinare le operazioni di soccorso mediante questo nuovissimo sistema gestionale delle emergenze. «Ho subito compreso la grande utilità di questo software - spiega Cattani - poiché permette alla sala operativa di conoscere in tempo reale l'esatta posizione delle squadre e di indirizzarle nei punti assegnati; tenete conto che sono stati setacciati ben 400 ettari durante le operazioni di ricerca».

E quali altri vantaggi offre questo nuovo sistema? «E' possibile anche l'esportazione dei dati per usarli in qualche altro software di mappatura, formendo agli operatori gli esatti percorsi fatti o punti non verificati, provvedendo poi a trasmettere anche alla magistratura un resoconto dettagliato di squadre in azione e percorsi fatti. Per fare un semplice esempio, assieme al comandante dei carabinieri di Andalo abbiamo verificato la copertura del ripetitore riuscendo, tramite apparato Tetra, ad avere un percorso Gps molto più preciso di quello fornito dall'operatore telefonico. Sono ormai tredici anni che vivo in questo meraviglioso mondo del soccorso, ma devo dire che sono rimasto compiaciuto di aver visto che tutto lo staff della Centrale unica di Trentino Network si sia adoperato per darmi tutto il supporto di cui avevo bisogno. E devo anche ammettere che non ero abituato ad avere risposte così precise in tempi molto rapidi, grazie a questa portentosa innovazione tecnologica».

Da oggi scatta la festa con «Fine estate a Mezombart»

MEZZOLOMBARDO - Parte oggi la festa di Fine estate a Mezzolombardo, organizzata dalla Pro Loco. Un appuntamento che quest'anno compie 15 anni di vita. Ed è prima di tutto la festa delle associazioni. Anche la Pro Loco di oggi, presidente Luca Toniatti, si muove con cura e dedizione. Del resto, il lavoro di organizzazione dura da diversi mesi.

Le 16 associazioni partecipanti proporranno innumerevoli e squisite pietanze annaffiate dal principe del vino, il Teroldego. «Tutto servito - sottolinea il presidente - all'interno di stand dove regnerà la simpatia, il sorriso e la voglia di mettere a proprio agio l'ospite che sarà coinvolto e si sentirà partecipe ad una delle feste più belle della nostra provincia. La semplicità fa rima con l'artigianalità, la bontà con la naturalità; i cuochi, i camerieri, i baristi e tutti i volontari concorreranno a fare di Mezzolombardo il centro del Trentino dove per tre giorni nessuno dovrebbe mancare, dove si assaporerà il valore dell'ospitalità». Sono ben 600 i volontari che si alterneranno a servizio delle migliaia di ospiti.

«La Pro Loco - chiosa Toniatti - è orgogliosa di rappresentare questi volontari che lavorano per mesi alla preparazione dell'evento ed i tre giorni della festa sono si molto impegnativi ma sono niente a confronto del lavoro che sta alla base di tutto, pertanto noi siamo grati a tutte queste persone che dedicano tempo, il loro tempo, agli altri al solo scopo di rendere il paese più bello, allegro e accogliente, trasmettendo quei valori del volontariato che sono alla base della cultura trentina».

Sul sito http://www.prolocomezzolombardo.it il programma completo. An. Lo.

Figure 4.36: *INSPECTOR* - Press. A local newspaper describing the usage of TETRA and INSPECTOR tool during a Search-and-Rescue operation (for missing person).

4.5 Conclusions

In this Chapter, location-based applications for the smart management of large fleet of personnel, vehicles and localized information are considered.

In particular, the illustrated *DSS* tool provides situation awareness to emergency-response operators and decision makers by means of historical data and real-time information streams acquired from distributed wireless sensor networks, online data-sources, military (i.e., *TETRA)* and civilian (*i.e., 3G,4G*) networks:

- vehicles of the fleet (i.e., many hundreds of vehicles and 5 helicopters equipped with TETRA radio);
- professionals and volunteers (i.e., almost four thousands of personnel equipped with TETRA hand-held radio);
- weather information (i.e., 263 weather station, 206 hydrometers, 52 snow sensors);

- road-traffic information (i.e., real-time events from public agencies, traffic data from Google Maps);
- critical infrastructures, points of interest (e.g., sites at risk, emergency stations, helicopters pads, hydrants).

The system has been experimentally validated in real scenarios by Civil Defense domain experts of Trentino region since 2015. The access was granted to the heads and situation room operators of the technical and medical emergency-response agencies as well as to the commanders in charge of all fire-fighters corps, actually there are 279 registered user accessing the system about 12 times per day.

Bibliography

[1] J. Riha, Home automation trends, diy network. Accessed on Dec. 27, 2012 from www.diynetwork.com.

[2] M. R. Alam, M. B. I. Reaz, and M. Ali, "A review of smart homes - Past, present, an future," *IEEE Trans. Syst., Man, Cybern., Syst.*, vol.42, no. 6, pp. 1190-1203, Nov. 2012.

[3] V. C. Gungor, D. Sahin, T. Kocak, S. Ergut, C. Buccella, C. Cecati, and G. P. Hancke, "Smart grid and smart homes," *IEEE Ind. Electron. Mag.*, pp. 18- 34, Dec. 2012.

[4] S. Helal, C. Chen, E. Kim, R. Bose, and C. Lee, "Toward an ecosystem for developing and programming assistive environment," *Proc. IEEE*, vol. 100, no. 8, pp. 2489-2504, Aug. 2012.

[5] T. J. Lui, W. Stirling, and H. O. Marcy, "Get smart," *IEEE Power Energy Mag.*, pp. 66-78, Jun. 2010.

[6] N. Langhammer and R. Kays, "Performance evaluation of wireless home automation networks in indoor scenarios," *IEEE Trans. Smart Grid*, vol. 3, no. 4, pp. 2252-2261, Dec. 2012.

[7] J. Han, C.-S. Choi, and I. Lee, "More efficient home energy management system based on ZigBee communication and infrared remote controls," *IEEE Trans. Consumer Electron.*, vol. 57, no. 1, pp. 85-89, Feb. 2011.

[8] M. Dong, P. C. M. Meira, W. Xu, and W. Freitas, "An event window based load monitoring technique for smart meters," *IEEE Trans. Smart Grid,* vol. 3, no. 2, pp. 787-796, Jun. 2012.

[9] F. G. Marmol, C. Sorge, O. Ugus, and G. M. Perez, "Do not snoop my habits: preserving privacy in the smart grid," *IEEE Commun. Mag.*, pp. 166-172, May 2012.

[10] B. Qela and H. T. Mouftah, "Observe, learn, and adapt (OLA) - An algorithm for energy management in smart homes using wireless sensors and artificial intelligence, " *IEEE Trans. Smart Grid*, vol. 3, no. 4, pp. 2262-2272, Dec. 2012.

[11] M. Kantarci and H. T. Mouftah, "Wireless sensor networks for cost-efficient residential energy management in the smart grid," *IEEE Trans. Smart Grid*, vol. 2, no. 2, pp. 314-325, Jun. 2011.

[12] D. Han and J. Lim, "Design and implementation of smart home energy management systems based on Zigbee," IEEE Trans. Consum. Electron., vol. 56, no. 3, pp. 1417-1425, Aug. 2010.

[13] Z. Zhu, S. Lambotharan, W. H. Chin, and Z. Fan, "Overview of demand management in smart grid and enabling wireless communication technologies," *IEEE Wireless Communications*, pp. 48-56, Jun. 2012.

[14] J. Byun, B. Jeon, J. Noh, Y. Kim, and S. Park, "An intelligent self adjusting sensor for smart home services based on Zigbee communications," *IEEE Trans. Consum. Electron.*, vol. 58, no. 3, pp. 794-802, Aug. 2012.

[15] A. J. D. Rathnayaka, V. M. Potdar, and S. J. Kuruppu, "Evaluation of wireless home automation technologies," *IEEE Int. conf. Digital Ecosystem and Technologies* (IEEE DEST2011), 31 May-3 June 2011, Daejeon, Korea, 2011.

[16] A. Hashizume, T. Mizuno, and H. Mineno, "Energy monitoring system using sensor networks in residential houses," *IEEE Int. Conf. on Advances Inf. Networking and Applications* (WAINA), 26-29 March 2012, pp. 595-600, 2012.

[17] K. Islam, W. Shen, and X. Wang, "Security and privacy considerations for wireless sensor networks in smart home environments," *IEEE Int. Conf. on Comp. Supported Cooperative Work in Design* (CSCWD), 23-25 May 2012, pp. 626-633, 2012.

[18] A. Sleman and R. Moeller, "SOA distributed operating system for managing embedded devices in home and buiding automation," *IEEE Trans. Consum. Electron.*, vol. 57, no. 2, pp. 945-952, May 2011.

[19] S. Junnila, H. Kailanto, J. Merilahti, A. Vainio, A. Vehkaoja, M. Zakrzewski, and J. Hyttinen, "Wireless, multipurpose in-home health monitoring platform: two case trials," *IEEE Trans. Inf. Tech. in Biomedicine*, vol. 14, no. 2, pp. 447-455, Mar. 2010.

[20] U. Cortes, C. Urdiales, and R. Annicchiarico, "Intelligent healthcare managing: An assistive technology approach," in *Proc. 9th IWANN*, San Sebastian, Spain, pp. 1045-1051, 2007.

[21] W. C. Mann, K. J. Ottenbacher, L. Fraas, M. Tomita, and C. V. Granger, "Effectiveness of assistive technology and environmental interventions in

maintaining independence and reducing home care costs for the frail elderly: A randomized trial," *Arch. Family Med.*, vol. 8, no. 3, pp. 210-217, 1999.

[22] A. Helal, W. Mann, H. Elzabadani, J. King, Y. Kaddourah, and E. Jansen, "Gator tech smart house: A programmable pervasive space," *IEEE Computer*, vol. 38, no. 3, pp. 64-74, Mar. 2005.

[23] C. D. Kidd, R. J. Orr, G. D. Abowd, C. G. Atkeson, I. A. Essa, B. Macintyre, E. Mynatt, T. E. Starner, and W. Newstetter, "The aware home: A living laboratory for ubiquitous computing research," *in Proc. 2nd Int. Workshop Cooperative Buildings*, pp. 191-198, Oct. 1999.

[24] S. S. Intille, K. Larson, E. Munguia Tapia, J. S. Beaudin, P. Kaushik, J. Nawyn, and R. Rockinson, "Using a live-in laboratory for ubiquitous computing research," in *Proc. 4th Int. Conf. Perv. Comput.*, Dublin, Ireland, pp. 349-365, May 2006.

[25] J. Marsh, "House Calls," *Rochester Rev.*, vol. 64, no. 3, pp. 22-26, 2002.

[26] D. J. Cook, M. Youngblood, E. O. Heierman, K. Gopalratnam, S. Rao, A. Litvin, and F. Khawaja, "MavHome: An agent-based smart home," in *Proc. 1st IEEE Int. Conf. Pervasive Comput. Commun.*, pp. 521-524, Mar. 2003.

[27] K. Ramamritham and P. K. Chrysanthis, *Advances in Concurrency Control and Transaction Processing*. Pitscataway, NJ: IEEE Computer Society Press, 1997.

[28] M. Chan, D. Esteve, C. Escriba, and E. Campo, "A review of smart homes - present state and future challenges," *Comput. Methods Progr. Biomed.*, vol. 91, no. 1, pp. 55-81, Jul. 2008.

[29] S. Intille, "Designing a home of the future," *IEEE Pervasive Comput.*, vol. 1, no. 2, pp. 76-82, Apr.-Jun. 2002.

[30] S. Intille, "A new research challenge: Persuasive technology to motivate healthy aging," *IEEE Trans. Inf. Technol. Biomed.*, vol. 8, no. 3, pp. 235-237, Sep. 2004.

[31] G. Le Bellego, N. Noury, G. Virone, M. Mousseau, and J. Demongeot, "A model for the measurement of patient activity in a hospital suite," *IEEE Trans. Inf. Technol. Biomed.*, vol. 10, no. 1, pp. 92-99, Jan. 2006.

[32] D. Dietrich, D. Bruckner, G. Zucker, and P. Palensky, "Communication and computation in buildings: a short introduction and overview," *IEEE Trans. Ind. Electron.*, vol. 57, no. 11, pp. 3577-3584, Nov. 2010.

[33] A. Gaddam, S. C. Mukhopadhyay, and G. S. Gupta, "Elder Care Based on Cognitive Sensor Network," *IEEE Sensors Journal*, vol. 11, no. 3, pp. 574-581, Mar. 2011.

[34] C. Lu, C. Wu, and L. Fu, "A reciprocal and extensible architecture for multiple-target tracking in smart home," *IEEE Trans. Cybern. - Part C: Applications and Reviews*, vol. 41, no. 1, pp. 120-129, Jan. 2011.

[35] B. Mrazovac, M. Z. Bjelica, D. Kukolj, B. M. Todorovic, and D. Samardzija, "A human detection method for residential smart energy based on Zigbee RSSI changes," *IEEE Trans. Consum. Electron.*, vol. 58, no. 3, pp. 819-824, Aug. 2012.

[36] R. Davenport, H. Elzabadani, J. Johnson, A. Helal, and W. Mann, "Pilot live-in trial at the GatorTech Smart house," *Top. Geriatr. Rehab.*, vol. 23, no. 1, pp. 73-84, 2007.

[37] A. V. Berlo, A. Bob, E. Jan, F. Klaus, H. Maik, and W. Charles, *Design Guidelines on Smart Homes: A COST 219bis Guidebook*. Brussels, Belgium: Eur. Commission, 1999.

[38] P. Rashidi, D. J. Cook, L. B. Holder, and M. Schmitter-Edgecombe, "Discovering activities to recognize and track in a smart environment," *IEEE Trans. Knowl. Data Eng.*, vol. 23, no. 4, pp. 527-539, Apr. 2011.

[39] D. Cook and M. Schmitter-Edgecombe, "Assessing the quality of activities in a smart environment," *Methods of Information in Medicine*, vol. 48, pp. 480-485, 2009.

[40] E. M. Tapia, S. S. Intille, and K. Larson, *Activity Recognition in the Home Using Simple and Ubiquitous Sensors*. Berlin, Germany: Springer- Verlag, pp. 158-175, 2004.

[41] M. Philipose, K.P. Fishkin, M. Perkowitz, D.J. Patterson, D. Fox, H. Kautz, and D. Hahnel, "Inferring activities from interactions with objects," *IEEE Pervasive Computing*, vol. 3, no. 4, pp. 50-57, Oct.- Dec. 2004.

[42] L. Liao, D. Fox, and H. Kautz, "Location-based activity recognition using relational Markov networks," *Proc. Intâl Joint Conf. Artificial Intelligence*, pp. 773-778, 2005.

[43] M. C. Mozer, "The neural network house: an environment that's adapts to its inhabitants," in *Proc. AAAI Spring Symp. Intell. Environ.*, pp. 110-114, 1998.

[44] H. Zheng, H. Wang, and N. Black, "Human activity detection in smart home environment with self-adaptive neural networks," in *Proc. IEEE Int. Conf. Netw., Sensing Control*, pp. 1505-1510, 2008.

[45] O. Brdiczka, J. L. Crowley, and P. Reignier, "Learning situation models in a smart home," *IEEE Trans. Syst., Man, Cybern. B, Cybern.*, vol. 39, no. 1, pp. 56-63, Feb. 2009.

[46] N. P. Couellan and T. B. Trafalis, "On-Line SVM learning via an incremental primal-dual technique" in Optimization Methods and Software, vol. 28, no. 2, pp. 256-275, Apr. 2013.

[47] P. Rocca, M. Benedetti, M. Donelli, D. Franceschini, and A. Massa, "Evolutionary optimization as applied to inverse problems," *Inverse Problems - 25th Year Special Issue of Inverse Problems*, Invited Topical Review, vol. 25, pp. 1-41, Dec. 2009.

[48] A. Sinha, A. Pandey, and K. Deb, "Solving high objective problems in fixed interactions with the decision maker," *IEEE Congress on Evolutionary Computation* (CEC2012), 10-15 June 2012, pp. 1-8, 2012.

[49] K. Jong-Hwan, H. Ji-Hyeong, K. Ye-Hoon, C. Seung-Hwan, K. Eun-Soo, "Preference-based solution selection algorithm for evolutionary multiobjective optimization," *IEEE Trans. Evol. Comput.*, vol. 16, no. 1, pp. 20-34, 2012.

[50] T. Yamazaki, "Beyond the smart home," in *Proc. Int. Conf. Hybrid Inf. Technol.*, pp. 350-355, 2006.

[51] P. Rashidi and D. J. Cook, "Keeping the resident in the loop: adapting the smart home to the user," *IEEE Trans. Systems, Man and Cybernetics, Part A: Systems and Humans*, vol. 39, no.5, pp. 949-960, Sep. 2009.

[52] T. Barger, D. Brown, and M. Alwan, "Health-status monitoring through analysis of behavioral patterns," *IEEE Trans. Systems, Man and Cybernetics, Part A: Systems and Humans*, vol. 35, no. 1, pp. 22-27, Jan. 2005.

[53] J. C. Augusto, "Ambient intelligence: the confluence of ubiquitous/pervasive computing and artificial intelligence," in *Intelligent Computing Everywhere*, A. Schuster, Ed. London, U.K.: Springer-Verlag, pp. 213-234, 2007.

[54] J. Dunlop, D. Girma, and J. Irvine, "Digital mobile communications and the TETRA system," John Wiley & Sons, 1999.

[55] E. Cavallo and I. Noy, "The economics of natural disasters - a survey," International Review of Environmental and Resource Economics, 2011.

[56] A. House, N. Power, and L. Alison, "A systematic review of the potential hurdles of interoperability to the emergency services in major incidents: recommendations for solutions and alternatives," Cognition, Technology and Work, vol. 16, pp. 319-335, Aug. 2014.

[57] European Community. (2015, Oct. 16) EU Programmes 2014-2020.

[58] S. Siqing, W. Li, L. Ling, and C. Yong, "An emergency response decision support system framework for application in e-government," *Journal of Information Technology and Management*, vol. 13, pp. 411-427, Dec. 2012.

[59] A. Polo, F. Robol, C. Nardin, S. Marchesi, A. Zorer, L. Zappini, F. Viani, and A. Massa, "Decision support system for fleet management based on TETRA terminals geolocation," *8th European Conference on Antennas and Propagation* (EUCAP 2014), The Hague, The Netherlands, pp. 1195-1198, Apr. 2014.

[60] F. Viani, L. Lizzi, P. Rocca, M. Benedetti, M. Donelli, and A. Massa, "Object tracking through RSSI measurements in wireless sensor networks," *Electronics Letters*, vol. 44, no. 10, pp. 653-654, May 2008.

[61] F. Viani, P. Rocca, M. Benedetti, G. Oliveri, and A. Massa, "Electromagnetic passive localization and tracking of moving targets in a WSN-infrastructured environment," *Inverse Probl.*, vol. 26, no. 074003, pp. 1-15, 2010.

[62] N. Patwari and J. Wilson, "RF sensor networks for device-free localization: Measurements, models, and algorithms," *Proc. IEEE*, vol. 98, no. 11, pp. 1961-1973, Nov. 2010.

[63] F. Viani, G. Oliveri, M. Donelli, L. Lizzi, P. Rocca, and A. Massa, "WSN-based solutions for security and surveillance," *40th European Microwave Conference 2010* (EuMC2010), Paris, France, September 26 - October 1, 2010.

[64] F. Viani, M. Donelli, M. Salucci, P. Rocca, and A. Massa, "Opportunistic exploitation of wireless infrastructures for homeland security," *Proc. 2011 IEEE AP-S International Symposium*, Spokane, USA, July 3-8, 2011.

[65] F. Viani, M. Donelli, P. Rocca, G. Oliveri, D. Trinchero, and A. Massa, "Localization, tracking and imaging of targets in wireless sensor networks," *Radio Science*, Vol. 46, No. 5, 2011.

[66] H. A. Nguyen, H. Guo, and K. Low, "Real-time estimation of sensor node's position using particle swarm optimization with log-barrier constraint," *IEEE Trans. Instrum. Meas.*, vol. 60, no. 11, pp. 3619-3629, Nov. 2011.

[67] F. Wen and C. Liang, "Fine-grained indoor localization using single acccess point with multiple antennas," *IEEE Sensors J.*, vol. 15, no. 3, 1538-1544, Mar. 2015.

[68] C. Loyez, M. Bocquet, C. Lethien, and N. Rolland, "A distributed antenna system for indoor accurate WiFi localization," *IEEE Antennas Wireless Propag. Lett.*, vol. 14, pp. 1184-1188, 2015.

[69] Y. Zhou, C. L. Law, and F. Chin, "Construction of local anchor map for indoor position measurement system," *IEEE Trans. Instrum. Meas.*, vol. 59, no. 7, pp. 1986-1988, Jul. 2010.

[70] H. Liu, J. Yang, S. Sidhom, Y. Wang, Y. Chen, and F. Ye, "Accurate WiFi based localization for smartphones using peer assistance," *IEEE Trans. Mobile Comput.*, vol. 13, no. 10, pp. 2199-2214, Oct. 2014.

[71] M. Marinova, A. Thielens, E. Tanghe, L. Vallozzi, G. Vermeeren, W. Joseph, H. Rogier, and L. Martens, "Diversity performance of off-body MB-OFDM UWB-MIMO," *IEEE Trans. Antennas Propag.*, vol. 63, no. 7, pp. 2187-3198, Jul. 2015.

[72] M. Addlesee, R. Curwen, S. Hodges, J. Newman, P. Steggles, A. Ward, and A. Hopper, "Implementing a sentient computing system," *Computer*, vol. 34, no. 8, pp. 50-56, Aug. 2001.

[73] C. Huang, L. Lee, C. C. Ho, L. Wu, and Z. Lai, "Real-time RFID indoor positioning system based on Kalman-filter drift removal and heron-bilateration location estimation," *IEEE Trans. Instrum. Meas.*, vol. 64, no. 3, pp. 728-740, Mar. 2015.

[74] A. Goldsmith, "Wireless Communications", 1st ed., Cambridge University Press, 2005.

[75] A. Bose, H. F. Chuan, "A practical path loss model for indoor WiFi positioning enhancement," 6th International Conference on Information, Communications & Signal Processing, pp.1,5, 10-13, Dec. 2007.

[76] P. Bahl and V. N. Padmanabhan, "RADAR: An In-Building RF-Based User Location and Tracking System," *Proc. IEEE INFOCOM*, vol. 2, pp. 775-784, 2000.

[77] M. Atia, A. Noureldin, and M. Korenberg, "Dynamic Online-Calibrated Radio Maps for Indoor Positioning In Wireless Local Area Networks," ," *IEEE Trans. Mobile Comput*, vol.12, no.9, pp.1774-1787, Sep. 2013.

[78] F. Viani, F. Robol, A. Polo, P. Rocca, G. Oliveri, and A. Massa, "Wireless architectures for heterogeneous sensing in smart home applications - Concepts and real implementations," *Proc. IEEE*, vol. 101, no. 11, pp. 2381-2396, 2013.

[79] M. McCracken and N. Patwari, "Hidden Markov estimation of bistatic range from cluttered ultra-wideband impulse responses," *IEEE Trans. Mobile Comput.*, vol. 13, no. 7, pp. 1509-1521, Aug. 2013.

[80] Y. Shen, W. Hu, M. Yang, J. Lio, B. Wei, S. Lucey, and C. T. Chou, "Real-time and robust compressive background subtraction for embedded camera networks," *IEEE Trans. Mobile Comput.*, vol. 15, no. 2, pp. 406-418, Feb. 2016.

[81] A. E. Kosba, A. Saeed, and M. Youssef, "RASID: A robust WLAN device-free passive motion detection system," *IEEE Pervasive Computing and Communications* (PerCom 2012), Lugano, Switzerland, March 19-23, 2012, pp. 180-189.

[82] P. Hillyard, N. Patwari, S. Daruki, and S. Venkatasubramanian, "You're crossing the line: Localizing border crossing using wireless RF links," *IEEE Signal Processing and Signal Processing Education Workshop* (SP/SPE 2015), Snowbird, UT, USA, August 9-12, 2015, pp. 249-254.

[83] Y. Zhao, N. Patwari, J. M. Phillips, and S. Venkatasubramanian, "Radio tomographic imaging and tracking of stationary and moving people via kernel distance," *12th international conference on Information processing in sensor networks* (IPSN 2013), Philadelphia, Pennsylvania, April 8-11, 2013, pp. 229-240.

[84] Z. Tian, L. Shao, M. Zhou, and X. Wang, "A highly-accurate device-free passive motion detection system using cellular network," *IEEE Wireless Communications and Networking Conference* (WCNC 2016), Doha, Qatar, April 3-6, 2016.

[85] G. Deak, K. Curran, J. Condell, D. Deak, "Detection of multi-occupancy using device-free passive localisation," *IET Wirel. Sens. Syst.*, vol. 4, no. 3, pp. 130-137, Jan. 2014.

[86] M. Seifeldin, A. Saeed, A. E. Kosba, A. El-Keyi, and M. Youssef, "Nuzzer: A large-scale device-free passive localization system for wireless environments," *IEEE Trans. Mobile Comput.*, vol. 12, no. 7, pp. 1321-1334, Jul. 2013.

[87] M. C. R. Talampas, and K. Low, 'An enhanced geometric filter algorithm with channel diversity for device-free localization', *IEEE Trans. Instrum. Meas.*, vol. 65 (2), pp. 378-388, 2016.

[88] Y. Gu, F. Ren, and J. Li, 'PAWS: Passive human activity recognition based on WiFi ambient signals', *IEEE Internet Things J.*, vol. 3 (5), pp. 796-806, 2016.

[89] S. Sigg, M. Scholz, S. Shi, Y. Ji, and M. Beigl, "RF-sensing of activities from non-cooperative subjects in device-free recognition systems using ambient and local signals," *IEEE Trans. Mobile Comput.*, vol. 13, no. 4, pp. 907-920, 2014.

[90] M. A. A. Al-qaness, and F. Li, 'WiGeR: WiFi-based gesture recognition system', *Int. J. Geo-Inf.*, vol. 5 (92), pp. 1-17, 2016.

[91] O. Kaltiokallio, H. Yigitler, R. Jantti, and N. Patwari, "Non-invasive respiration rate monitoring using a single cots tx-rx pair," *13th International Symposium on Information Processing in Sens*or Networks (IPSN 2014), Berlin, Germany, 15-17 April, 2014, pp. 59-69.

[92] X. Liu, J. Cao, S. Tang, J. Wen, and P. Guo, "Contactless respiration monitoring via off-the-shelf WiFi devices," *IEEE Trans. Mobile Comput.*, vol. 15, no. 10, pp. 2466-2479, Oct. 2016.

[93] M. Raja and S. Sigg, "Applicability of RF-based methods for emotion recognition: a survey," in *Proc. of the 5th IEEE COSDEO Workshop, in conjunction with the 14th IEEE International Conference on Pervasive Computing and Communications* (PerCom 2016), Sydney, Australia, March 14-18, 2016.

[94] E. Cianca, M. De Sanctis, and S. Di Domenico, "Radios as sensors," *IEEE Internet Things J.*, in press.

[95] M. Youssef, M. Mah, and A. Agrawala, "Challenges: Device-free passive localization for wireless environments," in *Proc. 13th ACM Int. Conf. Mobile Comput. Netw.*, Montreal, QC, Canada, Sep. 2007.

[96] M. Moussa and M. Youssef, "Smart devices for smart environments: device-free passive detection in real environments," *IEEE Pervasive Computing and Communications* (PerCom 2009), Dallas, Texas, March 16-20, 2009.

[97] J. Wilson and N. Patwari, "Radio tomographic imaging with wireless networks," *IEEE Trans. Mobile Comput.*, vol. 9, no.5, pp. 621.632, May 2010.

[98] C. Xu, B. Firner, R. S. Moore, Y. Zhang, W. Trappe, R. Howard, F. Zhang, and N. An, "SCPL: Indoor device-free multi-subject counting and localization using radio signal strength," *12th ACM/IEEE International Conference on Infor*mation Processing in Sensor Networks (IPSN 2013), Philadelphia, USA, April 8-11, 2013.

[99] S. Nannuru, Y. Li, Y. Zeng, M. Coates, and B. Yang, "Radio frequency tomography for passive indoor multi-target tracking," *IEEE Trans. Mobile Comput.*, vol. 12, no. 12, pp. 2322 - 2333, Dec. 2013.

[100] J. Wang, Q. Gao, X. Zhang, and H. Wang, "Device-free localisation with wireless networks based on compressive sensing," *IET Commun.*, vol. 6, no. 15, pp. 2395-2403, May 2012.

[101] C. Feng, W. Sy, A. Au, S. Valaee, and Z. Tan, Received-signal-strength-based indoor positioning using compressive sensing," *IEEE Trans. Mobile Comput.*, vol. 11, no. 12, pp. 1983-1994, Dec. 2012.

[102] J. Wang, Q. Gao, P. Cheng, Y. Yu, K. Xin, and H. Wang, "Lightweight robust device-free localization in wireless networks," *IEEE Trans. Ind. Electron.*, vol. 61, no. 10, pp. 5681-5689, Oct. 2014.

[103] F. Viani, P. Rocca, G. Oliveri, D. Trinchero, and A. Massa, "Localization, tracking, and imaging of targets in wireless sensor networks: An invited review," *Radio Science*, vol. 46, no. 5, Sep. 2011.

[104] V. Rampa, S. Savazzi, M. Nicoli, and M. D'Amico, "Physical modeling and performance bounds for device-free localization systems," *IEEE Signal Process. Lett.*, vol. 22, no. 11, pp. 1864-1868, Nov. 2015.

[105] J. Wilson and N. Patwari, "See through walls: motion tracking using variance-based radio tomography networks," *IEEE Trans. Mobile Comput.*, vol. 10, no. 5, pp. 612-621, May 2011.

[106] Y. Zhao and N. Patwari, ""Robust estimators for variance-based device-free localization and tracking," *IEEE Trans. Mobile Comput.*, vol. 14, no. 10, pp. 2116-2129, Oct. 2015.

[107] A. Saeed, A. E. Kosba, and M. Youssef, "Ichnaea: A low-overhead robust WLAN device-free passive localization system," *IEEE J. Sel. Topics Signal Process.*, vol. 8, no. 1, pp. 5-15, Feb. 2014.

[108] D. Pastina, F. Colone, T. Martelli, and P. Falcone, "Parasitic exploitation of WiFi signals for indoor radar surveillance," *IEEE Trans. Veh. Technol.*, vol. 64, no. 4, pp. 1401-1415, Apr. 2015.

[109] Y. Kim, Y. Chon, and H. Cha, "Smartphone-based collaborative and autonomous radio fingerprinting," *IEEE Trans. Syst., Man, Cybern. C, Appl. Rev.*, vol. 42. no. 1, pp. 112-123, Jan. 2012.

[110] C. Wu, Z. Yang, and Y. Liu, "Smartphones based crowdsourcing for indoor localization," *IEEE Trans. Mobile Comput.*, vol. 14, no. 2, pp. 444-458, Feb. 2015.

[111] M. Youssef and A. Agrawala, "The Horus WLAN location determination system," *Proc. Third Int'l Conf. Mobile Systems, Applications, and Services*, Seattle, WA, pp. 205-218, June 6-8, 2005.

[112] Y. Shu, C. Bo, G. Shen, C. Zhao, L. Li, and. F. Zhao, "Magicol: Indoor localization using pervasive magnetic field and opportunistic WiFi sensing," *IEEE J. Sel. Areas Commun.*, vol. 33, no. 7, pp. 1443-1458, Jul. 2015.

[113] H. Liu, H. Darabi, P. Banerjee, and J. Liu, "Survey of wireless indoor positioning techniques and systems," *IEEE Trans. Syst., Man, Cybern. C*, vol. 37, no. 6, pp. 1067-1080, Nov. 2007.

[114] T. Garcia-Valverde, A. Garcia-Sola, H. Hagras, J. A. Dooley, V. Challagan, and J. A. Botia, "A fuzzy logic-based system for indoor localization using WiFi in ambient intelligent environments," *IEEE Trans. Fuzzy Syst.*, vol. 21, no. 4, pp. 702-719, Aug. 2013.

[115] M. Ficco, C. Esposito, and A. Napolitano, "Calibrating indoor positioning systems with low efforts," *IEEE Trans. Mobile Comput.*, vol. 13, no. 4, pp. 737-752, Apr. 2014.

[116] S. Wyne, A. P. Singh, F. Tufvesson, and A. F. Molisch, "A statistical model for indoor office wireless sensor channel," *IEEE Trans. Wireless Commun.*, vol. 8, no. 8, pp. 4154-4165, Aug. 2009.

[117] S. A. Martinez, G. P. J. Molina, L. E. Egea, E. L. Esteban, V. A. Javier, J. L. Leandro, and G. H. Joan, "An accurate radio channel model for wireless sensor networks simulation," *J. Commun. Netw.*, vol. 7, no. 4, pp. 401-407, Dec. 2005.

[118] Y. Tian, Z. Tang, and Y. Yu, "Third-order channel propagation model-based indoor adaptive localization algorithm for wireless sensor networks," *IEEE Antennas Wireless Propag. Lett.*, vol. 12, pp. 1578-1582, 2013.

[119] J. Jung, J. Lee, Y. Kim, and S. Kim, "Ray-tracing-aided modeling of user-shadowing effects in indoor wireless channels," *IEEE Trans. Antennas Propag.*, vol. 62, no. 6, pp. 3412-3416, Jun. 2014.

[120] C. Figuera, I. Mora-Jimenez, A. Guerrero-Curieses, J. L. Rojo-Alvarez, E. Everss, M. Wilby, and J. Ramos-Lopez, "Nonparametric model comparison and uncertainty evaluation for signal strength indoor location," *IEEE Trans. Mobile Comput.*, vol. 8, no. 9, pp. 1250-1264, Sep. 2009.

[121] Z. Xiao, H. Wen, A. Markham, N. Trigoni, P. Blunsom, and J. Frolik, "Non-line-of-sight identification and mitigation using received signal strength," *IEEE Trans. Wireless Commun.*, vol. 14. no. 3, pp. 1689-1703, Mar. 2015.

[122] G. Destino and D. Macagnano, "Semantic positioning via structured sparsity models," *In Proc. 2014 IEEE World Forum on Internet of Things* (WF-IoT 2014), Seoul, South Korea, March 6-8, 2014, pp. 106-110.

[123] D. Macagnano, G. Destino, and G. Abreu, "Indoor positioning: a key enabling technology for IoT applications," *In Proc. 2014 IEEE World Forum on Internet of Things* (WF-IoT 2014), Seoul, South Korea, March 6-8, 2014, pp. 106-110.

[124] J. Trogh, D. Plets, L. Martens, and W. Joseph, "Advanced indoor localization based on the Viterbi algorithm and semantic data," *European Conference on Antennas and Propagation* (EUCAP 2015), Lisbon, Portugal, April 13-17, 2015, pp. 1-3.

[125] T. Moriyama, A. Polo, F. Viani, and A. Massa, "Improved wireless localization of mobile devices in smart indoor scenarios," *Proc. 2015 IEEE Mediterranean Microwave Symposium* (MMS 2015), Lecce, Italy, November 30 - December 2, 2015.

[126] R. Azaro, F. D. Natale, M. Donelli, A. Massa, and E. Zeni, "Optimized design of a multi-function/multi-band antenna for automotive rescue systems," *IEEE Trans. Antennas Propagat.*, vol. 54, no. 2, pp. 392-400, Feb. 2006.

[127] J. Robinson and Y. Rahmat-Samii, "Particle swarm optimization in electromagnetics," *IEEE Trans. Antennas Propagat.*, vol. 52, no. 2, pp. 397-407, Feb. 2004.

[128] W. Navidi, W. Murphy, Jr., and W. Hereman, "Statistical methods in surveying by trilateration," *Computational Statistics and Data Analysis*, vol. 27, no. 2, pp. 209-227, Apr. 1998.

[129] N. E. Huang, Z. Shen, S. R. Long, M. C. Wu and H. H. Shih, "The empirical mode decomposition and the Hilbert spectrum for non-linear and non-stationary time series analysis," *Proceedings of the Royal Society of London. Series A: Mathematical, Physical and Engineering Sciences*, vol.454, pp. 903-995, 1998.

[130] L. Zao, R. Coelho, and P. Flandrin, "Speech enhancement with EMD and Hurst-based mode selection," *IEEE/ACM Trans. Audio, Speech, Language Process.*, vol. 22, no. 5, pp. 899-911, May 2014.

[131] C. Luo, L. Cheng, M. C. Chan, Y. Gu, J. Li, and Z. Ming, "Pallas: Self-bootstrapping fine-grained passive indoor localization using WiFi monitors," *IEEE Trans. Mobile Comput.*, in press.

[132] I. Sabek, M. Youssef, and A. V. Vasilakos, "ACE: An accurate and efficient multi-entity device-free WLAN localization system," *IEEE Trans. Mobile Comput.*, vol. 14, no. 2, pp. 261-273, Feb. 2015.

[133] E. Hurst, "Long-term storage capacity of reservoirs," *Trans. Amer. Soc. Civil Eng.*, no. 11, pp. 770-799, Apr. 1951.

[134] A. V. Oppenheim and R. W. Schafer, *Digital Signal Processing*, Prentice Hall, Englewood Cliffs, N. J., 1975.

[135] R. Agrawal, C. Faloutsos, and A. Swami, "Efficient similarity search in sequence databases," *4th Int. Conference Foundations of Data Organization and Algorithms*, Chicago, IL, pp. 69-84, October 1993.

[136] N. Cristianini and J. Shawe-Taylor, *An Introduction to Support Vector Machines*. Cambridge, U.K.: Cambridge Univ. Press, 2000.

[137] V. N. Vapnik, *The Nature of Statistical Learning Theory*. New York: Wiley, 1999.

[138] H. W. Kuhn and A. W. Tucker, "Nonlinear programming," in *Proc. 2nd Berkeley Symp. Math. Statist. Probab.*, Berkeley, CA, USA, pp. 481-492, 1951.

[139] J. Platt, "Probabilistic outputs for support vector machines and comparison to regularized likelihood methods," in *Advances in Large Marging Classifiers*, A. J. Smola, P. Bartlett, B. Scholkopf, and D. Schuurmans, Eds. Cambridge, MA: MIT Press, 1999.

[140] Z. Yang, Z. Zhou, and Y. Liu, 'From RSSI to CSI: Indoor localization via channel response', *ACM Comput. Surv.*, vol. 46, (2), pp. 1-32, 2013.

[141] K. Wu, J. Xiao, Y. Yi, D. Chen, X. Luo, L. Ni, "CSI-based indoor localization," *IEEE Trans. Parallel Distrib. Syst.*, vol. 24, no. 7, pp. 1300-1309, 2013.

[142] F. Viani, A. Polo, E. Giarola, M. Salucci, and A. Massa, "Principal component analysis of CSI for the robust wireless detection of passive targets," *2017 International Applied Computational Electromagnetics Society Symposium*, ACES 2017, Firenze, Italy, March 26-30, 2017.

[143] Y. Wang, K. Wu, and L. M. Ni, "WiFall: Device-free fall detection by wireless networks," *IEEE Trans. Mobile Comput.*, vol. 16, no. 2, pp. 581-595, Feb. 2017.

[144] A. N. Kolmogorov, "Theory of transmission of information" *Amer. Math. Soc. Transl.,* Ser. 2, vol. 33, pp. 291-321, 1963.

[145] M. D. Migliore, "On electromagnetics and information theory," *IEEE Trans. Antennas Propag.*, vol. 56, no. 10, pp. 3188-3200, Oct. 2008.

[146] M. D. Migliore, "On the sampling of the electromagnetic field radiated by sparse sources," *IEEE Trans. Antennas Propag.*, vol. 63, no. 2, pp. 553-564, Feb. 2015.

[147] F. G. Filip, "Decision Support Systems," Ed. Tehnica, Bucharest, 2004.

[148] M. Demarest, "Technology and Policy in Decision Support Systems", Aug 2005. Available Online: http://dssresources.com/papers/features/demarest05/demarest07082005.html

[149] C. Coello Coello, D. Van Veldhuizen, G. Lamon, "Evolutionary algorithms for solving multi-objective problems," Kluwer Academic, 2002.

[150] A. Polo, F. Viani, L. Zappini, S. Marchesi, A. Zorer, and A. Massa, "Advances in decision-making support tools for fleet management in emergency and security applications," *Proc. 2014 IEEE Antenna Conference on Antenna Measurements and Applications* (IEEE CAMA 2014), Antibes Juan-les-Pins, France, pp. 1-3, Nov. 2014.

[151] K., Deb; A. Pratap; S. Agarwal; T. Meyarivan, "A fast and elitist multiobjective genetic algorithm: NSGA-II," *IEEE Trans. Evol. Comput.*, vol.6, no.2, pp.182,197, Apr 2002.

[152] L. Zappini, S. Marchesi, A. Polo, F. Viani, and A. Massa, "Evolutionary optimization strategies applied to wireless fleet management in emergency scenarios," *Proc. 2015 IEEE Mediterranean Microwave Symposium* (MMS 2015), Lecce, Italy, November 30 - December 2, 2015.

[153] D. A. Van Veldhuizen, G. B. Lamont, "Multiobjective Evolutionary Algorithm Research: A History and Analysis," Tech. Rep. TR-98-03, Dept. Elec. Comput. Eng., Graduate School of Eng., Air Force Inst.Technol., Wright-Patterson, AFB, OH, 1998.

[154] E. Zitzler, L. Thiele, "Multiobjective Evolutionary Algorithms: a Comparative Case Study and the Strength Pareto Approach," *IEEE Trans. Evol. Comput.*, vol 3, pp. 257-271, 1999.

[155] K. Deb, "Multi-objective Optimization Using Evolutionary Algorithms," John Wiley & Sons, 2001.

[156] D. Greiner, "Enhancing the multiobjective optimum design of structural trusses with evolutionary algorithms using DENSEA," 44th AIAA (American Institute of Aeronautics and Astronautics) Aerospace Sciences Meeting and Exhibit, AIAA-2006-1474, 2006.

[157] M. Reyes, C. Coello, "Improving PSO-based multi-objective optimization using crowding, mutation and 'ϵ-dominance'," in third international conference on evolutionary multicriterion optimization, EMO 2005. LNCS, vol. 3410. pp. 509-19, 2005.

[158] J. Kollat, P. Reed, "Comparison of Multi-Objective Evolutionary Algorithms for Long-Term Monitoring Design," Advances in Water Resources, vol. 29(6), pp. 792-807, 2006.

[159] H. Eskandari, "FastPGA: A Dynamic Population Sizing Approach for Solving Expensive Multiobjective Optimization Problems," Evolutionary Multi-Criterion Optimization, Springer, pp. 141-155, 2007.

[160] E. Zitzler, "Indicator-based selection in multiobjective search," Parallel Problem Solving from Nature (PPSN-VIII), Lecture Notes in Computer Science, Berlin/Heidelberg, Springer, 2004, pp.832-842

[161] A. J. Nebro, "A Cellular Genetic Algorithm for Multi-objective Optimization," Proceedings of the Workshop on Nature Inspired Cooperative Strategies for Optimization, Granada, Spain , pp.25-36, 2006.

[162] A. J. Nebro, "Optimal Antenna Placement using a New Multi-objective CHC Algorithm," Proceedings of the 9th Annual Conference on Genetic and Evolutionary Computation, London, England, pp.876-883, 2007.

[163] K. Deb, "A Fast Elitist Multi-Objective Genetic Algorithm: NSGA-II," *IEEE Trans. Evol.*, vol.6, pp.182-197, 2000.

[164] K. Deb, H. Jain, "An Evolutionary Many-Objective Optimization Algorithm Using Reference-Point- Based Nondominated Sorting Approach, Part I: Solving Problems With Box Constraints," *IEEE Trans. Evol. Comput.*, vol. 18, pp. 577-601, 2014

[165] J. Knowles and D. Corne, "The Pareto Archived Evolution Strategy: A New Baseline Algorithm for Multiobjective Optimization," *Proc. of the 1999 Congress on Evolutionary Computation*, Piscataway, N.J., pp. 98-105, 1999.

[166] D. Corne, "PESA-II: Region-based Selecion in Evolutionary Multiobjective Optimization," *Proc. of the Genetic and Evolutionary Computation Conference*, pp. 283-290, 2001.

[167] N. Beume, "SMS-EMOA: Multiobjective selection based on dominated hypervolume," *European Journal of Operational Research*, vol. 181(3), pp. 1653-1669, 2007.

[168] E. Zitzler, "SPEA2: Improving the Strength Pareto Evolutionary Algorithm For Multiobjective Optimization," CIMNE, Barcelona, Spain, 2002.